NUMERICAL SIMULATION OF THE FLOW FIELD IN 3D ECCENTRIC ANNULAR AND 2D CENTERED LABYRINTH SEALS FOR COMPARISON WITH EXPERIMENTAL LDA DATA

A Thesis

by

ANAND VIJAYKUMAR

Submitted to the Office of Graduate Studies of
Texas A&M University
in partial fulfillment of the requirements for the degree of

MASTER OF SCIENCE

December 2010

Major Subject: Mechanical Engineering

Numerical Simulation of the Flow Field in 3D Eccentric Annular and 2D Centered Labyrinth Seals for Comparison with Experimental LDA Data

NUMERICAL SIMULATION OF THE FLOW FIELD IN 3D ECCENTRIC ANNULAR AND 2D CENTERED LABYRINTH SEALS FOR COMPARISON WITH EXPERIMENTAL LDA DATA

A Thesis

by

ANAND VIJAYKUMAR

Submitted to the Office of Graduate Studies of
Texas A&M University
in partial fulfillment of the requirements for the degree of

MASTER OF SCIENCE

Approved by:

Chair of Committee,	Gerald L. Morrison
Committee Members,	Je C. Han
	Robert E. Randall
Head of Department,	Dennis O' Neal

December 2010

Major Subject: Mechanical Engineering

ABSTRACT

Numerical Simulation of the Flow Field in 3D Eccentric Annular and 2D Centered Labyrinth Seals for Comparison with Experimental LDA Data.

(December 2010)

Anand Vijaykumar, B.S., Vellore Institute of Technology, India

Chair of Advisory Committee: Dr. Gerald L. Morrison

The flow field in an annular seal is simulated for synchronous circular whirl orbits with 60Hz whirl frequency and a clearance/radius ratio of 0.0154 using the Fluent Computational Fluid Dynamics (CFD) code. Fluent's Moving Reference Frame model (MRF) is used to render the flow quasi-steady by making transformations to a rotating frame. The computed flow fields for velocity, pressure and shear stress measurements are compared with the experimental data of Winslow, Thames and Cusano. The CFD predictions are found to be in good agreement with the experimental results. The present CFD methodology can be extended to other whirl frequencies and clearances. The dynamic wall pressure distributions in an annular seal for non-circular whirl orbits were obtained using CFD. The simulations were performed using a time dependant solver utilizing Fluent's Dynamic Mesh model and User Defined Functions (UDFs). The wall pressure distributions obtained from the simulations are compared with data of Cusano. The CFD simulations over predicted the pressure field when compared to experimental results however the general trends in pressure contours are similar. The flow fields for

varying rotor eccentricities are also studied by performing coordinate transformations and rendering the flow quasi-steady at set eccentricities using Fluent's MRF model. The computed velocity and pressure fields are compared with the time dependant solution obtained using Fluent's Dynamic Mesh model and UDFs for the same eccentricity. Good agreement in the velocity fields is obtained; however the pressure fields require further investigation. 2D Labyrinth seal simulations were performed for comparisons with experimental LDA data from Johnson. The velocity fields match the experimental LDA data to a fair degree of extent; however, Fluent simulations under predicted the secondary recirculation zones in Labyrinth Backward Swirl (LBS) case.

ACKNOWLEDGEMENTS

I would sincerely like to thank my committee chair, Dr. Gerald L. Morrison for his constant source of support and encouragement which kept me motivated throughout my research. I would also like to express my gratitude to Dr. Je C. Han and Dr. Robert E. Randall for their guidance and for taking time out to serve on my committee.

I would like to acknowledge the support of Turbomachinery Research Consortium which made it all possible. I would also like to thank the Department of Mechanical Engineering, Texas A&M University for giving me this opportunity.

NOMENCLATURE

c	Nominal clearance between rotor and stator (1.27 mm)
d	Rotor diameter
e	Rotor eccentricity ratio
ε	rotor eccentricity
L	Rotor length (37.3 mm)
P	Static pressure
P*m	(P-Pout)/(Pin-Pout)
R	Rotor radius (82.05 mm)
Re	Reynolds number = (2Uc)/(ν)
Ta	Taylor number = $(\rho W_{sh} c \mu)/(2c/D)^{1/2}$
Ux	Mean axial velocity m/s
Um	Bulk averaged axial velocity, 7.4 m/s
Ur	Mean radial velocity m/s
Ut	Mean azimuthal velocity m/s
Wsh	Surface rotational speed of shaft
μ	Dynamic viscosity
ν	Kinematic viscosity
ρ	Density of fluid
Cp	Sommerfeld Journal Bearing Coefficient $Cp= P^{*}c^{2}/ (6\mu\omega R^{2})$
β	whirl ratio

γ	carry over coefficient
χ	percentage kinetic energy
Cd	coefficient of discharge

TABLE OF CONTENTS

CHAPTER Page

CHAPTER Page

LIST OF TABLES

CHAPTER I

INTRODUCTION

Turbomachinery seals interface between rotating parts such as rotors, blade tips and stationary parts such as housings. Seals help isolate regions of different pressures and are non-contacting; resulting in leakage flow across the seal.

Annular seals and Labyrinth seals are leakage control devices minimizing secondary flow in turbomachines. Although the annular seals are geometrically similar to plain journal bearings, they show a different flow structure which may be dominated by turbulence and inertia effects. Labyrinth seals consist of series of constrictions and cavities through which energy is dissipated.

The secondary flow through the seal is unwanted as it reduces the efficiency of the machine. Operating conditions unique to seals are large axial pressure gradients and small clearance to radius ratios. The flow is important to analyze since it affects the performance of the seal as well as the forces which act upon the rotor. Computational Fluid Dynamic (CFD) simulations will be performed using flow parameters from the experiments of Winslow [1], Thames [2], Cusano [3], Johnson [4] and Robic [5] so that the ability of CFD simulations to directly represent various flow fields in annular seals can be verified. CFD simulations will be performed on 2D labyrinth seals to compare flows fields and investigate the effects of pre-swirl, clearance and Reynolds numbers. Discharge coefficient, carry over coefficient and percentage kinetic energy dissipated are plotted as a function of the tooth with preceding cavity. CFD simulations can be helpful

---

This thesis follows the style of the Journal of Applied Mechanics.

in providing a faster and cheaper estimate of the flow field for a wide variety of operating conditions and flow parameters compared to experimental investigations.

The impetus for the present study is two-fold. First is to test the accuracy of the CFD model and the physical models utilized to simulate these types of problems where coordinate transformations are made. Flow fields for various eccentricities can be estimated by rendering the flow quasi-steady. The second is to apply the same methodology for similar types of flows in labyrinth seals and to validate the accuracy of commercial code for labyrinth seals by comparisons with experimental data.

The flow field in annular and labyrinth seals is highly turbulent and hence it is important to analyze the flow in order to determine the seal performance and forces acting on it. Johnson [4] and Morrison et. Al, [6] measured the flow field inside a eccentric and whirling annular seal with the help of a pioneering laser measurement system that was developed at Turbo machinery laboratory at Texas A&M University.

Extensive data is available on annular seals and labyrinth seals through experimental studies. But complexities with the current experimental setups make it difficult to obtain information for a wide range of operating and flow conditions. CFD provides an excellent alternative to determine flow fields and turbulence measurements for different operating conditions and flow fields.

The orbits for 3600 rpm with varying whirl ratios revealed that the orbits at higher whirl ratios are more and more non-circular. It was impossible to measure the pressure data around the rotor instantaneously as the pressure measurements were taken

at fixed azimuthal locations along the stator while the rotor is rotating. Instantaneous and phase averaged wall pressure for annular seals with dynamic eccentricities and a whirl ratio of one were recorded by Winslow [1] and for different whirl ratios at a given eccentricity by Cusano [3]. LDV measurements of flow fields in labyrinth seals were performed by Johnson [4]. The current work focuses on obtaining the velocity and pressure fields distribution in an annular seals and labyrinth seals using CFD. The Fluent-based CFD analysis was performed on data of Winslow [1], Thames [2], Cusano [3] and Johnson [4] to compare velocity and pressure fields.

CFD provides an excellent alternative to determine flow fields and turbulence measurements for different operating conditions and flow fields.

CHAPTER II

LITERATURE REVIEW

Annular Seal

Experimental

Fluid flow investigations in annular seals began in the 1970's due to their contributions to turbo-machinery instabilities. Hirs [7] developed a bulk flow model for turbulent flow between thin films. It differed from earlier methods in the empirical constants used. The comparisons with law of wall theory for turbulent flow in bearings were better for high Reynolds number. Brenn [8] investigated the nature of the flow in the annulus between concentric cylinders to analytically determine the influence of whirl motion on flow conditions. Lessen [9] performed the analytical study of dynamically eccentric whirling annular seal at a Taylor number within the Taylor regime. The axial flow through the seal was modeled as a plug flow by assuming high momentum transport by Taylor vortices. Other findings by Lessen [9] include the presence of Goertler disturbances which are similar to Tollmein-Schlichting waves induced by the curvature of the boundary surfaces. Research in measuring the flow field inside eccentric and whirling annular seals began with Johnson [4] and Morrison et. Al [6], when a pioneering laser measurement system was developed at Turbo machinery laboratory at Texas A&M University. Morrison et. Al [6] investigated the flow field inside an annular seal with 1.27 mm clearance using 3-D Doppler anemometer system. The seal was operated at a Reynolds number 18,600 and a Taylor number of 4500. They found that the azimuthal value of velocity continuously increases as the fluid moves downstream.

Based on the Reynolds normal stress components, they found the production of anisotropic turbulence as the flow progresses through the annular seal.

Johnson [4] performed detailed flow measurements of both smooth and labyrinth seals It was found that there is a large entrance region where the radial velocity decayed from 0.08U to zero in the first x/c = 1 length of the seal. This effect was reported by Morrison et. al and further confirmed by Thames [2] and was identified as a vena contracta. Thames [2] made measurements using 3D Laser Doppler Velocimeter and found that there is a region of high axial momentum at the inlet on the pressure side of the clearance that migrates around the seal to the suction side at the exit. This confirmed the recirculation zone discovered by Johnson and was called the 'saddle back effect'. Das [10] studied the effect of eccentricity ratio on the flow field. The flow field was investigated using a 3D Laser Doppler Velocimeter in annular and labyrinth seals. The eccentricity ratio was 0.10 and 0.50 for annular and labyrinth seals respectively. He found that the maximum axial velocity migrates from the pressure side to suction side as the flow goes downstream and the magnitude of the migration was dependant on the eccentricity of the seal. He observed that labyrinth seal showed larger regions of recirculation at the inlet due to its higher eccentricity. Winslow [1] studied the dynamic pressure and wall-shear measurements for different eccentricities with a whirl ratio 1. He observed that for larger eccentricities there is a peak in mean pressure followed by a gradual decay until the near the exit of the seal where pressure begins to increase again. Suryanarayanan [11] studied the effect of whirl-ratio on a 50% eccentric annular seal and made experimental wall pressure measurements. Cusano [3] experimentally found

the wall pressure distribution on a 25 % eccentric annular seal and studied the effect of whirl ratio on the flow field. He found that Childs [12] correlations could not be applied to find the rotordynamic coefficients as the rotor moves in non-circular orbits about the stator center.

Numerical

Athavale et al [13] simulated the turbulent flow field in an annular seal with large clearance/radius ratio (0.015) and the whirling rotor was simulated using the 3-D CFD code SCISEAL. The flow field was rendered quasi-steady by making transformation to rotating frame. The computed flow field in terms of velocity and pressure was compared with experimental results and a good agreement was established. He predicted that the behavior of the flow has anisotropic turbulence, both in quantitative and qualitative terms. Arghir Frene [14] performed perturbed Navier Stokes calculations and compared results with Morrison et al [6]. They observed that for a large c/L ratio the influence of downstream conditions on upstream flow are more important than usually accounted for in rotor dynamic calculations. Robic [5] studied the effect of pre-swirl on whirling annular and labyrinth seals. For annular seals Robic [5] found that predicted axial velocity contours matched well with experimental results but he did not take into account wakes of swirl generator in his calculations. The turbulent kinetic energy was slightly over predicted near the walls. Sekaran [15] studied the impact of orbit path, whirl ratio and clearance on the flow field and rotordynamic coefficients of annular seals. She observed that the flow field varies greatly with change in orbit and clearance. The velocity, pressure and force magnitudes were found to be much larger for linear as

compared to circular orbits. The force predictions and rotordynamic coefficients matched theory better for smaller clearances. Flow in smaller clearances was viscosity dominated while in larger clearances was inertia dominated.

Labyrinth Seal

Experimental

Mean flow measurements in a nine cavity labyrinth seal was performed by Deich et al [16] and it was found that the flow remains unchanged after the fourth cavity of the seal. The measurements were made with a LDA system. Hauck [17] made turbulent measurements in eccentric annular seal in order to understand the eccentricity effects on the flow field. Turbulence kinetic energy and dissipation rate were compared for the turbulence model. Stator wall roughness and honeycomb structures were found to have a large effect on the labyrinth seals design. Iwatsubo et. al [18] evaluated the stability and leakage of a rotor system for labyrinth seals with arbitrary configurations by applying theory of straight and stepped type seal. Dareli and Eser [19] studied gas flow through straight-through labyrinth seal. They calculated leakage and pressure distribution using Neumann Modified method and circumferential velocity was calculated using Moody Friction-Factor model. Martin [20] provided the most primitive form of leakage model which is still in use today and was purely analytical and based on work done to attain a pressure drop. He did not validate his findings with experimental data. Das [10] measured the flow field inside a labyrinth seal using 3D Doppler velocitmeter. He also saw the maximum velocity is not observed over the maximum clearance and the labyrinth seal had large axial recirculation zone at the inlet of the cavity due to the large

eccentricity. He found that the turbulence generation was dominant over the first third of the seal. Gamal [21] as a part of his doctorate thesis, investigated the leakage and rotordynamic characteristics of pocket damper seals and see-through labyrinth seals. He found that both blade profile and thickness affected the leakage. Cavity depth was found to have negligible effect on seal leakage however leakage increased with eccentricity. He also suggested the importance of carry over coefficient and suggested a modified carry over coefficient.

Numerical

Stoff [22] studied incompressible flow in a labyrinth seal using finite difference code using a k-epsilon turbulence model; he also measured mean flow and turbulence intensities. He compared his finite difference code with back scattering laser-Doppler anemometer. Rhode [23] et. al did a numerical study of labyrinth seals. He studied the effect of inlet conditions on the flow fields and was a major impetus in the current research. He applied a Navier-Stokes code to predict the leakage from upstream and downstream pressures. A rather unexpected finding is that a dramatic increase in swirl occurs at the discharge of small clearance annular seal which is not observed in labyrinth seals. He observed that free shear layer and tooth throttling had little effect on turbulent length scale. Robic [5] presented dynamic and mean pressure measurements on labyrinth and annular seals for different inlet swirls -45, 0, +45 degrees. He also performed an analysis of the effect of swirl on the pressure field. He compared the computer simulations for pressure and velocity data with LDV measurements taken at the Turbomachinary Laboratory. Demko et al. [24], performed a numerical study and

predicted the existence of secondary recirculation zone when the Taylor number is large compared to the Reynolds number. Labyrinth seal investigations were discussed by Cogan [25] and Gamal [21] and they explored a number of leakage models and compared results with experimental data. Al-Ghasem [26] explored the effectiveness of commercial Fluent code to predict the leakage in a windback seal. They studied the effects of seal clearance, tooth pitch, cavity depth and tooth number on leakage, velocity and pressure distribution. Collins [27] with the help of CFD studied the performance of worn abradable honeycomb labyrinth seals.

CHAPTER III

OBJECTIVES

The work is comprised of four objectives; first, to study the flow field in an annular seal as the rotor traces non-circular orbits about the stator center. The flow field in an annular seal was predicted by means of a CFD code. Fluent simulations were performed on the annular seal for arbitrary whirl orbits. The simulations were made possible using Fluent's Dynamic Mesh Modeling (MDM) and the arbitrary whirl motion assigned to the rotor using Fluent's User Defined Functions (UDFs). Standard k-ε models with wall-functions were used for turbulence. The pressure contours were compared with experimental data from Cusano [3]. Simulations were performed for 3600 rotor rpm and 24 Hz whirl frequency.

Second, to predict the flow field for circular whirl orbits with synchronous whirl by rendering the flow field quasi-steady using suitable transformations to a rotating frame. Fluent's MRF (Moving reference Frame) model was used for coordinate transformation and simulations were performed with a steady solver using k-ε model and wall functions to represent turbulence. The computed flow fields for pressure and shear stress measurements were compared with experimental data of Winslow [1], Robic [15], Thames [2] for 60 Hz whirl and circular orbit. A good degree of conformance was observed between simulation and experimental results.

Third, to predict flow field for varying rotor eccentricities by performing coordinate transformations and rendering the flow field quasi-steady at the set eccentricities under similar flow conditions. The velocity and pressure contours were

compared for the coordinate transformation case and the Deforming Mesh case for same eccentricity. A good estimate of the flow conditions at varying rotor eccentricities is made possible by rendering the flow quasi-steady at set eccentricities by coordinate transformations using Fluent's MRF. The coordinate transformations involve a steady solver and hence the simulations are much faster compared to moving mesh simulations which involve an unsteady-solver. Then the dynamic solution is obtained by using the steady-state solution for each eccentric location of the orbit.

Fourth, to simulate the flow field in 2D labyrinth seal for No Swirl, Forward Swirl, Backward Swirl, High Taylor number and low clearance cases. Compare the simulation results with experimental LDA data by Johnson [4]. Using Hodkinson [28] model, predict and plot the carry over coefficient and percentage kinetic energy. Calculate and plot the coefficient of discharge against each tooth with preceding cavity. Establish the effect of Reynolds number, clearance and swirl on the flow field in 2D labyrinth seals.

The most important objective of the study is to show that a database of flow fields for varying rotor eccentricities using the quasi-steady state approach can be utilized such that the flow field for any particular orbit can be estimated by matching from the database.

CHAPTER IV

ANNULAR SEALS

Numerical Methodology for Annular Seals

The computations are performed using Fluent 6.3.26 which uses a control volume technique with a pressure based solver using segregated algorithms which solve the governing equations sequentially. The solution is iterated until a converged solution is obtained.

The present study utilizes the experimental work of Cusano [3], Thames [2], Winslow [1], and Robic [5] to compare with the CFD results. The 3D model is built using Gambit (Ver 2.4.6). The geometry of the model has the following dimensions- L =37.3mm, R =82.05mm and clearance= 1.27mm (50 mil). The rotor is maintained initially at an eccentricity of 50% (25mil). The 3D modeling is based on the actual seal geometry used in the experiments. The entire geometry is meshed using a hexahedral grid which consists of more than a million node. The mesh is shown in Fig. 1. The grid has high aspect hexahedral cells as the variations along the tangential direction are small. In order to capture the flow conditions accurately near walls, the boundary layers along the rotor and stator walls must be resolved to y+ values of less than 5. The whirling motion of the rotor about the stator center was made possible using Fluent's Dynamic Mesh Model. The mesh is deformed every time step by treating the mesh as a series of interconnected springs. This is enabled using the 'rpsetvar' command. The rotor is made to move along specific orbits paths by using User Defined Functions (UDF's) in Fluent, which are programs written in C programming language. Arbitrary orbit paths are

represented by a polynomial equation. The rotor wall inside the meshed region was made to move along this orbit using UDFs in C language. Suitable transformations had to be made to ensure that orbit path makes an x intercept equivalent to 0.000635 m corresponding to the eccentricity of the rotor. Another UDF was written to print the centroid of the rotor after each timestep. The centroid coordinates were then compared with the curvefit equations to ensure that the rotor moves along specified orbit paths as it is not possible to observe the rotor motion in 3D due to complexity of grid and 3D rendering problems.

The Fig 1 shows the 3D mesh model which consists of 3 parts- Swirl ring, the region between the rotor and the stator and the step region after the seal where the clearance increases. The swirl ring merely provides the inlet boundary condition for clearance and hence a relatively course mesh was used. The clearance region was meshed with a very fine mesh to ensure wall y+ values within specified limits. The space after the outlet is the region of larger clearance and is created long enough in order to prevent backflow from taking place at the outlet plane. The boundary condition for inlet plane is set as ‘mass flow rate’. The mass flow rate was set to 4.87 kg/sec for Reynolds number of 24000. The boundary conditions for turbulent parameters like turbulent kinetic energy and dissipation rate are set at 2.26 m^2/s^2 and 431.2 m^2/s^3 respectively. The steady state simulation was performed first to provide an initial guess for the unsteady simulation. Unsteady simulations were performed once the steady solution converged. The good initial guess shortens the computational time. The unsteady simulations were

performed at each time step until the residuals for x,y,z velocities, turbulent kinetic energy, turbulent viscosity and continuity went below 1e-04.

Fig. 3 shows the geometry along with the dimensions of the test rig. The working fluid used is water with density of 998.2 kg/m3 and dynamic viscosity of 0.00103 kg/m-s. A shaft speed of 3600 RPM corresponds to a Taylor number 6600. The inlet mass flow boundary condition was specified with a mass flow rate of 4.87 kg/s for a Reynolds number of 24,000. Standard k-ε models and wall-functions with pressure gradient effects were used to model the turbulence. The enhanced wall treatment is necessary to capture flow characteristics accurately in the viscous sublayer next to the wall. The standard wall function does not sufficiently resolve the viscous sublayer, and is not very effective when the wall is moving rapidly or when there are high pressure gradient effects. Ideally the wall y+ values should be below 1 but Fluent allows wall y+ values as large 5 as long as the first layer of the mesh lies in the viscous sublayer. The wall y+ value is equal to or below 5 throughout the seal except for the entrance region. Fig 4 show the wall y+ distribution obtained in this study. Fig. 7 shows the flow chart for the dynamic mesh scheme. The coordinate transformations were performed using Fluent's Moving Reference Frames model (MRF) which renders the flow field quasi steady thereby enabling steady state simulations.

Numerical Simulation Model

Five Test Cases Were Run

1. 50Mil clearance, 25Mil eccentricity, Circular orbit, 60hz case with whirl.

2. 50Mil clearance, 25Mil eccentricity, Circular orbit 60hz, Coordinate transformation.
3. 50Mil clearance, 25Mil eccentricity, statically eccentric case.
4. 50Mil clearance, 25Mil eccentricity, 18hz arbitrary orbit.
5. 50Mil clearance, 25Mil eccentricity, Circular orbit 18hz, Coordinate transformation.

Operating at the Following Conditions

Eccentricity: 50 % of seal-stator clearance, Re= 24000, flow rate =4.87 kg/s, Rotor speed: Ta=6600 (3600 rpm, 60Hz), Whirl ratio: 0.3, 1 positive whirling. The first case was run for 50Mil clearance, 25Mil eccentricity, and circular orbit with whirl frequency of 60 Hz. The flow was rendered quasi-steady using Fluent's MRF model. The results were compared with experimental results from Thames [2], Winslow [1] and Robic [5]. The next run was for the same case with deforming mesh using Fluent's Dynamic mesh model and UDFs. The results were compared with experiments and with results from the coordinate transformation case. The simulations at 0.3 whirl ratio and non-circular whirl orbits were carried out to compare with instantaneous wall pressure distribution from experiments by Cusano [3].

To compare simulations results with experiments, the orbital data were processed to generate x and y coordinates of whirl orbits as functions of time. Coordinate data from experiments are curvefit using Tablecurve 2D which produces the x and y curves as functions of time. The same curvefit equations are incorporated in UDFs to ensure rotor follows the specified orbit. The UDF calculates the position of each node element in the

seal model for each time step. In Cusano [3], the stator whirled to simulate the whirling of the rotor while the rotor itself is rotating about a fixed axis. Due to small c/D ratio the effect on the fluid is similar. The orbit path chosen corresponded to 18Hz whirl frequency as the variations in orbit per block were minimum. For all other whirl ratios there were high variations in consecutive orbits paths and hence could not be used. The orbit used is acquired at the test condition of 3600 rpm rotor speed and 0.3 whirl ratio (18Hz), positive whirl- whirling direction being the same as rotor's revolution. The reason why this orbit was chosen is because this is almost a circle.

Boundary Conditions for Annular Seal

For turbulent flow computations, additional boundary conditions need to be specified for turbulence parameters. This information is supplied in the form of derived quantities like turbulent intensity, length scale, viscosity ratio and hydraulic diameter. The default boundary conditions should be representative of the flow field else errors will be introduced. For internal flows the turbulent intensity and hydraulic diameter are specified based on $I = 0.16.Re^{-1/8}$. Periodic boundary conditions were assumed in the circumferential direction. Mass flow inlet condition was specified at the inlet of the swirl ring along the axial direction and outlet of seal was outflow.

Solution Process

1. The solution is initialized with the boundary conditions at the inlet. The turbulence hydraulic diameter and turbulence intensity ratio are specified.

2. A good initial guess for turbulence is made by trial and error and based on experimental data.

3. The solver is run in steady state for few iterations and the steady state solutions is used as an initial guess for transient simulations

4. Convergence is judged by monitoring velocity pressure, forces and by checking repeatability in pressure contours/trends.

Grid Independence Study

The model used a grid with 15 nodes in the seal clearance and the preliminary run showed turbulence y+ beyond 5 and high gradients and leakage. The grid independence was established by Sang Hyun Park [29] by increasing the number of nodes along the radial direction in the clearance region. The variation in mass flow rate with number of nodes in the clearance region is shown in figure 2 where it was seen that increasing the number of nodes from 25 to 35 in the clearance region led to little change in the mass flow rate showing that grid independence was established. The final mesh consisted of 35 nodes across the clearance.

Steps to Achieve Grid Independence

1. Obtain grid.

2. Adapt the grid based on wall Y+ and pressure gradient.

3. If large gradients in pressure are expected, concentrate the grid in that region, eg boundary layer.

4. Adapt grid – data from original grid is interpolated to the finer grid.
5. Continue calculation to convergence.

6. Compare results obtained with different grids.

7. Establish grid independence.

Solver

Fluent 6.3.26 uses a control volume technique with a pressure based solver using segregated algorithms which solve the governing equations sequentially and the solution is iterated until a converged solution is obtained.

Finite Volume Technique

Fluent uses a control volume technique which involves division of the domain into control volumes, integration of individual control volumes to obtain algebraic equations, linearization of discretized equations, and solving the system to obtain values of variables.

Under Relaxation Factors (URF's)

URF's are used to stabilize the iterative process in a segregated solver. Decreasing the URF's stabilizes the solution but increases time to convergence. Appropriate URFs are learnt through trial and error and from experience.

The following sequence of steps is followed:

1. Fluid properties like density, viscosity, specific heat including turbulent viscosity are updated based on the current solution.
2. Momentum equations are updated one after the other using recently updated values of pressure and face mass fluxes.
3. Pressure correction equations are solved using recently updated values of pressure and face mass fluxes.

4. Face mass fluxes, pressure and velocity field are corrected using pressure correction obtained from previous step.
5. The equations are solved for additional scalars, if any, such as turbulent quantities, energy, species, and radiation intensity using current values of solution variables.
6. Source which arise from interactions between different phases (source term for carrier phase due to discrete particles) are updated.
7. Convergence for these equations is checked.

CHAPTER V

DYNAMIC MESH MOTION

The grid is deformed at every time step using the Dynamic Mesh Motion scheme in Fluent by treating the edges between nodes as a series of interconnected springs, while the motion of the rotor is specified using User Defined Functions (UDFs). The spacing between the nodes in the initial mesh is taken as the equilibrium condition. Dynamic mesh capability of Fluent updates the volume mesh after everytime step. There are three commonly available mesh motion methods to update the deforming volume mesh. The methods are smoothing, dynamic layering and local remeshing. The method used in the simulations is spring based smoothing for hexahedral grid. Spring based smoothing is enabled by default only for tetrahedral, to enable it for hexahedral grid we need to enable it using the syntax –

(rpsetvar 'dynamesh/spring/all-element-type? #t)

Describing Rotor Motion Using UDF

A UDF in Fluent can be used for various applications like specified Mesh Motion or Velocity profiles. UDF's are written in C language and are dynamically linked to the solver. For defining the motion of the rotor the equations of motion are supplied as a C code. A number of inbuilt macros are used to associate the motion of the grid with the UDF. In the Dynamic Mesh Technique the mesh changes shape as a function of time while in Moving Reference Frames the mesh is static.

Description of UDF

Description of UDF includes assigning surface velocity to rotor, writing out centroid coordinates of the rotor and assigning rotor motion profile. The surface velocity of the rotor is assigned using the surface velocity UDF. The begin_f_loop iterates over each node on the rotor and assigns the shaft speed to each node based on calculations of the centroid of the rotor. The x component of the surface velocity and the y component of surface velocity are assigned to each node on the rotor to simulate the rotation of the rotor.

The arbitrary motion of the rotor is specified by reducing the left and right probe position recorded on the test rig to x, y coordinates as a function of whirl angle and theta. The x and y coordinates as a function of theta are curve fit using Table Curve 2D. The curve fitting is done using a higher order polynomial. The higher order polynomials are coded in C language to ensure that the rotor follows the polynomial equation. The mesh is treated like a series of interconnected springs and each node is translated by giving it a small displacement del_x and del_y as a function of time. The translation of nodes makes the problem unsteady. The begin_f_loop calculates the centroid of each node and the del_x and del_y are added to calculated centroids. The nodes are then updated using the built in Fluent function NODE_POS_NEED_UPDATE.

As it is virtually impossible to observe the motion of the rotor in 3D and since there is no way to ensure that the rotor is actually following the intended rotor path. A small code snippet was written on the same lines as assigning surface velocity to the rotor. The centroid of rotor was calculated by iterating using begin_f_loop over all the

nodes of the rotor and averaging the centroid of each cell to get the rotor centroid. The rotor centroid were then printed on screen and compared with equations to confirm that at each time step the rotor was tracing out the correct profile. In the experimental setup the stator is whirling about a stationary rotor. But simulations were performed with stationary stator as the variations along the radial direction are very minor and both simulations can be considered the same. The simulations were performed with stationary stator and whirling rotor as it was more convenient to assign a surface velocity to the rotor and simulate whirling motion of the rotor.

CHAPTER VI

MOVING REFERENCE FRAMES

Many engineering problems involve flows through domains which contain rotating components. Examples of such flow include pump impellers, axial turbine blades and flow through propellers. The fluid flow equations can be solved using moving reference frame if the domain does not change shape as it moves (Rigid Motion). The equations are solved by adding additional Coriolis acceleration terms to the momentum equations. The solution is rendered steady with respect to the moving reference frame. The moving reference frames can be coupled with stationary frames through interfaces. For domains which change shape as they move we can solve equations using Dynamic Mesh Techniques.

Modeling Moving Reference Frames

The moving reference frame consists of a flow field which is rotating at a constant speed with respect to a stationary axis. The flow fields which are unsteady when viewed from a stationary frame become steady when viewed from a rotating frame.

The advantage of using rotating reference frames is that boundary conditions are simpler, lower computational cost and utilization of resources, post processing and analysis is easier.

Following Considerations Need to Be Ensured for Using MRF

1. Walls which move with fluid domain may assume any shape.

2. Walls which are stationary with respect to a fixed frame must be surfaces of revolution.

Equations in Rotating Frames

Equations can be solved in absolute or relative reference frames. Equations solved in relative velocity formulation are obtained by transforming the stationary frame Navier Stokes equations to a rotating frame. Relative Velocity Formulation uses relative velocity and relative total internal energy as dependant variables. Absolute velocity formulations are derived from relative velocity formulation uses absolute velocity and absolute total internal energy as dependant variables. In Relative Velocity Formulations, rotational source terms appear in momentum equations. For multiple zones which include stationary and rotating domains, governing equations are solved in each fluid zone. At interfaces between rotating and stationary zones approximate transformations for velocity vectors and velocity gradients are performed to compute fluxes of mass momentum, energy and other scalar. Flow is assumed to be steady in each zone.

Equations in Moving Reference Frames

Conservation of mass

$$d\rho/dt + \nabla.\ \rho\vec{v} = 0$$

Conservation of momentum

$$\frac{d\rho\vec{v}}{dt} + \nabla.(\rho\vec{v}\vec{v}) + \rho(2\vec{\omega}\ x\ \vec{v} + \vec{\omega}\ x\ \vec{\omega}\ x\ \vec{r}) = -\nabla(\rho) + \nabla\left(\vec{\Gamma}\right) + \vec{F}$$

Conservation of energy

$$\frac{d\rho E}{dt} + \nabla.\ (\rho\vec{v}\vec{H}) = \nabla.(k\nabla\vec{T} + \vec{\Gamma}.\vec{v}) + Sh$$

where,

2ω x v is the Coriolis acceleration

ω x ω x r is the centripetal acceleration

Γ is the viscous stress

E is the relative internal energy

H is the relative total enthalpy also known as the rothalpy

Drawbacks of Moving Reference Frames (MRF)

- MRF ignores relative motion of zones with respect to each other.
- It does not account for fluid dynamic interactions between rotor and stator and is called as frozen rotor approach.

Dynamic Mesh Motion vs. Moving Reference Frames (MRF)

In the moving grid approach, the whirling of the rotor causes the computational domain to continuously deform with every time step. The grid is regenerated or deformed like a series of interconnected springs at every time step to generate time-dependant accurate flow solutions. However, the time-dependant flow solutions are costly and time consuming. For the case in which the rotor whirls in a circular orbit, we can render the flow quasi steady by switching the reference frame to a rotating frame. The momentum equations need to be solved with an additional force terms called

Coriolis term. The boundary conditions need to be changed appropriately. The flow can now be solved with a steady solver.

Mesh Requirements for Turbulent Flow

Turbulent flow occurs when all transport quantities like mass, momentum and energy exhibit periodic, irregular fluctuations in time and space. The flows are classified based on Reynolds number Re> 2300 (internal flows)

Mesh requirements for laminar flow may not be acceptable for turbulent flows. The turbulent boundary layer is subdivided into several regions. Based on the specific region of interest, the location of the first cell adjacent to boundary or wall is determined. To capture the flow characteristics in the viscous sub-layer, enhanced wall treatment should be used. Choices of different near wall treatments are provided in Table 1. Depending on the choice of near wall treatment, some constraints are imposed on the placement of the first cell from the wall.

Table 1-Wall Functions

Enhanced Wall Treatment (EWT)	Y+ =1, can go upto y+ <=5 First cell in Laminar Sublayer	Low Re flows, better drag, pressure-drop prediction
Standard Wall Functions (SWF)	Y+ >=30-300, First cell in Log Layer	High Re flows, little gain by resolving sublayer
Non-Equilibrium Wall Functions	Limits same as SWF, Accounts for Δp effects	For mildly separating and reattaching flows

When generating a mesh, care is taken to ensure that the first cell next to the wall doesn't lie in the buffer layer, y+=5-30. Cell height calculations are based on cell centroid locations. Enhanced wall treatment with pressure gradients is used for accurate prediction of frictional drag, pressure drop, separation.

Mesh Motion Preview

Fluent dynamic mesh simulations cannot be investigated by visually observing the simulations. The 3D grid deformations cannot be observed and hence in order to ensure the orbits paths specified are correctly traced by the rotor, we need to write to a file the coordinates of the centroid of the rotor at every time-step using Fluent UDF code. The coordinates are then compared with curve-fit data from Tablecurve 2D Software which produces x and y coordinates as a function of time. The coordinates printed out by Fluent should exactly match with the curve-fit data, which ensures correct orbits paths followed by rotor.

CHAPTER VII

RESULTS FOR ANNULAR SEAL

Circular Orbit, 50% Eccentricity, 60Hz Whirl

For this flow case the flow rate is 4.87 l/s with 60Hz whirl frequency with a rotor rpm of 3600 (Wsh= -30.9 m/s). The Reynolds number is 24000, the Taylor number is 6600 and the eccentricity is 50%. The path of flow of fluid in the seal is show in Fig 6. The plenum ensures uniform flow into the seal and ensures there is no debris in the flow. The plenum was followed by a swirl ring to produce an inlet swirl for the flow entering the seal. The swirl angle was increased by placing an annular diffuser after swirl blades which slows the axial velocity at the same time increasing the swirl angle. There were no swirl blades installed for these simulations. The flow experiences a slight step at the inlet of the seal owing to difference in clearances from the exit of the diffuser to the inlet of the seal. The step has a considerable effect on the flow field in the seal.

The Fig 8.a-c, 9.a-c, 10.a-c, 11.a-c, 12.a-c, 13.a-c show the axial, radial, and tangential velocity fields at the seal inlet plane and at a location 85% downstream of the seal entrance. The experimental data are from Thames [2]. Also included in each figure are the results from the two different CFD techniques used to simulate the whirl ratio of 1, 50% eccentric ratio, circular orbit seal results. The rotor is rotating and orbiting in the counter-clockwise direction. The axial velocity near the inlet shows an accelerating flow near the pressure side with low velocities on the suction side. Fig 5 defines the pressure and suction side locations. As the flow progresses further downstream, the largest velocity magnitude region shifts from the pressure side towards the suction side. The

highest velocity drops slightly half way down and increases again towards the exit of the seal. The numerical simulation results are in good agreement with the experimental results, however the numerical simulation results show a much thicker boundary layer compared to experimental results. This could be attributed to the LDA system's inability to make measurement near surfaces and because the graphics program Tecplot 360 linearly interpolates from the last measurement position to the wall.

As the flow moves downstream, the peak axial momentum which was located at the inlet of the seal reaches wider clearances causing a slight decrease in the axial velocity. The axial velocity profile is more evenly distributed through out the seal. The radial velocities decrease as the flow is being directed down the seal and remain more or less constant. The radial velocities at the upstream and downstream positions are low throughout the seal. With the decrease in axial momentum, the tangential velocities increase. As the maximum axial velocity rotates around the seal the towards the suction side, the tangential velocities continue to increase towards the pressure side. Fig 14. a-b and Fig 15. a-b show the axial and tangential velocity fields at Z/L = 0, 0.22, 0.49, 0.86 and 0.99 locations for UDF mesh motion and coordinate transform (MRF) cases.

The CFD azimuthal velocities at the seal inlet compare well to the experimental data. The small band of high axial velocity at the rotor surface is about the same for the both the experimental case and the Fluent simulations. Further downstream from inlet, the location of maximum axial velocity is convected around the seal accompanied by an increase in the tangential velocity component. There is good agreement between the experimental data with the Fluent simulations. However, the UDF mesh motion case

predicts larger bands of high tangential velocity compared to the coordinate transformation case.

The tangential velocities at the inlet region show areas of low velocities. The Fluent UDF mesh motion case compares well with the experimental data however the coordinate transformed case predicts a larger region of low velocity. Both the Fluent simulations predict the small band of high tangential velocity at the high side along the rotor surface.

The coefficient of pressure plots for the UDF mesh motion case and the coordinate transformed case are presented in Fig 16.a-b. The high Cp and low Cp regions appear at the same locations at the seal entrance. However, there is a slight shift in regions of high Cp for the Moving Reference Case which is more in agreement with measurements by Winslow [1].

Circular Orbit, Statically Eccentric Case

For this flow case, the flow rate is 4.87 l/s with zero whirl ratio and a rotor rpm of 3600 (Wsh = -30.9 m/s). The Reynolds number is 24000, the Taylor number is 6600 and eccentricity ratio is 50%. The eccentric annular seal geometry exhibits a pressure distribution very similar to a journal bearing. As the rotor is eccentric about the stator center, the spinning of the rotor creates a pressure distribution which is very similar to the pressure and suction sides of a journal bearing. The region of constricting clearance position is called the pressure side and the suction side corresponds to expanding clearance position (Relative to positive θ direction). The largest and smallest clearance positions are called the high side and low side respectively. The different seal positions

are show in Fig 5. Contours of non-dimensionalized axial (Ux/Um) and azimuthal velocity (Ut/Um) are presented for the Maximum Clearance position, Minimum Clearance position, Pressure side and Suction side in Fig 17.a-c., 18.a-c., 19.a-c., 20.a-c., 21.a-c., 22.a.c., 23.a.c., 24.a.c. and compared with LDV measurements by Johnson [4] and Shresta [30].

The axial velocities are the largest at the high and suction side at the inlet and largest at the pressure side at the exit of the seal. The Minimum clearance position shows regions of high axial velocity at the inlet of the seal. The Fluent simulations over predicts the magnitude of axial velocities compared to experimental results as seen in Fig. 19.a-c. The peak in the axial velocity occurs in center of the minimum clearance position and this could also be due to the ineffectiveness of the laser system to measure velocities accurately near the walls owing to the small size of the clearance region. The axial flow characteristics can be explained based on journal bearing pressure field. As the flow enters the seal it gets pushed towards the regions of high side and region of low pressure field which constitutes the suction side. Hence axial velocities are higher on the suction side when compared to the pressure side. As the flow moves downstream it gets pulled towards the pressure side owing to the wall shear stress of the spinning rotor. The spinning causes the axial momentum to be built up and move towards the pressure side. The experimental results from LDA data have been non-dimensionalized using the average leakage velocity of 7.32 m/s. The results of Fluent 6.3.26 simulations for the static reference frame have been compared with the results from the coordinate transformed frame. The azimuthal velocities are higher on the low side compared to the

high side and larger on the suction side compared to pressure side. Based on the comparisons it can be concluded that the Coordinate transformation mimics the UDF mesh motion and both kinds of simulations show similar trends, however the Fluent-based simulations do not compare well against the experimental LDA for smaller clearances. The suitability of Fluent-based simulations with transformed coordinates to predict flow field in statically eccentric seals has been addressed; however the predictions of high axial velocities in lower clearances still remain unanswered. Further investigations are needed to gauge the suitability and feasibility of coordinate transformation for statically eccentric case in terms of computational time and availability of resources.

Mean Pressure and Mean Shear Stress Distribution for Circular Orbit, 50% Eccentricity

For this flow case the flow rate is 4.87 l/s with a 60Hz whirl frequency with a rotor rpm of 3600 (Wsh = -30.9 m/s). The Reynolds number is 24000, the Taylor number is 6600 and the eccentricity ratio is 50%. The results for the pressure drop compare well with data obtained by Winslow [1] as seen in Fig 25.a-b. Upstream of the seal inlet, the mean shear (Fig 25. c-d) is low and the pressure is high. However, as the flow enters the seal they increase gradually due to restriction in the flow which occurs as the flow enters from a region of larger clearance to a smaller gap. A large pressure drop, Fig 25. a-b, occurs as the flow moves past the inlet region into the annulus. This has been found to be proportional to the eccentricity. The mean pressure recovers slightly past the inlet region owing to a ‘vena contracta effect’ which causes a small recirculation zone on the rotor surface. The experimental results show a steeper pressure drop as

compared to numerical simulations. As the flow moves downstream, the pressure decreases linearly with axial direction. This can be attributed to frictional losses occuring in the seal.

The mean shear stress, Fig 25. c-d, is strongly effected by axial and azimuthal velocity gradients in the radial direction at the walls. The mean shear stresses are low at the inlet of the seal, however they increase as the fluid flows past the inlet. They remain fairly constant along the interior of the seal until at the exit where it rises rapidly. The Fluent simulations underpredict the mean shear stress measurements and show a more uniform profile, unlike the experimental data which has a fluctuating profile. The initial drop in mean shear stress downstream of the inlet can be attributed to the developing boundary layer which fully spans the clearance past Z/L = 0.2.

Non-Circular Whirl Orbits at 18Hz and 24Hz Whirl

For this flow case the flow rate is 4.87 l/s with 18Hz and 24Hz whirl frequencies (whirl ratios, β, of 0.3 and 0.4) with the rotor spinning at an rpm of 3600 (Wsh = -30.9 m/s). The Reynolds number is 24000, the Taylor number is 6600 and the whirl orbits are non-circular with varying eccentricity ratios as shown in Fig. 30. b. The simulations were performed for whirl ratios of 0.3and 0.4.

Contours of coefficient of pressure distributions (Fig 26) are presented for experimental (Cusano [3]) and simulation results. C_p is derived as a variation of Sommerfeld Journal Bearing equation. The axes presented show % cycle and Z/L which represent percentage cycle and normalized downstream position in the annular seal.

Fig 26.a-b shows the contour plots of coefficient of pressure Cp for whirl frequency of 18Hz (β=0.3). The experimental results indicate that at the inlet the minimum pressure is located at 20% of the cycle and the maximum pressure at 70%. However, as the flow progresses through the seal, the low and high pressure regions exchange positions with the maximum pressure occurring at 20% and the minimum at 70%. This same exchange was documented by Winslow [1] for the same seal with a whirl ratio of 1. The Cp values for the 24Hz whirl frequency are presented in Fig 26.c-d. The exchange is not as obvious with the contours from the exit plane extending and decreasing in amplitude in the upstream direction. The magnitude of Cp is larger for the higher whirl ratio. For both whirl ratios, the Fluent UDF motion based simulations (time dependent simulations of the varying orbit path) over predicted the Cp values compared to experminental results by Cusano [3]. The Fluent Simulations exhibit regions of high and low Cp which present opposite trends at the downstream and upstream postions for the same % cycle, the same trend can be seen from experimental results by Cusano [3]. The switch is more prominent in the 24Hz whirl case (β =0.4). Further investigation into the differences between the experimental data and the CFD simulations is however necessary.

The time dependent, UDF motion based computer simulations are very computer resource intensive. In an effort to determine if a more efficient simulation approach is viable, an assumption of quasi-steady state was made. This assumption is similar using the quasi-Couette flow assumption to represent the flow inside a tilt pad bearing. The current goal was to determine if the flow field present in a circular orbit flow case, which

can be represented as a steady state calculation using the coordinate transform technique, can accurately represent the flow present with a varying orbit seal when the eccentricity ratios of both are the same. This would allow the simulation of a set number of steady state, circular orbit eccentricity ratios which would then be used to represent the flow whenever the non-circular orbit has the same instantaneous eccentric ratio. Fig 27. a-c, presents the static pressure contours for the coordinate transformation case and the UDF mesh motion case. Two UDF mesh motion results are presented. Both have the same eccentric ratio as the coordinate transform case but one was obtained from non-circular orbit with the same eccentricity ratio, as the eccentricity was increasing and the other while the eccentricity was decreasing. The results show that the shape of the pressure contours is the same for all three cases. The two UDF mesh motion simulations are almost identical with respect to contour shape and pressure variation magnitude. This provides credence that the flow can be represented by a quasi-steady state assumption. The use of the coordinate transform steady state solution to provide this quasi-steady state solution is questionable. The contour shapes are very similar but the pressure levels are significantly different; a variation of 50 kPa for the coordinate transform case compared to 125 kPa for the UDF mesh motion. This factor of 2.5 times difference is unacceptable. Additional analysis is required to resolve the issue.

The flow fields predicted for the three cases presented in Fig 27 are presented in Fig 28 and 29. Radial-azimuthal planes are presented at a location Z/L = 0.4 into the seal. Fig 28 illustrates that the magnitudes of the axial velocity are similar for all three cases. The region of maximum axial velocity for the two UDF cases brackets the

location for the coordinate transform case. This indicates that even though the pressure distributions did not show memory of the previous seal eccentricity, the axial velocity does. Fig 29 shows the results for the azimuthal velocity component. All three cases are essentially identical.

Cusano recorded a number of different orbits for the same whirl ratio from the left and right proximeter probe. The recorded orbits at higher whirl ratios are not circular and show large variations. The orbits are not similar and hence an approximation was made by averaging all the left and right proximeter readings and the averaged orbit was simulated using Fluent. The approximation could also be one of the reasons for slight discrepancies in the pressure contours. The legends FCT, FDT, FAT, FAB, FBB represent the different probe positions. The different orbit paths and the simulated orbit is show in Fig. 30. a. The experimental orbit path observed by Cusano [3] and simulated orbit path are shown in Fig. 30. b. The rotor is initially set at an eccentric position of ε = 25Mil with18Hz whirl ratio,and c = 50Mil.

Unsteady UDF mesh motion based simulations can be solved using a steady solver by transforming coordinates to a rotating frame. The simulation results indicate that a good estimate of the flow field can be obtained at a particular eccentric ratio by coordinate transformation technique using set number of circular orbit steady state iterations. The steady state simulations take considerable less computational time. The coordinate transformation has been found to be more effective for nearly circular orbits with larger clearances where rotor stator interactions are weak.

CHAPTER VIII

LABYRINTH SEAL

Numerical Methodology for Labyrinth Seals

Commercial ANSYS 12 version of Fluent was used for this section. The k-ε solver was found to be effective in solving turbulent flows in labyrinth seals. A pressure based solver with finite volume method of discretization was used. The grid was adapted for resolving pressure gradients and for ensuring wall Y+ plus was below 5 throughout the seal. Wall Y+ based adaptation were performed to ensure that the flow was sufficiently resolved in the near wall region. The geometry of the seal was based on the Johnson [4] experimental model and the entire grid was created in Gambit 2.4.6 using quad cells. The mesh distribution was not uniform with a course mesh in the interior of the cavity and in the annular region and a dense mesh near the walls. The mesh for the reduced clearance case had a very fine mesh in the reduced clearance region to accurately resolve the gradients. The geometry consists of an inlet swirl ring, the seal portion and the region with increased clearance. The flow enters the swirl ring through a plenum and the flow is imparted sufficient swirl by the swirl ring. The seal portion is sufficiently long to ensure that the flow is fully developed. The flow leaves through the region of large clearance. The compressibility effects were neglected in the simulations and water was used as the fluid.

A representative mesh is show in Fig. 31. The geometry of the model will consist of the following dimensions- L =33.5 mm, R =82.05 mm and clearance= 1.27 mm (50 mil). Fig. 31 shows the geometry of the labyrinth seal along with dimensions of the test

rig used. The working fluid used is water with density of 998.2 kg/m3 and dynamic viscosity of 0.00103 kg/m-s.

The effects of swirl, clearance and Reynolds numbers for the centered seal have been investigated for the cases presented in Table 2.

Table 2-Labyrinth Seal Simulations

Type of seal	Rpm	Re	Ta	Swirl	clearance
Labyrinth seal	3600	24000	6600	none	1.27 mm
Labyrinth seal	3600	24000	6600	Forward (+45°)	1.27 mm
Labyrinth seal	3600	24000	6600	Backward (-45°)	1.27 mm
Labyrinth seal	5300	15000	10300	none	1.27 mm
Labyrinth seal	3600	24000	6600	none	0.127 mm

The computed flow field 1.27 mm cases will be compared with experimental LDA data from Johnson [4]. In order to study the effect of flow parameters, Reynolds number, and clearance, on the carry over coefficient, a number of simulations were

performed and the carry over coefficient was plotted as a function of the tooth with preceding cavity as shown in Fig. 33

Grid Independence Study

Grid independence study was performed by adapting the grid based on pressure gradient and Wall Y+ until the wall Y+ is below 5 in the seal and the regions with high pressure gradients were sufficiently refined. Grid independence is established by monitoring the force values on the seal until constancy is achieved. The grid was adapted until further refinement of the grid did not change the solution.

Boundary Conditions

The boundary conditions are mass flow inlet and outlet boundary condition at the exit. The rotor was imparted shaft rotation by specifying the rpm of the rotor. The standard k-ε model was selected with law of wall functions with pressure gradient effects. The under relaxation values (URF´s) were default and work well for all the cases. Owing to the complexity of the flow, the grid for Higher Taylor Number (LHT) case and reduced clearance was very fine.

CHAPTER IX

CARRY OVER COEFFICIENT

Labyrinth seal is a leakage control device. It dissipates the kinetic energy of the fluid passing through the annulus by increasing friction. The goal is to get maximum possible energy dissipation as possible. The labyrinth seal reduces fluid leakage by increasing the friction to the fluid flow in the annular path by dissipation of kinetic energy. As fluid moves across each tooth a part of the fluid goes over to the next tooth while another portion re-circulates in the cavity. Carry over coefficient 'γ 'gives an index of the amount of kinetic energy dissipated in the cavity and can be calculated based on the angle Beta (β).

Calculation of β Angle

The carry over coefficient is calculated based on Hodkison's model [28] as shown below:

$$\gamma^2 = 1/\ 1-\chi$$

$$\tan \beta = c\ (1-\ \gamma)/\ \chi s$$

The divergence angle (β) is measured from the streamline positions of fluid which recirculates in cavity to the free flow fluid in the annulus region as shown in Fig. 32. The divergence angle Beta (β) can be found by noting the position on the downstream tooth where the radial velocity is zero. The exact position needs to be recorded for accurate determination of Beta (β). Using Tecplot 360 after suitable magnification and limiting the range of measurement, the probe tool was used to probe and extract regions of least

radial velocity which correspond to stagnation points in the cavity. The region of very low radial velocity was used in the determination of angle Beta (β).

Experimental labyrinth seal data are available for 1, 3, 5 and 7 cavities for the LNS (Labyrinth No Swirl), LFS (Labyrinth Forward Swirl), LBS (Labyrinth Backward Swirl), NS (No Swirl), LHT (Labyrinth High Taylor). The simulation results are compared with these LDA data from Johnson (1989). Post processing was done by cutting iso-planes and monitoring sections of the cavities in Tecplot 360. There is no LDA data available to compare for reduced clearance case (c = 0.127mm). Johnson's [4] data was reduced in order to compare with simulations results and good correlations were found between the two. The small discrepancies were due to the fact that the laser measurements were not very effective near the walls due to the small clearances. Also for the No-swirl case, small amounts of swirl were recorded which are not seen in the simulations results. The suitability of CFD based simulations has been verified for simulating turbulent flows in Labyrinth seals.

The seal with seven teeth was considered for the simulation, the geometry of the seal was considered axisymmetric and two dimensional. The geometry and mesh was created in Gambit 2.4.6 with quadrilateral nodes, the grid independence study was established until the average forces on the seal wall attained a constant value. The mesh was refined based on pressure and velocity gradient. The wall y+ were ensured less than 5 throughout the seal by using Fluent's enhanced wall function with pressure gradient effects. The percentage kinetic energy, carry over coefficient and coefficient of discharge were calculated using Hodkinson's [28] model and plotted as a function of tooth with

preceding cavity for all the cavities. The three quantities showed variations for the first cavity however they remained same for the downstream cavities.

Simulations were performed for higher Taylor number case which showed a more pronounced recirculation zone on the front side of the downstream cavity. The carry over coefficient for all the cases remains more or less constant except of the first cavity. The carry over coefficient for the lower clearance deviates a little from expected behavior. The percentage kinetic energy (χ) for the No Swirl and Forward swirl decreases from first to third and more or less remains constant whereas for backward swirl it increases from first to third and then remains constant. The percentage kinetic energy (χ) for the lower clearance case is low throughout. The percentage kinetic energy and carry over coefficient are plotted against tooth with preceding cavity in Fig. 33-34. The discharge coefficient for all the cases is the same at the start and increases from first to third and decreases slightly to only remain constant along the downstream direction as see in Fig. 35.

Effect of Clearance and Shaft Speed on Carry Over Coefficient

For a given Reynolds number the higher the clearance, the higher is the carry over coefficient. This effect can be best described by Hodkinson's [28] theory. For the same Reynolds number there is more fluid flow in the annulus between the tooth and the stator when more clearance is available for the fluid and this explains a higher χ with increase in c. As the clearance increases a larger portion fluid owing to inertia flows through the annulus and less amount of impingement occurs in the cavities, resulting in

lesser kinetic energy dissipation by means of turbulent viscosity interactions with cavity and hence an increase in carry over coefficient is observed.

The effect of shaft speed is found to be negligible on the carry over coefficient, % kinetic energy and discharge coefficient. The same was reiterated by Saikishan's [31] using improved leakage prediction methods. Saikishan [31] obtained the same result for teeth on stator. The location of the tooth on the rotor or stator does not affect the flow field in the seal. However the simulations show slight variations between NS, FS, BS and LHT cases. The plots for Carry over coefficient (γ), % Kinetic energy (χ) and Coefficient of discharge (Cd) are presented after the flow field results in Fig. 33-35.

The carry over coefficient increases by a small amount with decrease in Reynolds number for a giver clearance in the LHT case. The higher Taylor number has a higher shaft speed and lower Reynolds number as seen from the Table. 2. This is contrary to the carry over coefficient behavior predicted by Saikishan [31]. Higher carry over coefficient, indicates more amount of energy is being convected out of the seal cavity without being dissipated in the cavity. This implies that the seal is less effective at high Taylor numbers.

CHAPTER X

DISCHARGE COEFFICIENT

The discharge coefficient has been calculated based on following relation.

$$\mathrm{Cd} = m/\sqrt{(A2\rho(P1 - p2)\ )}$$

The discharge gives an index of the total losses that occur as the fluid flows through the cavity and above the tooth. Cd is a representation of the frictional losses that occur in the tooth and dissipation in the cavity.

The discharge coefficient has been calculated based on the Reynolds number and has been found to be significantly dependant on Reynolds number but variations for the same Reynolds number are minimal. The discharge coefficient is however largely affected by clearance. The discharge coefficient decreases significantly with decrease in clearance. The discharge coefficient of the first tooth varies in comparison with other tooth. The value of discharge coefficient of the first tooth is significantly lower than the other teeth. The discharge coefficient of the subsequent teeth was slightly different than the first tooth and this could be attributed to the fact that the velocity profile upstream of the first tooth differs considerable from the subsequent tooth. The velocity profile of the first tooth differs considerable from the subsequent teeth owing to the vena-contracta effect which is caused by fluid accelerating from a large plenum over the first tooth into a the labyrinth seal with smaller clearance.

Effect of Shaft Speed and Reynolds Number on Discharge Coefficient

The discharge coefficient gives a quotient of the loss that occurs when fluid flows through the cavity and in the annulus for flow in labyrinth seals. Based on the leakage mass flow rate and inlet and exit pressures across tooth, the discharge coefficient can be calculated.

The discharge coefficient from the plots is found to vary only with Reynolds number based on clearance, which was further reiterated by Saikishan [31]. As we move downstream the discharge coefficient attains a constant value after some variations at the inlet of the seal.

The discharge coefficient is found to be higher for larger clearances. The variations in discharge coefficient for variations in shaft speed have been found to be negligible. A detailed investigation on variation of discharge coefficient with shaft speed needs to be performed; however it is beyond scope of this thesis.

CHAPTER XI

RESULTS FOR LABYRINTH SEALS

Labyrinth No Swirl (LNS)

The velocity profiles for the labyrinth seal are presented in Fig. 36-53. The left columns are the Fluent 12 simulations and right columns in are the experimental LDA data from Johnson [4]. Flow field comparisons have been made for first, third, fifth and seventh cavities.

There is a small acceleration at the inlet of the seal attributed to the vena contracta effect owing to the fluid being compressed from a large to a small clearance. The vena-contracta effect is however more pronounced in the experimental LDA data compared to numerical simulations.

There is a flow separation over the first tooth however flow separation is suppressed over the inlet of the third tooth as seen in Fig. 36 Inside the seal cavity the recirculation zone had negative radial velocity on the front side of the downstream tooth and positive radial velocity on the back side of the upstream tooth. The recirculation zone strength was found to be higher in the first cavity compared to the subsequent cavities. The first cavity shows a larger region of high radial velocity compared to the third, fifth and seventh cavities owing to the vena contracta effect as seen in Fig 36-39. The radial velocities for the subsequent tooth are lesser than the first tooth but exhibit more or less constant profiles. There is a slight increase in the tangential velocity component as we go downstream from the first to seventh. There is an increase in swirl in each cavity as you go downstream. It is interesting to note that the azimuthal

component goes on increasing from cavity to cavity in the downstream direction and hence never becomes fully developed. The effect of swirl and pre-swirl has been examined by Johnson [4] using pre-swirl blades. The peak axial velocity for the first cavity in experimental result is near the inlet of the cavity but shifts towards the center for the third cavity. The simulation results show more or less similar profiles of axial velocity but with no migration of peak axial velocity. Due to the presence of the upstream swirl the effect of vena contracta has weakened.

Labyrinth Seal Forward Swirl (LFS) and Labyrinth Seal Backward Swirl (LBS)

The axial, radial and azimuthal velocity contours for the forward swirl (LFS) and backward swirl (LBS) are show in Fig. 40-47. The contours remain more or less the same as we move downstream but the azimuthal velocity shows a slight increase. The first cavity, Fig. 40 shows a large radial velocity for the backward swirl case showing the effect of vena contracta however the simulation results show a comparatively lower radial velocity. The region of radial velocity decreases slightly as we move downstream from the first to the seventh cavity showing the weakening in the vena contracta effect. There is a small migration in the region of peak axial velocity from close to the inlet for the first cavity to mid cavity for the third cavity as seen in Fig. 41. The azimuthal velocity remains very low in the annular region however the cavity region shows a slight amount of increase and recirculation as we move downstream. The azimuthal velocity region goes on increasing confirming that the flow is not yet fully developed. For forward swirl case, azimuthal velocity has adjusted and does not change much after third cavity unlike the backward swirl case which keeps on adjusting until the seventh cavity

as seen from Fig. 44-47. It is surprising to note that the radial velocity decreases by a small amount as we go downstream for the backward swirl and no swirl cases however the radial velocity increases slightly from the first to third cavity and remains more or less constant after that for the forward swirl case indicating a slight increase in the recirculation zone.

Higher Taylor Number (LHT) and Reduced Clearance

The high Taylor number case also shows the presence of a secondary recirculation zone in the front side of the downstream cavity. Simulations for the reduced clearance case showed lower coefficient of discharge values as expected. The flow field for Higher Taylor Number (LHT) and reduced clearance are show in Fig. 48-54. The recirculation zone strength decreases slightly from the first to the third cavity and after that the recirculation zones show a small rise. The azimuthal velocity for the high Taylor number case shows a marginal increase as we go downstream and this can be attributed to the increase in centrifugal acceleration as flow goes downstream. For the lower clearance, Fig. 52 the axial velocity is high in the annulus region while remaining low in the cavity. There is a small region of stagnation velocity at the sharp corner of the inner face of each tooth. The azimuthal velocity goes on increasing as we move along the downstream direction. The experimental simulations show a stronger recirculation zone compared to simulations results for the Higher Taylor Number (LHT) case. The turbulent flow in the LHT and lower clearance cases has not fully developed which can be registered from the fact that the radial and tangential profiles for the two cases are still not fully developed. The fluid in the lower clearance overshoots the first cavity and

hence axial velocity is considerably low in the first cavity. The flow field in the reduced clearance case becomes fully developed by the fifth cavity and variations in flow field between fifth and seventh cavity are negligible.

Comparison between LDA and Fluent Simulations

The numerical Fluent-based simulations compare well against the experimental LDA data. The Fluent-based simulations accurately mimic the experimental LDA data by exhibiting similar profiles and predicting regions of peak axial velocity, recirculation zones and regions of strong swirl accurately. This provides credence to the fact that Fluent-based simulations with standard k-ε turbulence models can be used for predicting turbulent characteristics in labyrinth seals in for a wide range of operating conditions. The numerical simulation results present a more uniform profile with fewer spikes. The wiggles in experimental data are due to software used for contouring and due to fluctuation in data and do not represent any physical phenomena. Also detailed measurements of flow reversal region or near the wall could not be possible due to limitation of laser anemometry. The numerical simulations predict the existence of a secondary recirculation zone seen in the experimental LDA data for the LHT case, thereby further validating the usefulness of CFD based simulations in accurately predicting flow field in labyrinth seals. Based on the computed 2D flow field, carry over coefficient and coefficient of discharge for the labyrinth seal are calculated. Both carry over coefficient and coefficient of discharge show a strong dependence on the clearance and negligible dependence on shaft speed. The Discharge Coefficient for the first tooth shows a value greater that one due to the vena-contracta effect. The Discharge

Coefficient for the first tooth differs considerable from other tooth. The velocity fields together with the carry over coefficient and discharge coefficient give a good estimate of the effectiveness of the seal. The Fluent 12 based simulations do a fairly good job in predicting the flow field and the associated flow physics in a 2D labyrinth seal.

Future Work

The current simulations deals with turbulent flow simulations in a labyrinth seal in which the rotor is centered about the stator. Future work could investigate the turbulent flow field in an eccentric seal in which the rotor is eccentric about the stator center. Also the present simulations are 2D centered Labyrinth seal simulations. The 3D models of the seal could be constructed and simulated for circular whirl orbits by transformations to a rotating frame using Fluent's Moving Reference Frame (MRF) approach. The MRF simulations being steady state simulations would consume less time compared to transient simulations.

CHAPTER XII

CONCLUSIONS

3D CFD simulations of a whirling smooth annular seal are performed. Flow field comparisons are made between Fluent‘s Dynamic Mesh model which used a time dependant solver and Fluent’s Moving Reference Frame (MRF) model which renders the flow quasi-steady. The flow field in the transformed frame shows a good agreement with experimental results for statically eccentric case and circular orbit. The axial pressure distributions and the mean shear stresses matched experimental data for Fluent’s simulations in static frame as well as the transformed frame. However the contours of Cp show slight variations between the coordinate transformed frame case and the UDF mesh motion case.

The phase averaged wall pressure distributions aid in understanding the complex fluid processes occurring within the seal. The simulations were performed under zero pre-swirl conditions.

The general trends for 18Hz and 24Hz non-circular whirl orbits look similar however the Fluent simulations over predict the magnitude of the wall pressure distributions. Also the trends appear a little offset; this could be attributed to different whirl orbits recorded by Cusano [3] for the same whirl frequency. The Fluent simulations simulate an averaged orbit of all the experimental orbits recorded by the probes at each downstream position.

A good estimate of the flow field and pressure distribution in an annular seal for different eccentricities can be made by statically setting the rotor at that eccentricity and

using Fluent's Moving Reference Frame model to compute the flow field in the transformed frame using a steady solver.

The complex flow field in a whirling annular seal can be simulated by transforming to a rotating frame to render the flow quasi-steady. In this frame the computed flow fields show a good agreement with experimental data and present a consistent picture of the flow field and associated physics. More flow cases however need to be simulated for further code validation and also to explore other turbulence models.

2D centered labyrinth seal simulations were performed for comparison with experimental LDA data. The existence of secondary recirculation zones has been predicted well by Fluent 12 code which is further verified from experimental LDA results. However for Labyrinth Backward Swirl (LBS) case the radial velocity contours are under predicted in simulations. The plots for carry over coefficient, % kinetic energy and coefficient of discharge are plotted against tooth with preceding cavity which represent the effect of clearance and Reynolds number on the flow field and give a good indication of the effectiveness of the seal. The three quantities show minor variations except at the inlet, for variation in Reynolds number but seem to vary a lot with variation in clearance indicating a strong dependence on the clearance to pitch ratio of the seal.

The velocity field for computer based simulations and experimental LDA measurements appear similar, indicating that a good estimate of the flow field in a turbulent labyrinth seal can be obtained by numerical simulation. Also the effect of pre-

swirl, clearance and Reynolds number can be estimated to a fair degree of extent. The predicted leakage values were further verified using Saikishan's [32] leakage models.

The Fluent-based simulations in the transformed frame might show discrepancies if the clearance is very small as for small clearances the flow becomes viscous dominated and rotor stator interactions are not weak which is an essential pre-requisite for Moving Reference Frames based Fluent simulations. The similarity in the flow field between UDF mesh motion and Moving Reference suggests that whirling rotors can be simulated by transforming coordinates.

Future work needs to be done in order to refine CFD techniques for more accurate predictions. The grid refinement, wall functions and turbulence models used need further investigation.

CHAPTER XIII

RECOMMENDED FUTURE WORK

1. Apply coordinate transformation for lower clearances and check the applicability of Moving Reference Frames for lower clearances where the rotor stator interactions are not weak
2. Introduce swirl and try to check the validity of input swirl on the flow field in 3D eccentric annular seals and compare results with experimental LDA data
3. More research needs to be done on Moving Reference Frames and the applicability of k-ε model needs to be further validated. The `presto´ scheme needs to be verified by performing simulations for a wide range of operating conditions
4. Apply the MRF technique used in annular seals to simulate the flow field in labyrinth seals.
5. Perform labyrinth seals simulations for eccentric seals as present simulations were for centered seals.
6. Try to validate the prediction correlations by verifying results with other prediction methods.
7. Develop a 3D labyrinth seal model and compare flow fields in terms of velocity and pressure with experimental LDA data.
8. Try to understand the effect of tooth and cavity on the flow field in labyrinth seals

9. The effect of clearance has been investigated but effect of variation in tooth width on the flow field needs to be considered as well.
10. Check the applicability of MRF for lower clearance cases in labyrinth seals.

REFERENCES

[1] Winslow, R.W., 1994, "Dynamic Pressure and Shear Stress Measurements on the Stator Wall of Whirling Annular Seals," M.S Thesis, Texas A&M University, College Station.

[2] Thames, H.D., 1992, "Mean Flow and Turbulence Characteritics in Whirling Annular Seal," M.S. Thesis, Texas A&M University, College Station.

[3] Cusano, D., 2006 "Experimental Phase-Averaged Wall Pressure Distributions for a 25% Eccentric Whirling Annular Seal" M.S. Thesis, Texas A&M University, College Station.

[4] Johnson, M.C., 1989, "Development of a 3-D Laser Doppler Anemometry System: With Measurements in Annular and Labyrinth Seals," Ph.D. Dissertation, Texas A&M University, College Station.

[5] Robic, B.F., 1999, "Experimental and Numerical Analysis of the Effect of Swirl on the Pressure Field in Whirling Annular and Labyrinth Seals," Ph.D. Dissertation, Texas A&M University, College Station.

[6] Morrison, G.L., Johnson, M.C., Tatterson, G.B., 1991 "Three-Dimensional Laser Anemometry Measurements in an Annular Seal," Journal of Tribology, **113,** pp**.** 421-427.

[7] Hirs, G. G., 1973, "A Bulk Flow Theory for Turbulence in Lubricant Films," Journal of Lubrication Technology, April, **95**(2), pp. 137-146.

[8] Brennen, C., 1976, "On the Flow in an Annulus Surrounding a Whirling Cylinder," Journal of Fluid Mechanics, **75**(1), pp. 173-191.

[9] Lessen, M., 1987, "Turbulent Flow in Shaft Seals and Bearings," STLE Tribology Transactions, **31**, pp. 391-396.

[10] Das, P.G., 1993, "3-D Laser Doppler Velocimetry Measurements of Eccentric Annular and Labyrinth Seals," M.S. Thesis, Texas A&M University, College Station.

[11] Suryanarayanan, A., 2003, "Experimental Measurement and Analysis of Wall Pressure Distribution for a 50% Eccentric Whirling Annular Seal," M.S. Thesis, Texas A&M University, College Station.

[12] Childs, D. W., 1982, "Finite-Length Simulations for Rotordynamic Coefficients of Turbulent Annular Seals," ASME Journal of Lubrication Theory, **105**, pp. 429-436.

[13] Athavale, M.M, Hendricks, R.C, Steinetz, B.M, 1995, "Numerical Simulation of Flow in a Whirling Annular Seal and Comparison with Experiments", 31st Joint Propulsion Conference and Exhibit, San Diego, California.

[14] Arghir, M and Frene, J. July 1997b, "Analysis of a Test Case for Annular Seal Flows," Transactions of the ASME, **119**, pp. 408-414

[15] Sekaran, Aarthi., 2009, "Study of Impact of Orbit Path, Whirl Ratio and Clearance on the Flow Field and Rotordynamic Coefficients for Smooth Annular Seals", M.S. Thesis, Texas A&M University, College Station.

[16] Deich, M.E., Shkvar, A. Ya., and Solomko, V.I., "Investigations of Straight-Flow Labyrinth Seals, "Izvestiya Akademii Nauk SSSR. Energetika I Transport, **16**(4), pp. 146-152, 1978.

[17] Hauck, L., 1982, "Measurement and Evaluation of Swirl-Type Flow in Labyrinth Seals of Conventional Turbine Stages," Presented at the Rotordynamic Instability

Problems in High-Performance Turbomachinery, NASA Conference Publication 2250, West Germany.

[18] Iwatsubo, T., 1980, "Evaluation of Instability Forces of Labyrinth Seals in Turbines and Compressors," NASA CP 2133, Proceedings from a Workshop on Rotordynamic Instability Problems in High Performance Turbomachinery, May 12-14, Texas A&M University, College Station, TX, pp. 205-222.

[19] Esser, D. and Kazakia, J.Y., 1995, "Air Flow in Cavities of Labyrinth Seals," International Journal of Engineering Science, **33**(15), pp. 2309-2326.

[20] Martin, H. M., 1908, "Labyrinth Packings," Engineering, pp.35-36

[21] Gamal, A.M., 2007, "Leakage and Rotodynamic Effects of Pocket Damper Seals and See-Through Labyrinth Seals," Ph.D. dissertation. Texas A&M University, College Station.

[22] Stoff, H., 1980, "Incompressible Flow in Labyrinth," Journal of Fluid Mechanics, **100**, pp. 817-829.

[23] Rhode, D.L. and Hibbs,R.I., 1993, " Clearance Effects on Corresponding Annular and Labyrinth Seal Flow Leakage Characteristics," Journal of Tribology, **115**, pp. 699 – 704.

[24] Demko, J.A., Morrison, G.L., Rhode, D.L., 1987, "Effect of Shaft Rotation on Incompressible Flow in Labyrinth Seal," *Proceedings of the 5th International Conference on Numerical Methods in Laminar and Turbulent Flow*, pp. 171-176, Montreal, Canada.

[25] Cogan, K.C., 1982, "Leakage Prediction of Incompressible Fluids in Labyrinth Seals", M.S. thesis, Texas A&M University, College Station.

[26] Morrison, G.L. and Al-Ghasem, A., 2007, "Experimental and Computational Analysis of a Gas Compressor Windback Seal," GT2007-27986 , *Proceedings of ASME Turbo Expo 200*, Montreal, Canada, May 14-17.

[27] Collins, D., Amaral Teixeira, J.A. and Crudgington, P., "Insight into the Performance Degradation of Abradable Honeycomb Labyrinth Seals Due to Wear", Institution of Mechanical Engineers-10th European Fluid Machinery Congress: Advances in Optimization , Design and Maintenance of Process Machinery, IMechE, pp. 91-102, 2008

[28] Hodkinson, B., 1939, "Estimation of the Leakage through a Labyrinth Gland," *Proceedings of the Institution of Mechanical Engineers*, **141**, pp. 283–288.

[29] Park, S.H., 2006, "How to prepare the 3-D Mesh with whirling rotor using deforming mesh", Tutorial, Texas A&M University, College Station.

[30] Shresta, S., 1993, "The Effects of Pre-swirl on Flow Through Centered and Eccentric Annular Seals," M.S. Thesis, Texas A&M University, College Station.

[31] Suryanarayanan, Saikishan, 2009, "Labyrinth Seal Leakage Equation", M.S. Thesis, Texas A&M University, College Station.

[32] Stodola, A.,1927, Steam and Gas Turbines, 6th ed., The McGraw-Hill Book Company, New York.

APPENDIX A

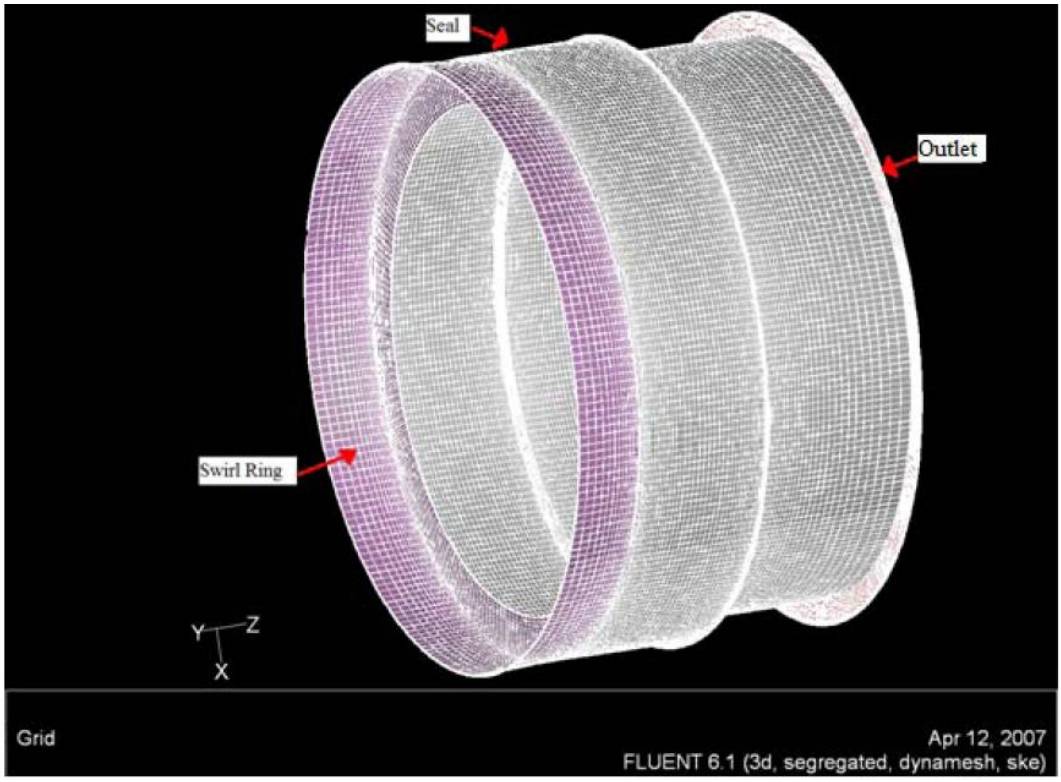

Fig. 1 Meshed Seal Geometry (from ref. 14)

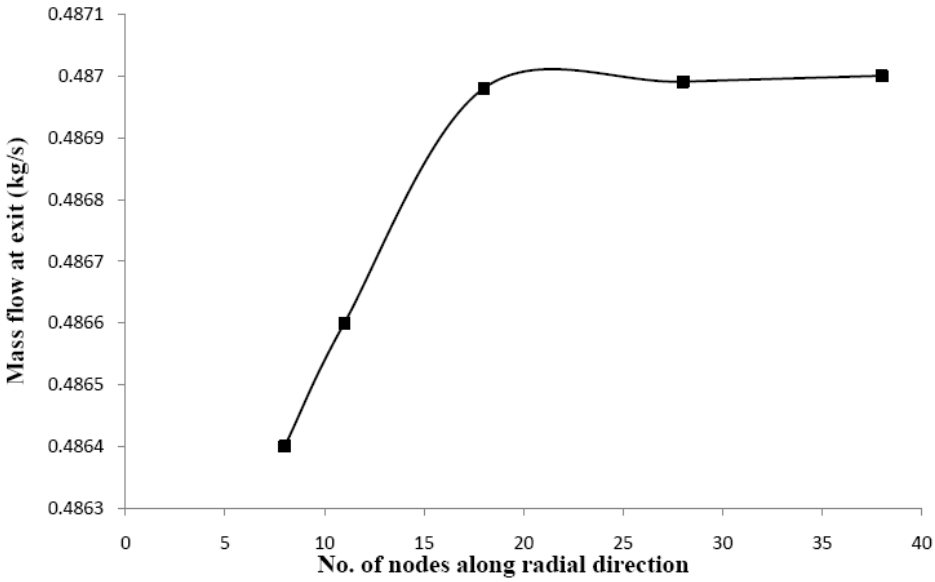

Fig. 2 Grid independence study (from ref. 14)

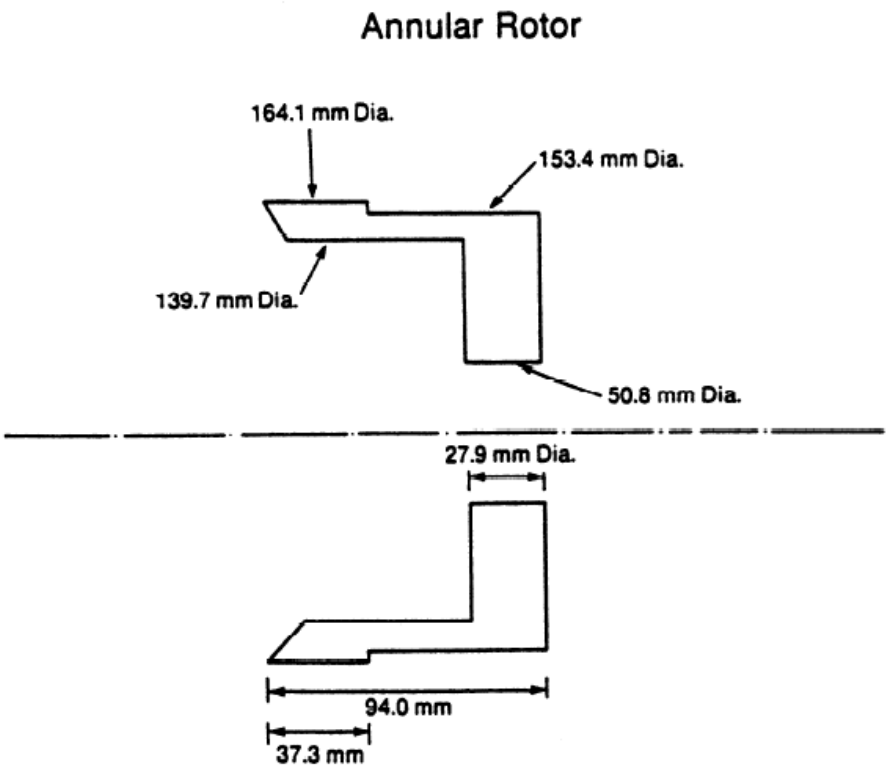

Fig. 3 test setup with dimensions (from ref. 6)

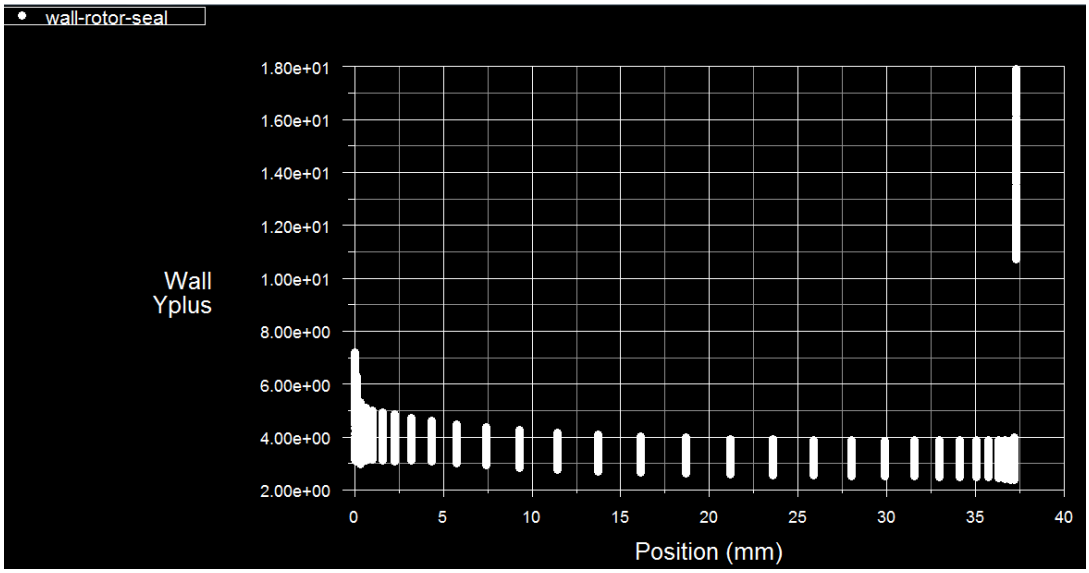

Fig. 4 XY plot of Wall Yplus Vs Position of seal

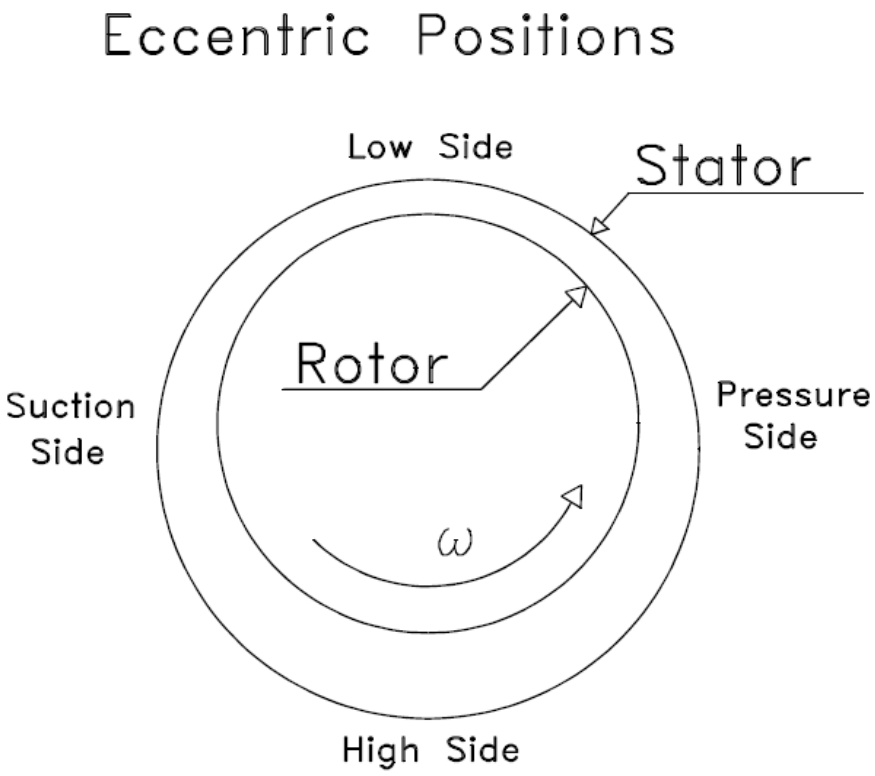

Fig. 5 Seal positions (from ref. 7)

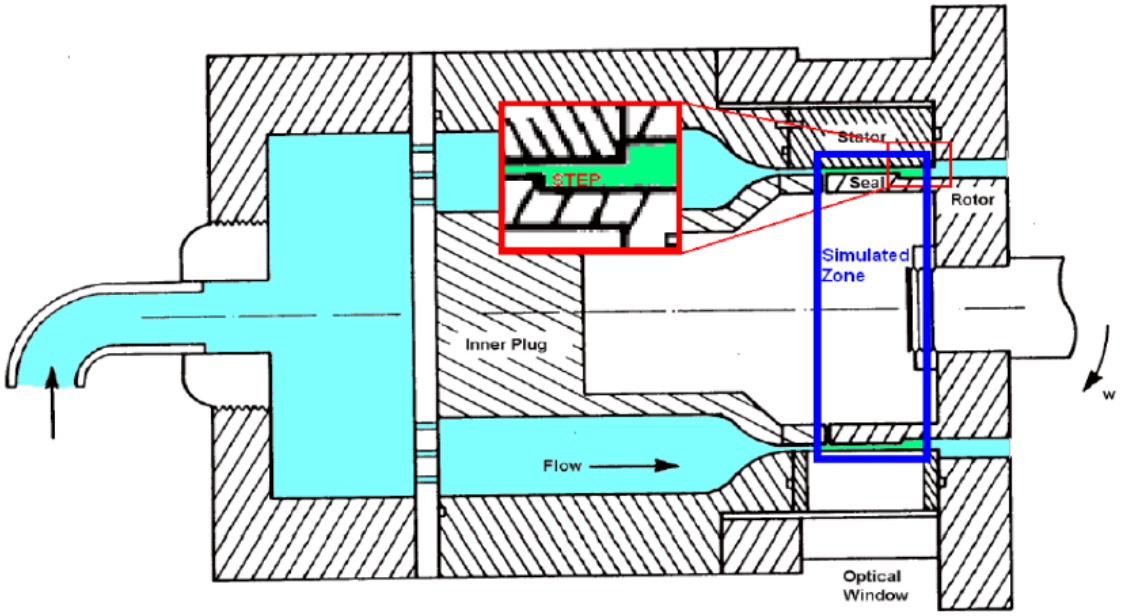

Fig. 6 Path of fluid in seal (from ref. 3)

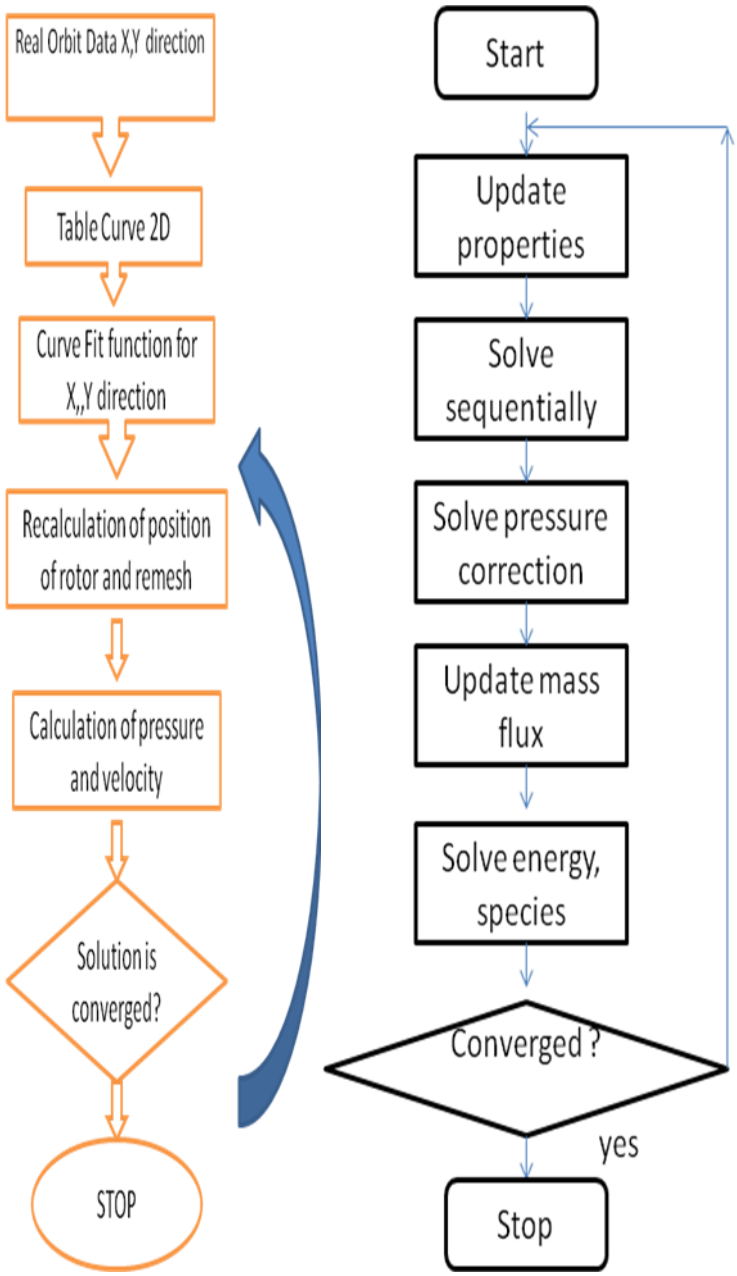

(a) (b)

Fig. 7 Flowchart of dynamic mesh scheme

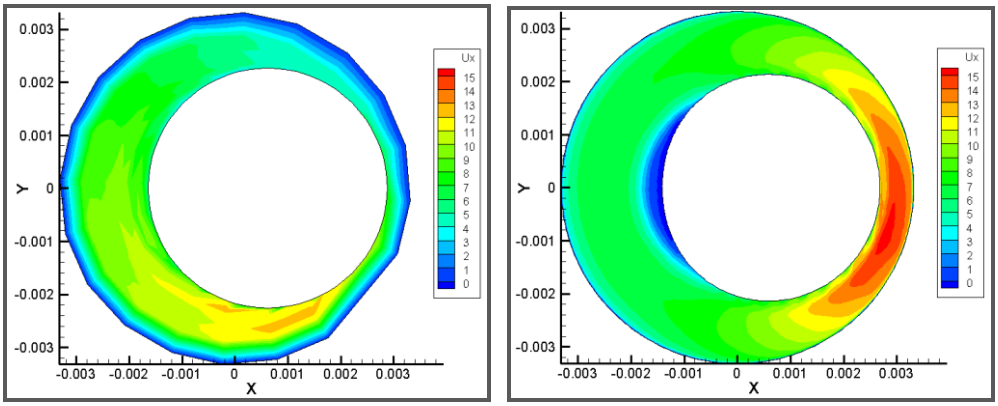

(a) LDA (experimental) (b) UDF Mesh motion

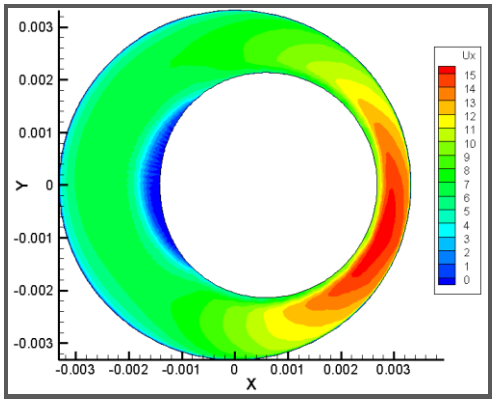

(c) Coordinate Transform (MRF)

Fig. 8 contours of Ux at Z/L = 0. Seal whirl and spin in counterclockwise direction, clearances have been exaggerated for clarity

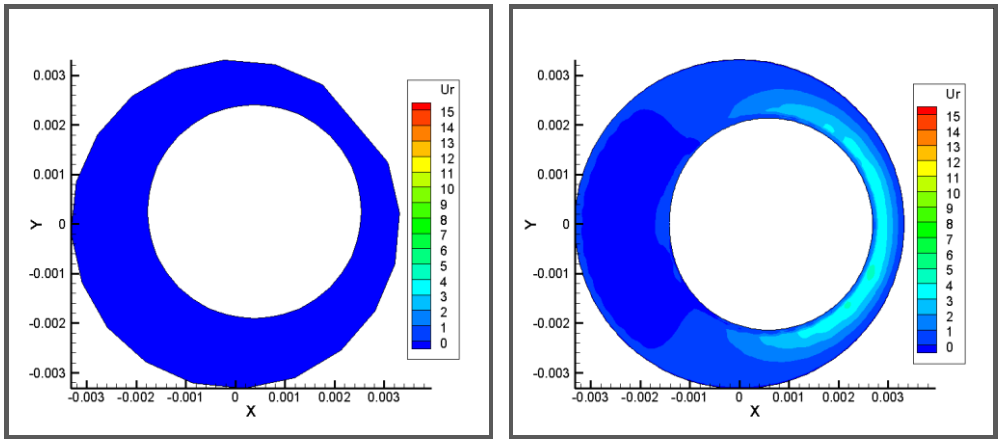

(a) LDA (experimental) (b) UDF Mesh motion

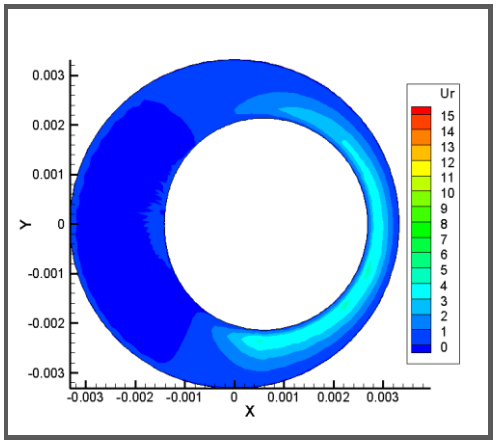

(c) Coordinate Transform (MRF)

Fig. 9 contours of Ur at Z/L = 0. Seal whirl and spin in counterclockwise direction, clearances have been exaggerated for clarity

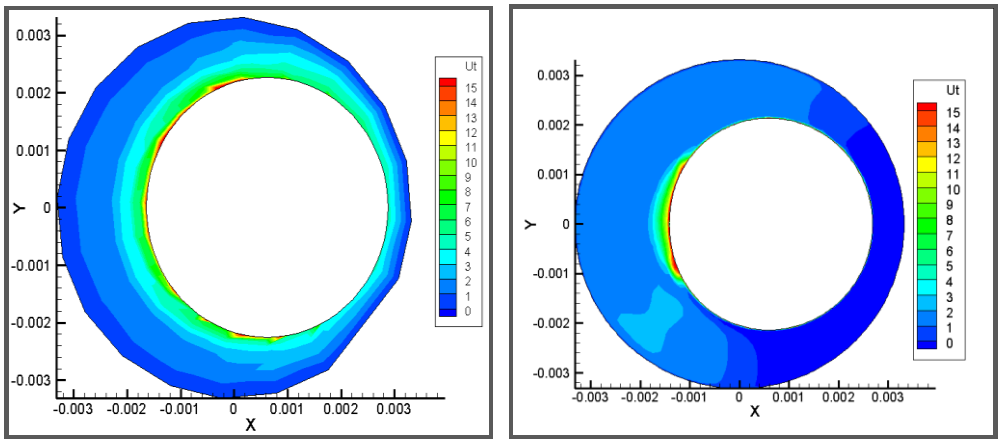

(a) LDA (experimental) (b) UDF Mesh motion

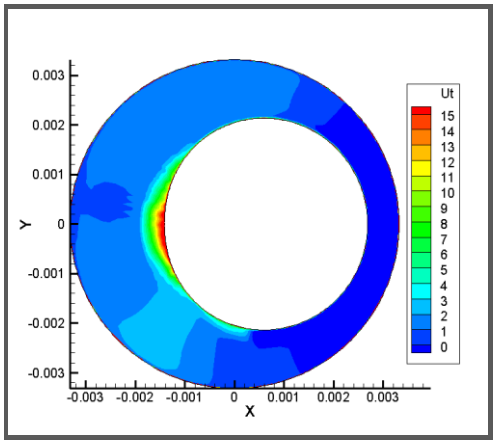

(c) Coordinate Transform (MRF)

Fig. 10 contours of Ut at Z/L = 0. Seal whirl and spin in counterclockwise direction, clearances have been exaggerated for clarity

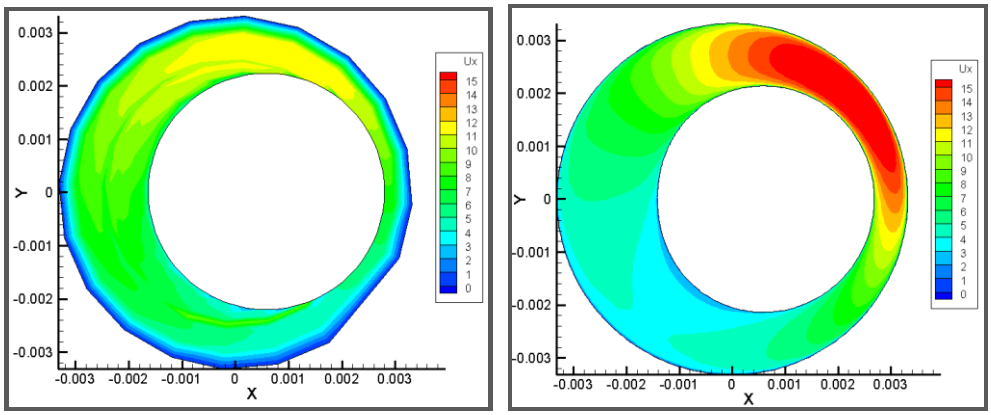

(a) LDA (experimental) (b) UDF Mesh motion

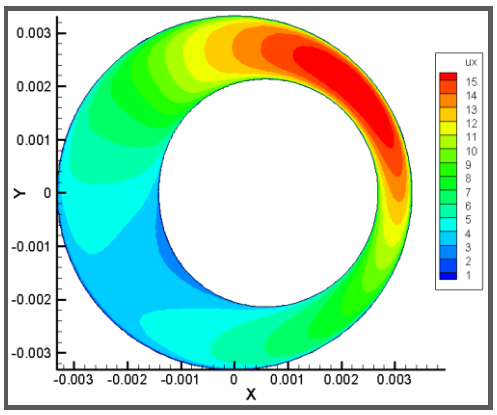

(c) Coordinate Transform (MRF)

Fig. 11 contours of Ux at Z/L = 0.850. Seal whirl and spin in counterclockwise direction, clearances have been exaggerated for clarity

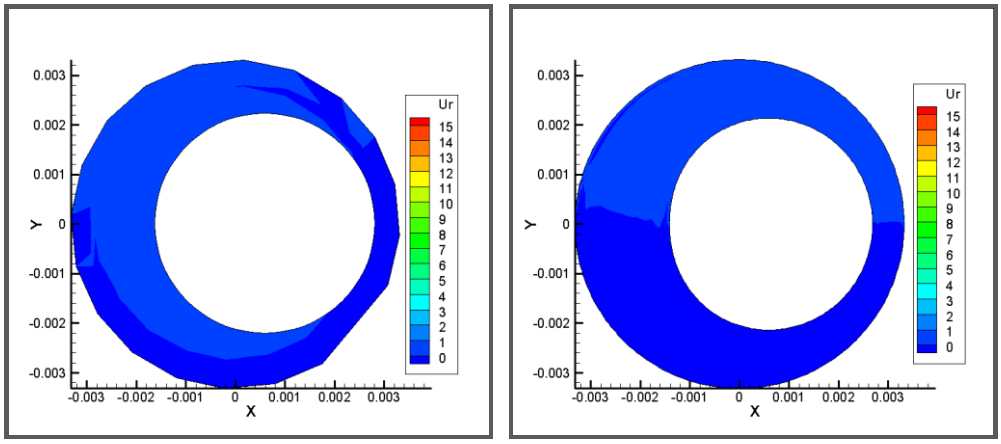

(a) LDA (experimental) (b) UDF Mesh motion

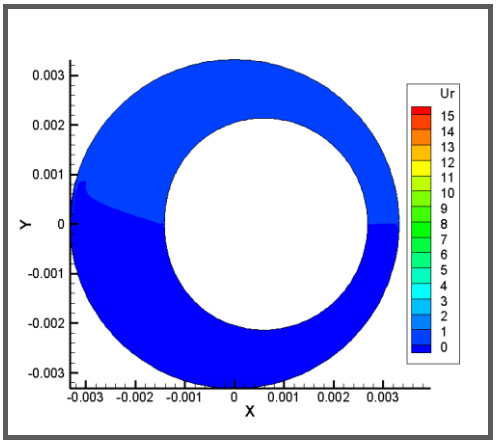

(c) Coordinate Transform (MRF)

Fig. 12 contours of Ur at Z/L = 0.850. Seal whirl and spin in counterclockwise direction, clearances have been exaggerated for clarity

.

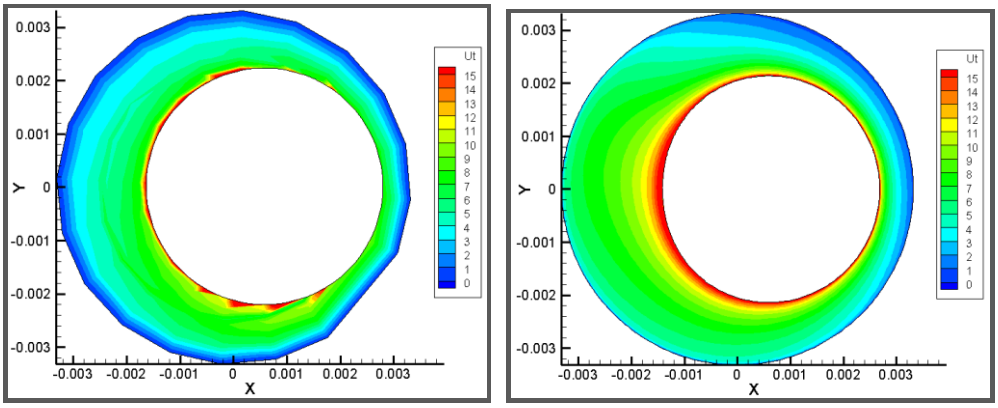

(a) LDA (experimental) (b) UDF Mesh motion

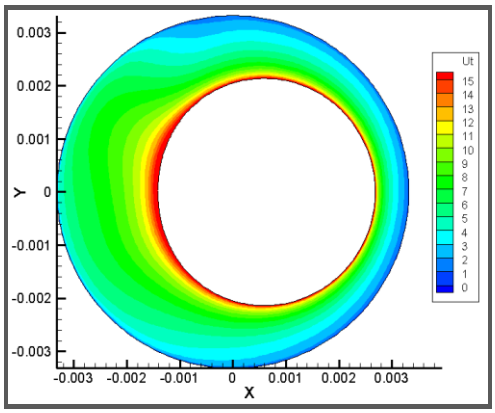

(c) Coordinate Transform (MRF)

Fig. 13 contours of Ut at Z/L = 0.850. Seal whirl and spin in counterclockwise direction, clearances have been exagerrated for clarity

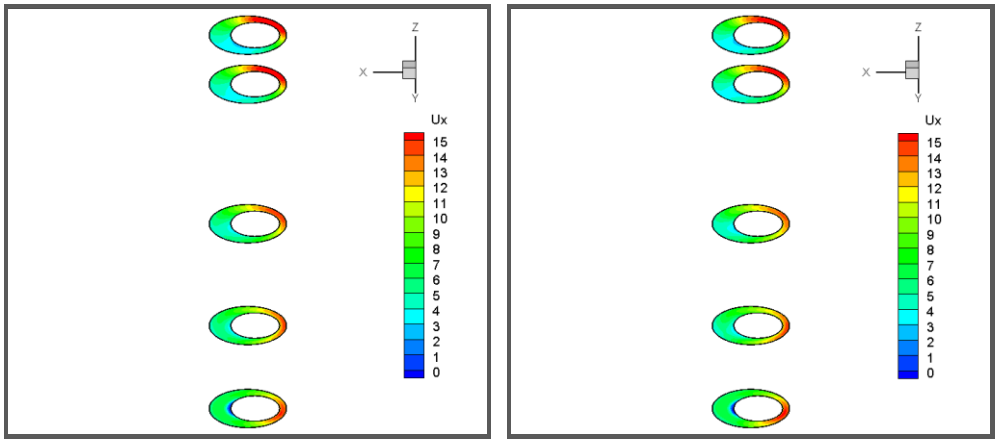

(a) UDF (b) MRF

Fig. 14 contours of Ux at Z/L = 0, 0.22, 0.49, 0.86, 0.99. Seal whirl and spin in counterclockwise direction, clearances have been exagerrated for clarity

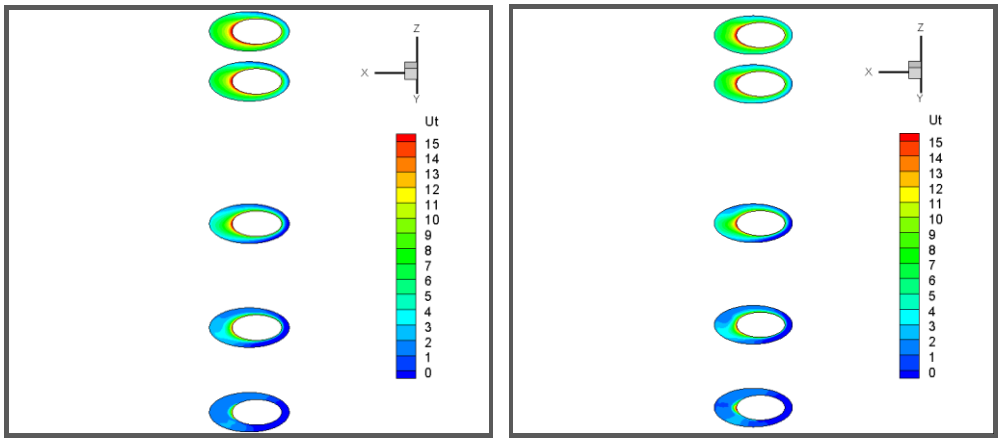

(a) UDF (b) MRF

Fig. 15 contours of Ut at Z/L = 0, 0.22, 0.49, 0.86, 0.99. Seal whirl and spin in counterclockwise direction, clearances have been exagerrated for clarity

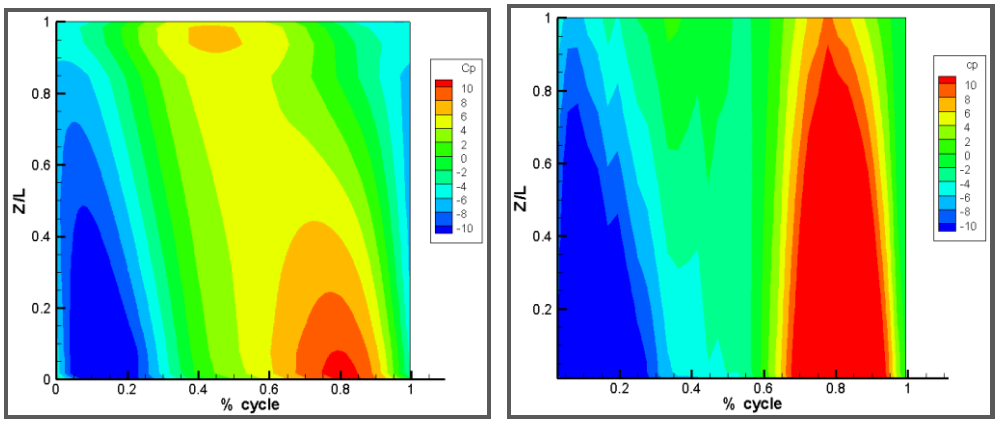

(a) Coordinate transform (ε =50%, β=1) (b) UDF mesh motion (ε =50%, β=1)

Fig. 16 Contours of Coefficent pressure for coordinate transform case and UDF mesh motion case

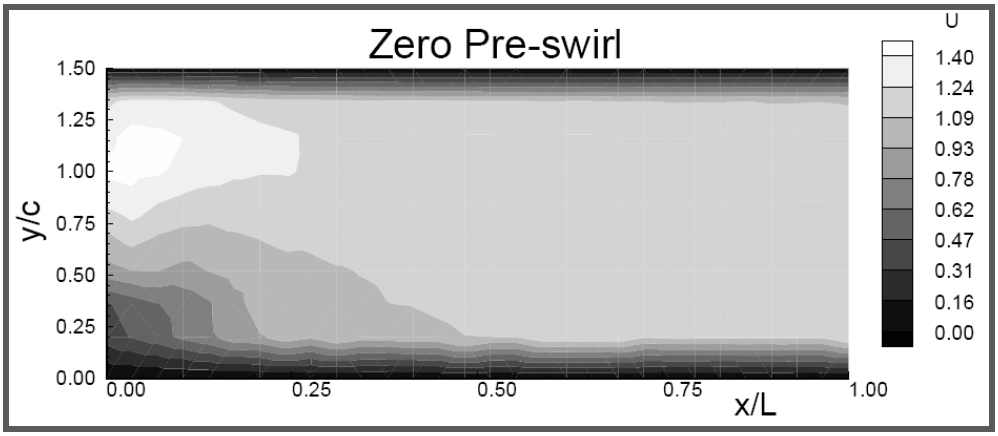

(a) LDV(experimental, from ref. 30)

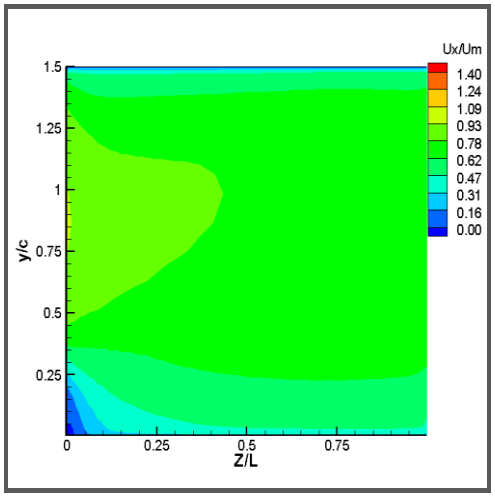

(b)UDF mesh motion

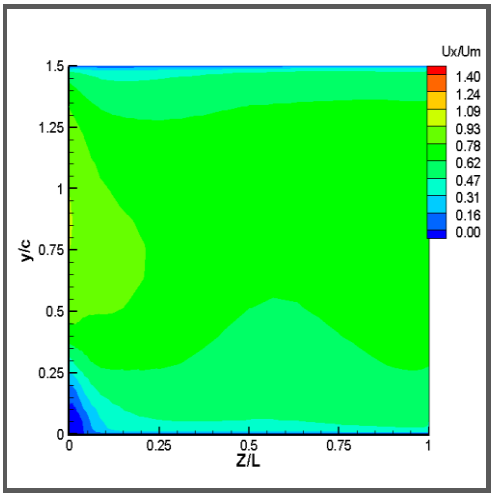

(c)Coordinate Transform

Fig. 17 Contours of axial velocity for Maximum clearance position

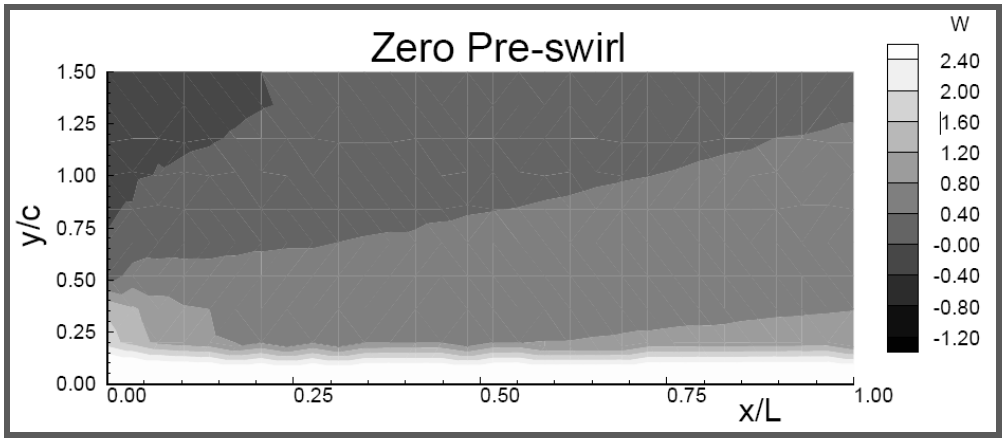

(a) LDV(experimental, from ref. 30)

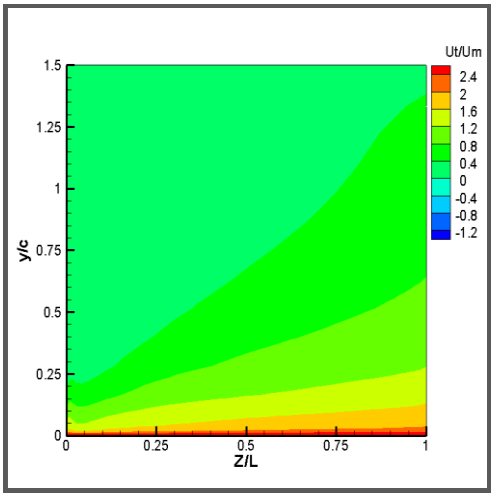

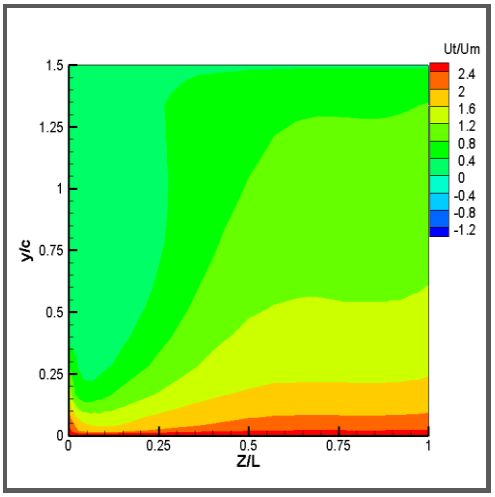

(b)UDF mesh motion (c)Coordinate Transform

Fig. 18 Contours of tangential velocity for Maximum clearance position

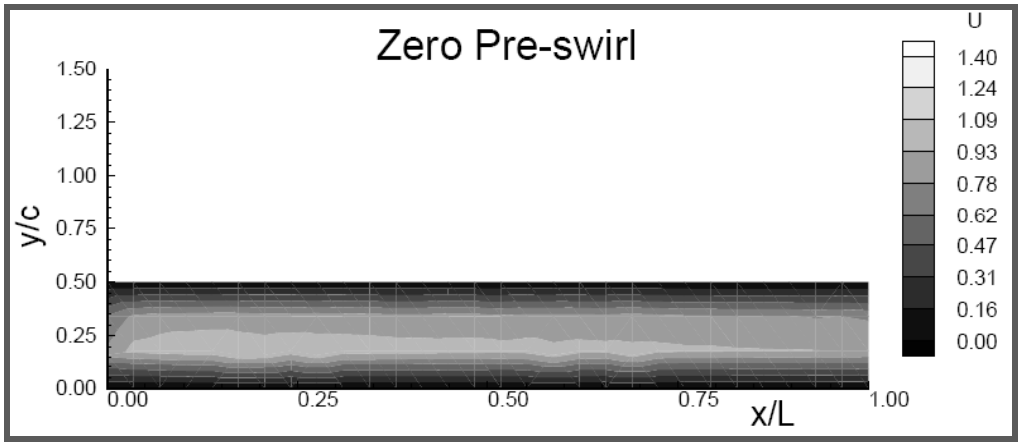

(a) LDV(experimental, from ref. 30)

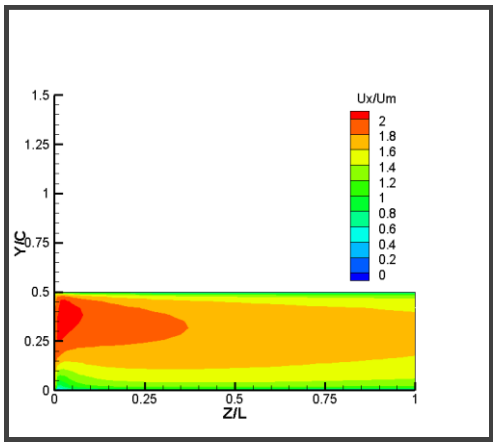

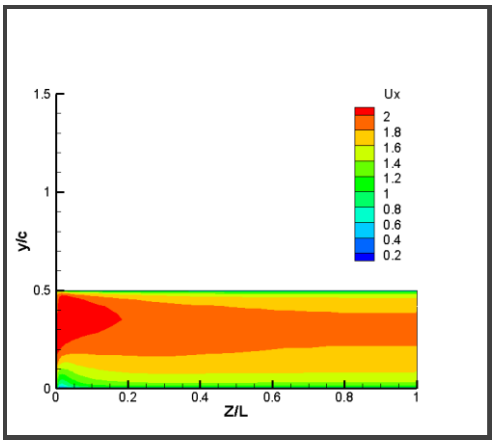

(b)UDF mesh motion (c) Coordinate Transform

Fig. 19 Contours of axial velocity for Minimum clearance position

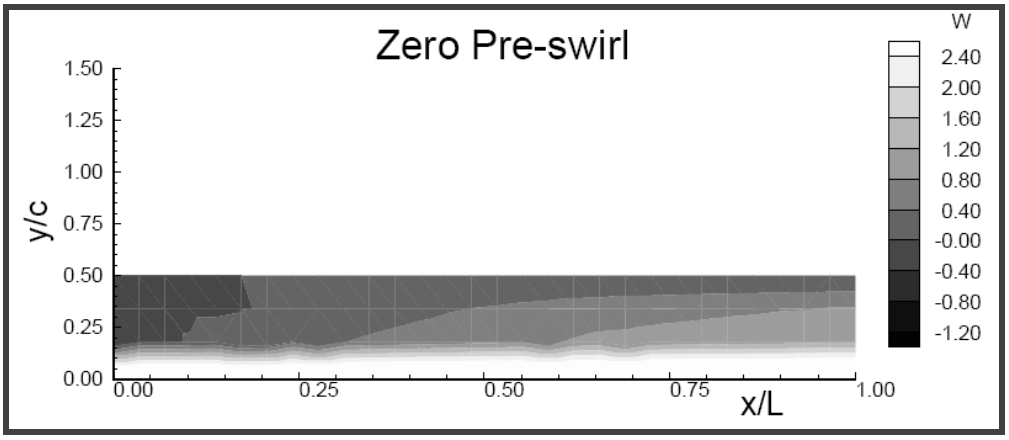

(a) LDV(experimental, from ref. 30)

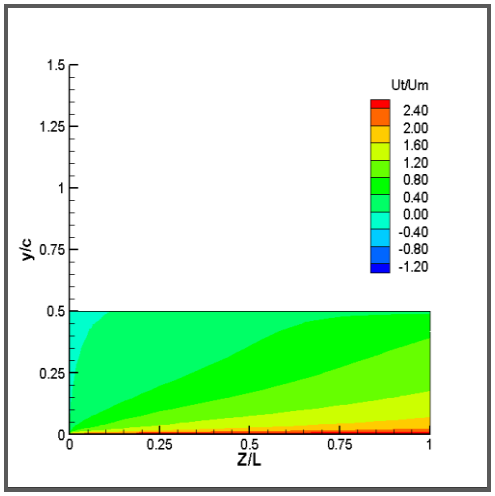

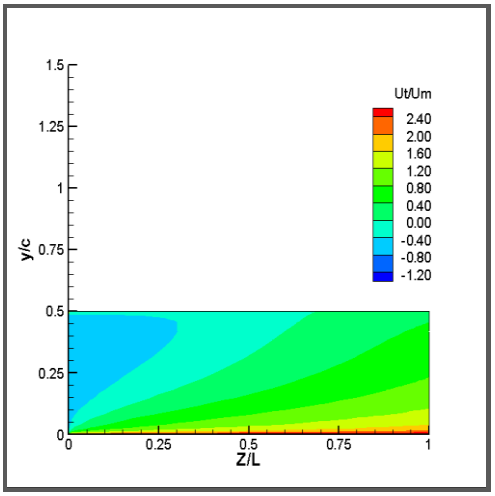

(b)UDF mesh motion (c)Coordinate Transform

Fig. 20 Contours of tangential velocity for Minimum clearance position

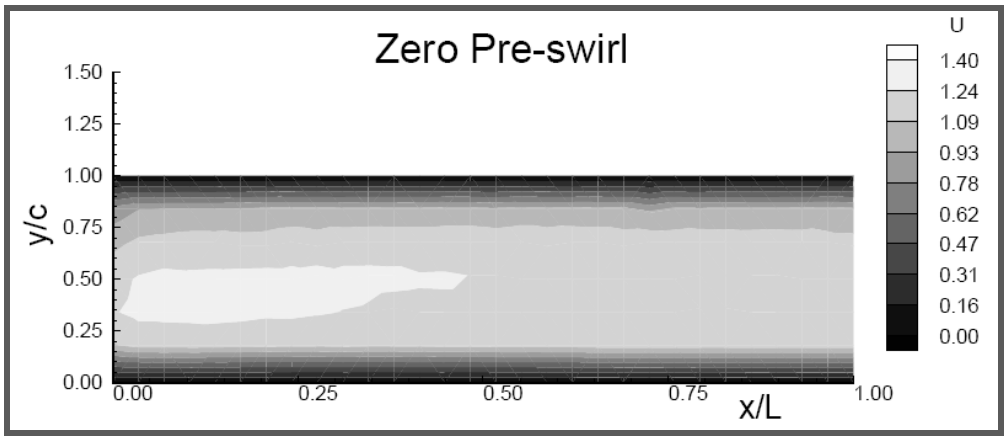

(a) LDV(experimental, from ref. 30)

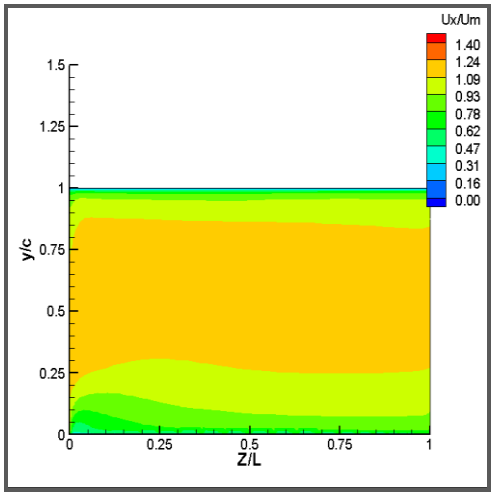

(b)UDF mesh motion

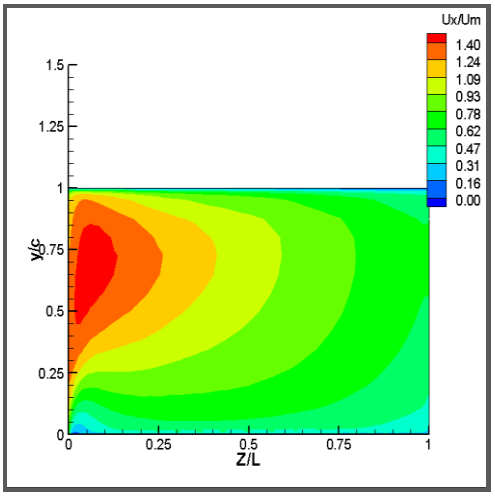

(c)Coordinate Transform

Fig. 21 Contours of axial velocity for Suction side

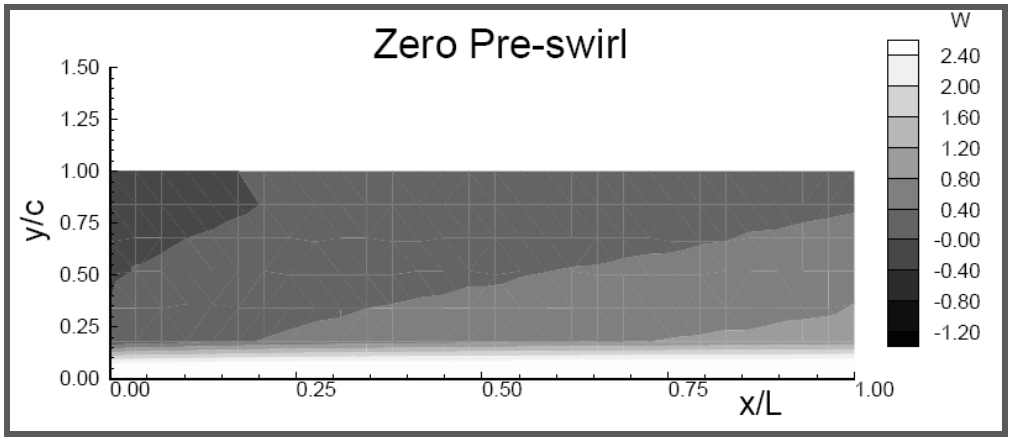

(a) LDV(experimental, from ref. 30)

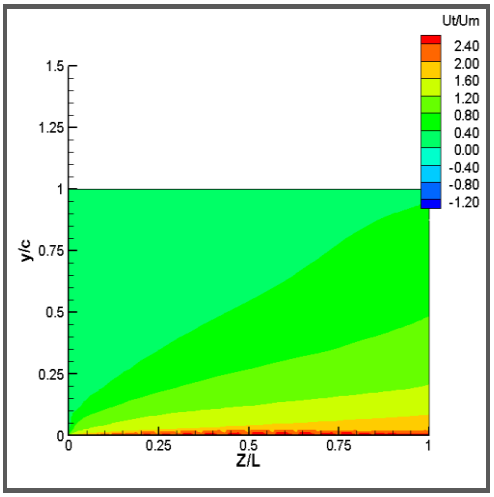

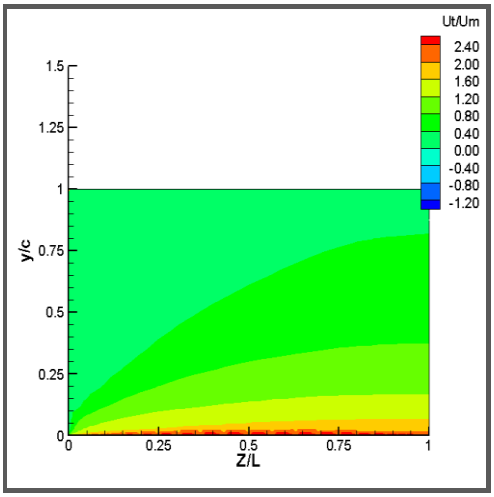

(b)UDF mesh motion (c)Coordinate Transform

Fig. 22 Contours of tangential velocity for Suction side

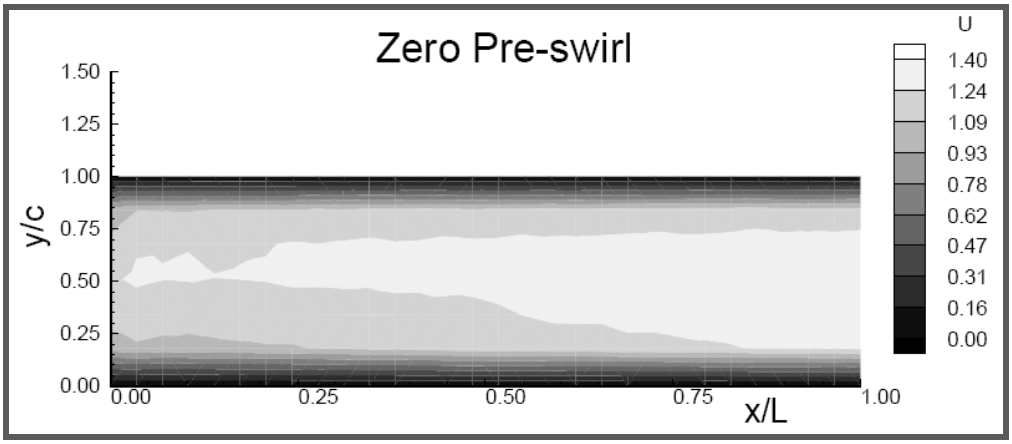

(a) LDV(experimental, from ref. 30)

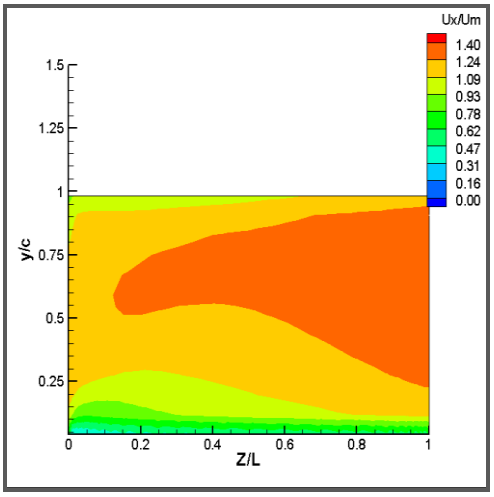

(b)UDF mesh motion

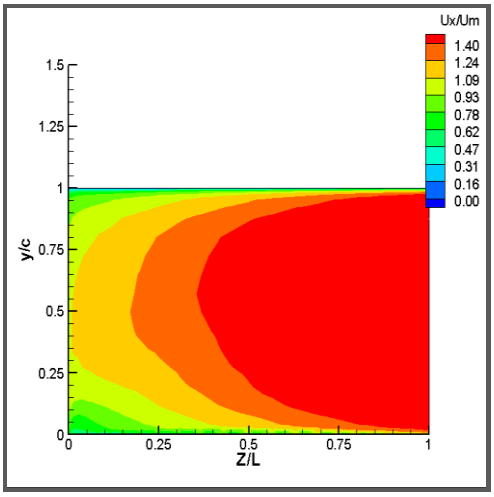

(c)Coordinate Transform

Fig. 23 Contours of axial velocity for Pressure side

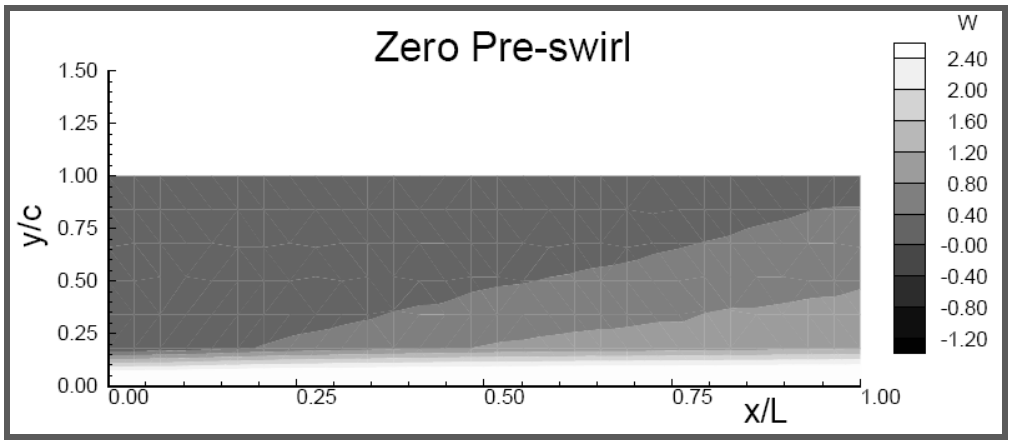

(a)LDV(experimental, from ref. 30)

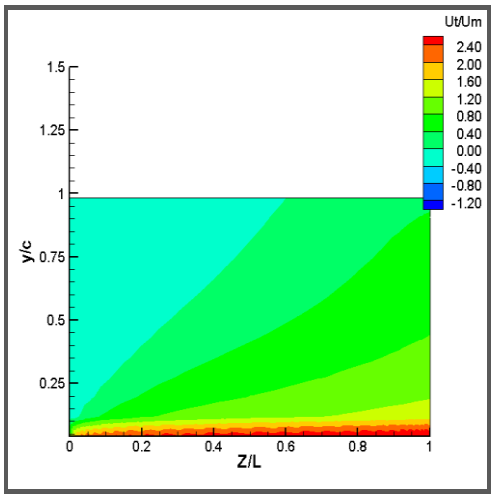

(b)UDF mesh motion

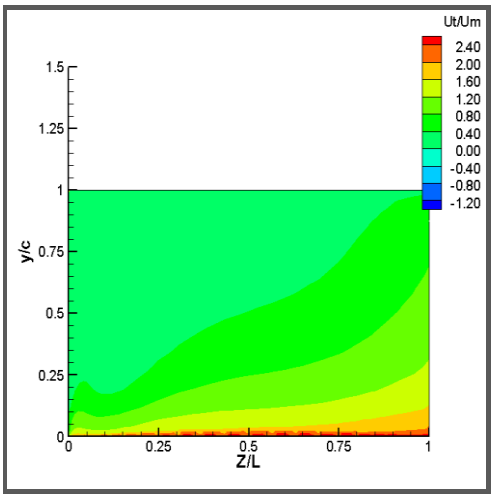

(c) Coordinate Transform

Fig. 24 Contours of axial velocity for Pressure side

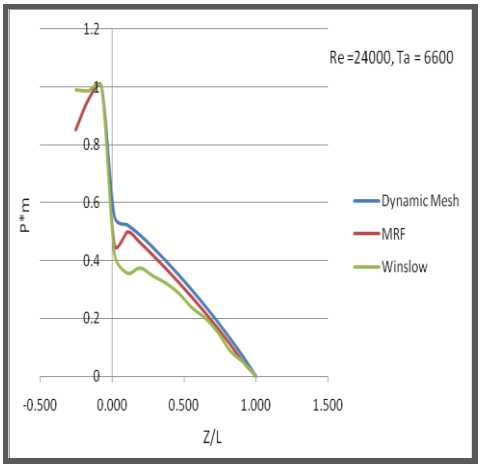

(a)

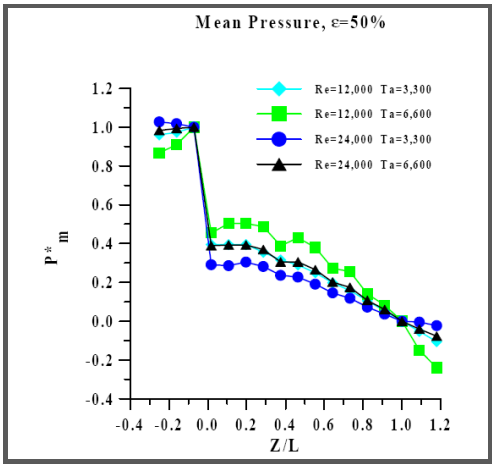

(b) Experimental, from ref. 1

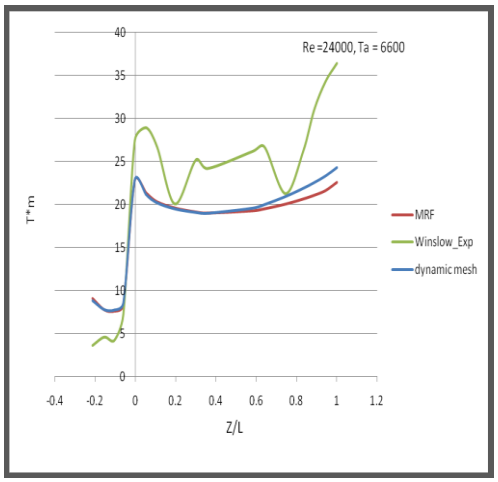

(c)

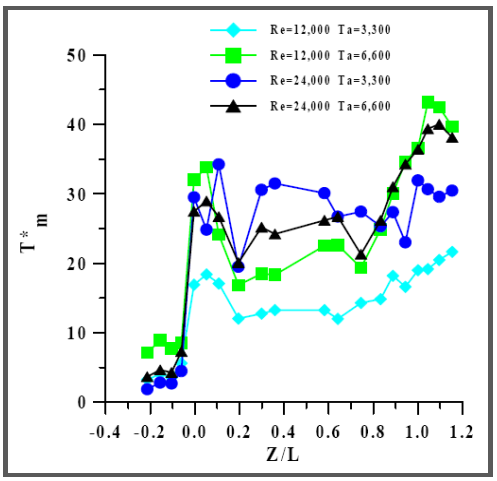

(d) Experimental, from ref. 1

Fig. 25 Plots of P*m Vs Z/L and T*m Vs Z/L

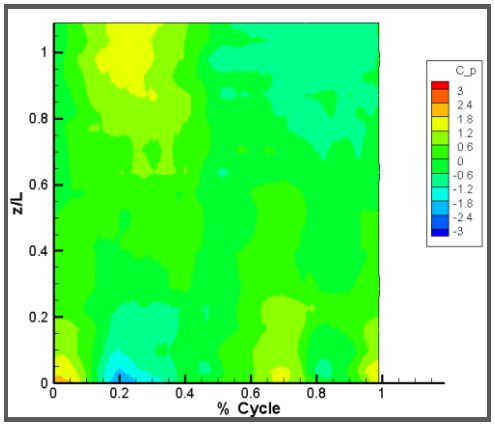

(a) β= 0.3(experimental, from ref. 3)

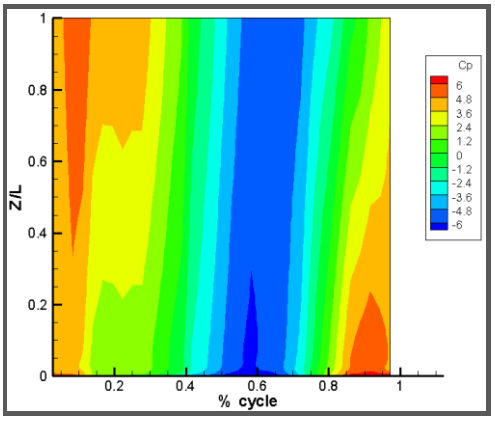

(b) β= 0.3

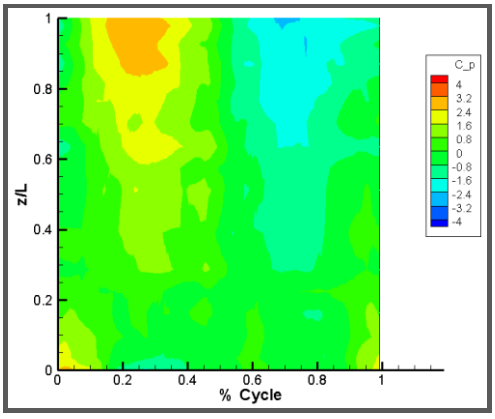

(c) β= 0.4(experimental, from ref. 3)

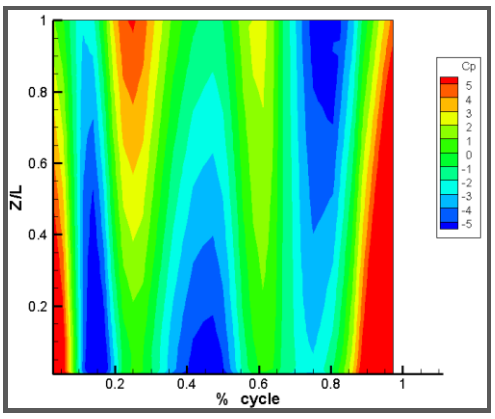

(d) β= 0.4

Fig. 26 Phase Averaged Pressure (Cp), Re=24000, ε =50%, Ta=6600

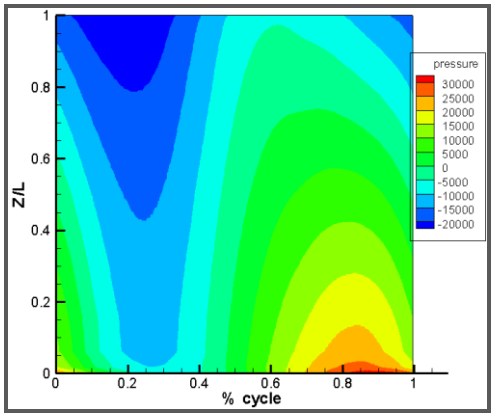

(a) Coordinate Transform (ε =15mil)

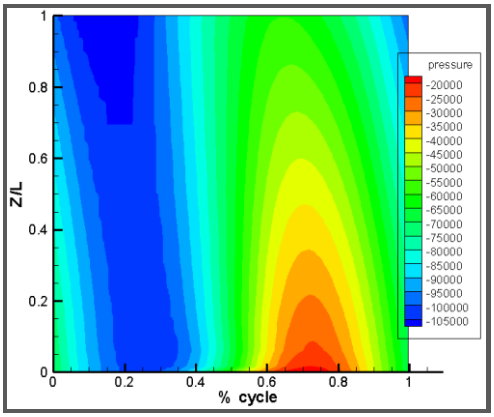

(b) UDF -254^{o} Whirl (ε =15mil)

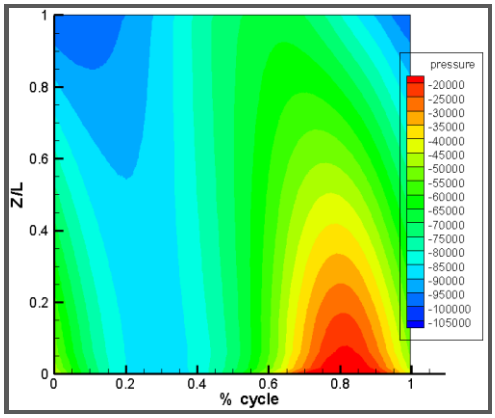

(c) UDF -219^{o} Whirl (ε =15mil)

Fig. 27 Contours of static pressure as a function of Z/L and % cycle for ε = 0.4 mil and β=0.3

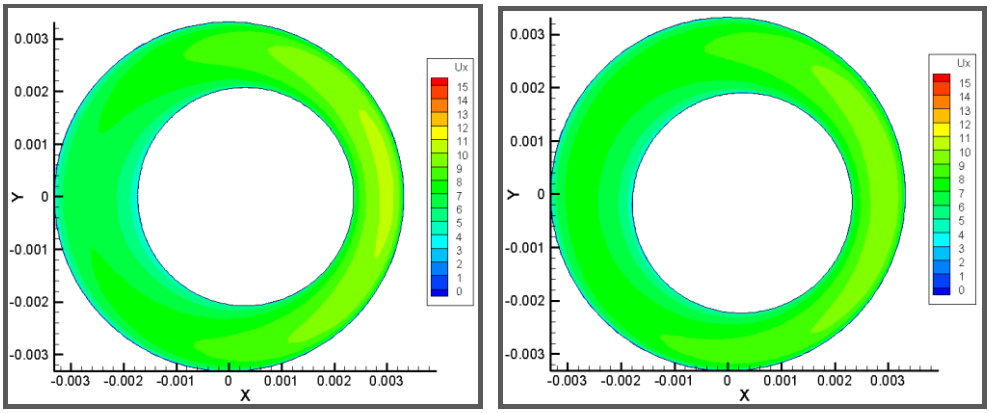

(a) Coordinate Transform (ε=15 mil) (b) UDF -254^{o} Whirl (ε=15mil)

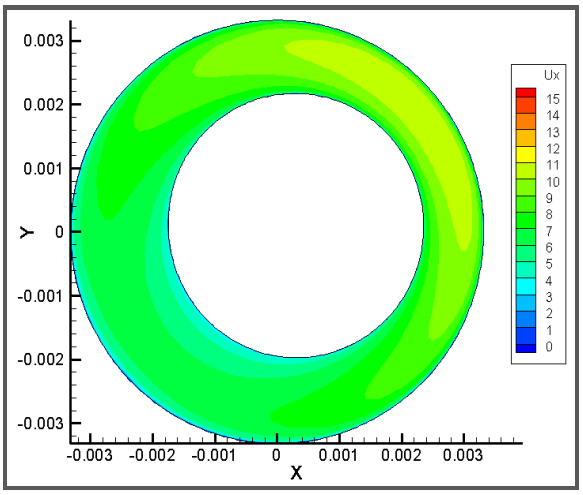

(c) UDF -219^{o} Whirl (ε =15mil)

Fig. 28 Contours of axial velocity at Z/L= 0.4, ε =15mil and β=0.3

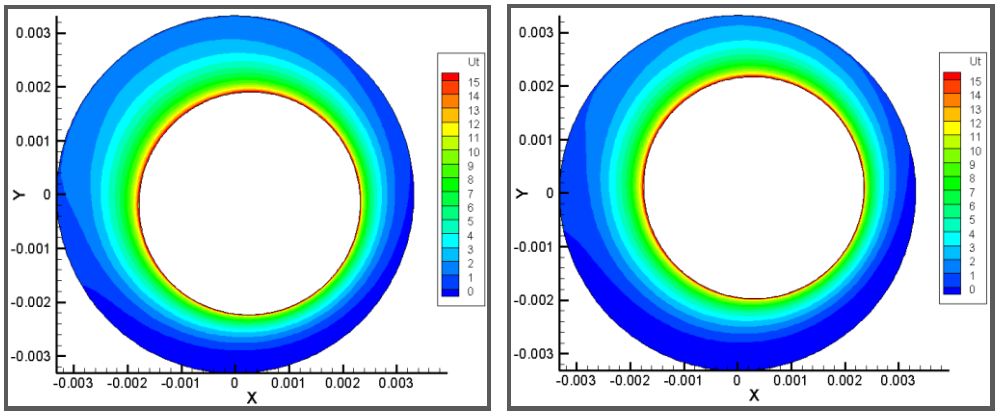

(a) Coordinate Transform (ε=15 mil) (b) UDF -254^{o} Whirl (ε=15 mil)

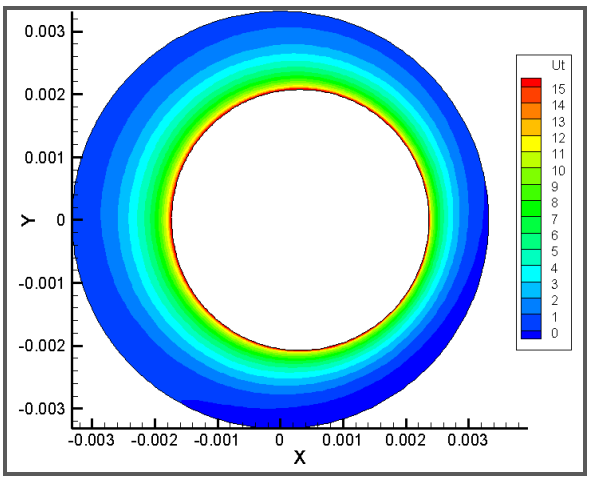

(b)UDF mesh motion-219^{o} Whirl (ε =15mil)

Fig. 29 Contours of tangential velocity at Z/L= 0.4, ε =15mil and β=0.3

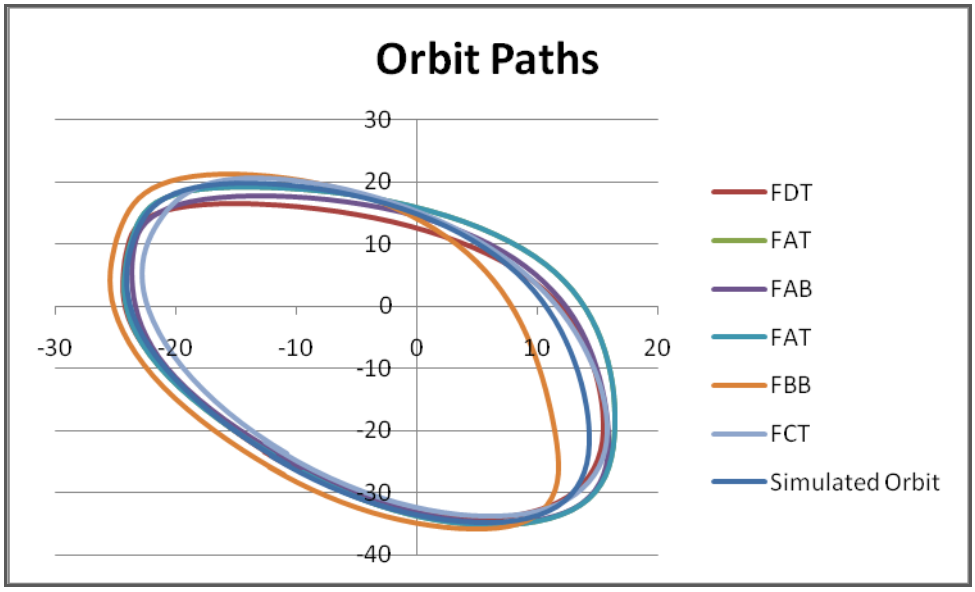

(a)

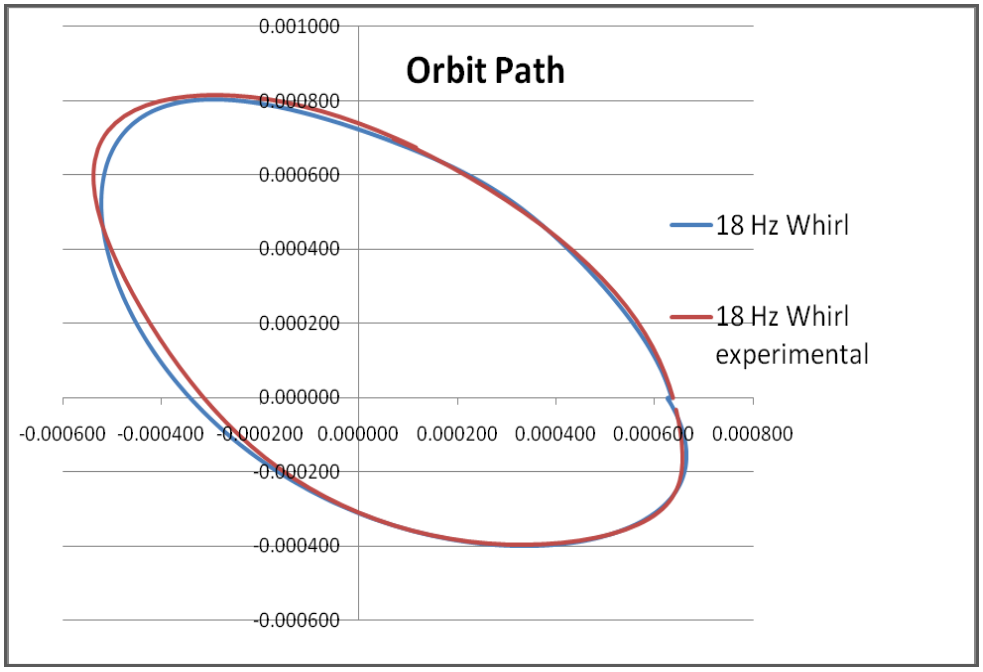

(b)

Fig. 30 recorded probe positions and simulated orbit path

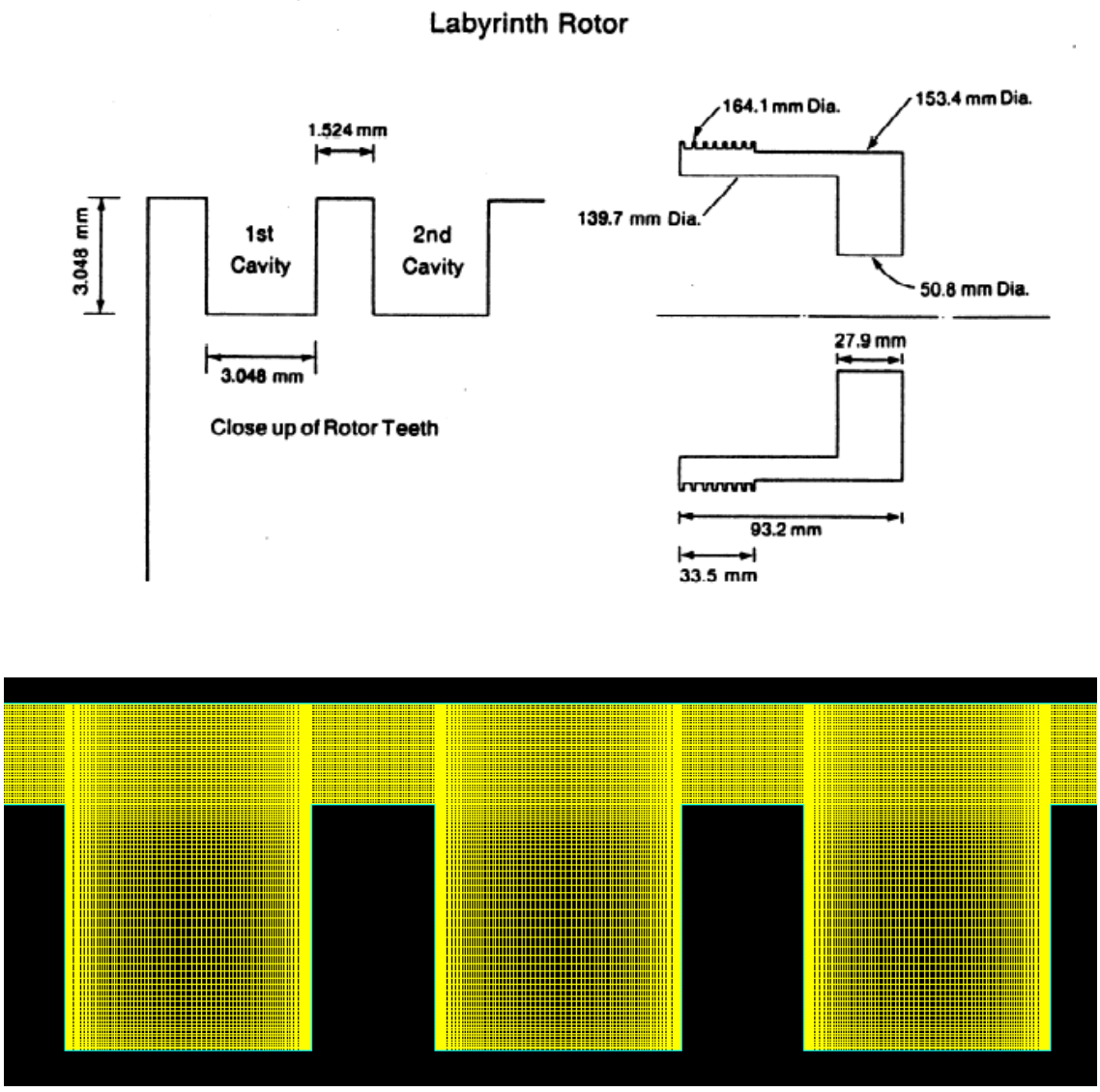

Fig. 31 Labyrinth seal rotor geometry and representative mesh

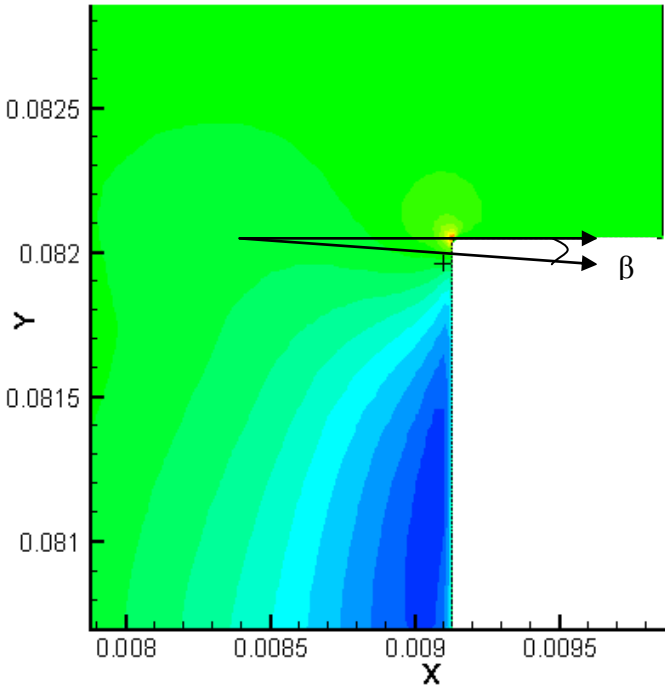

Fig. 32 determination of β angle

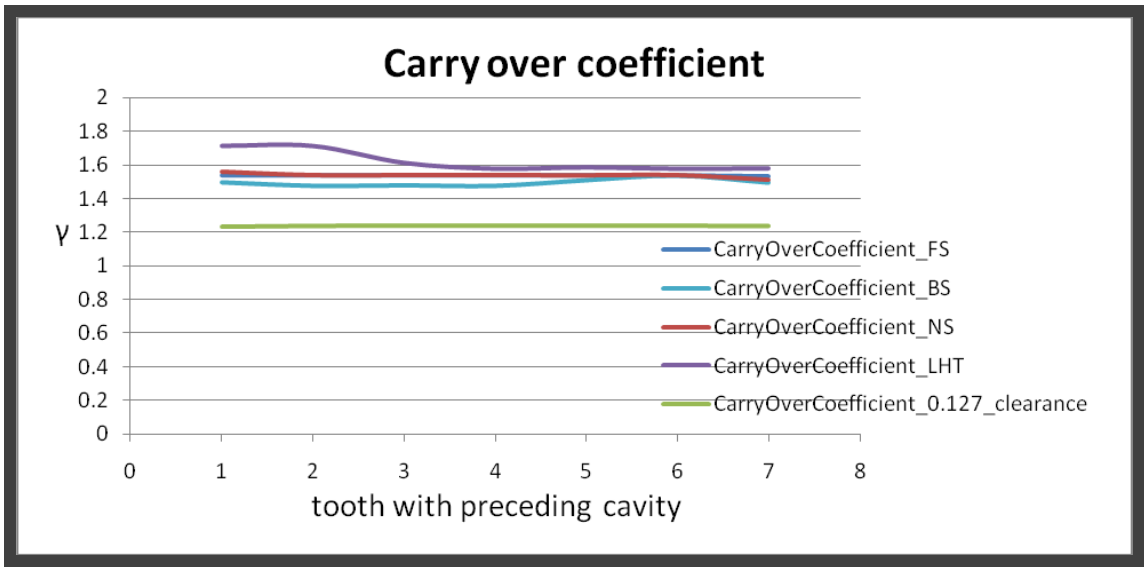

Fig. 33 Carry over coefficient vs. tooth with preceding cavity

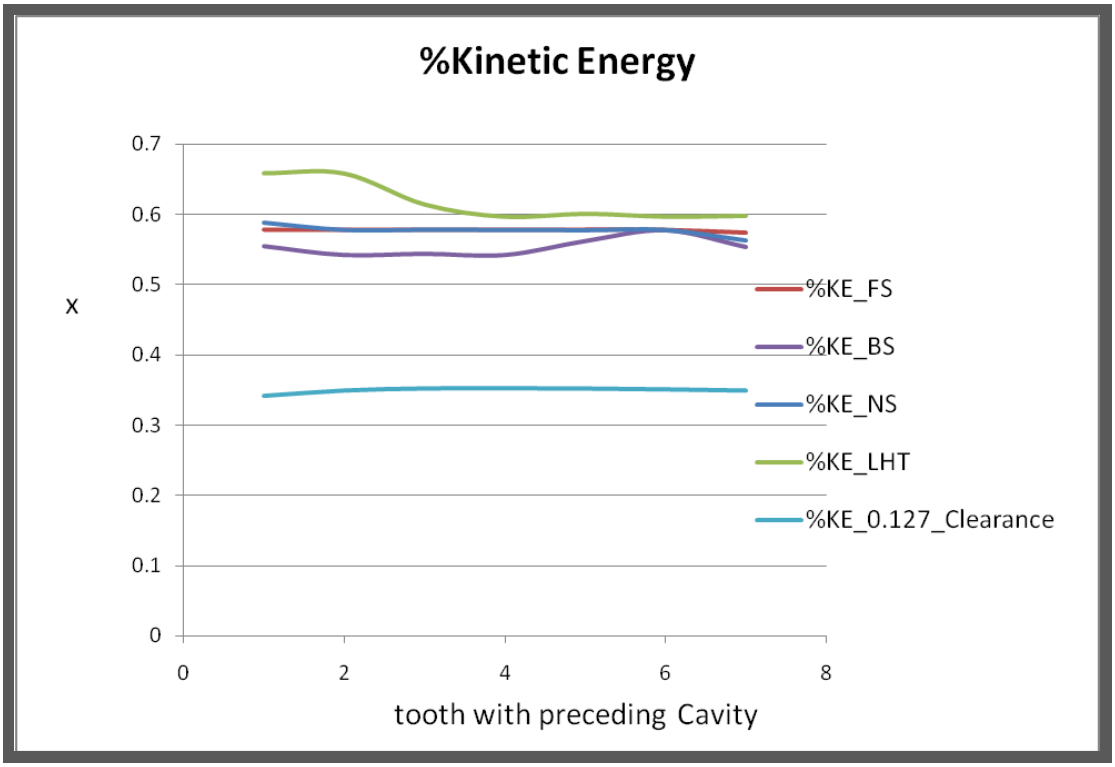

Fig. 34 % Kinetic energy vs. tooth with preceding cavity

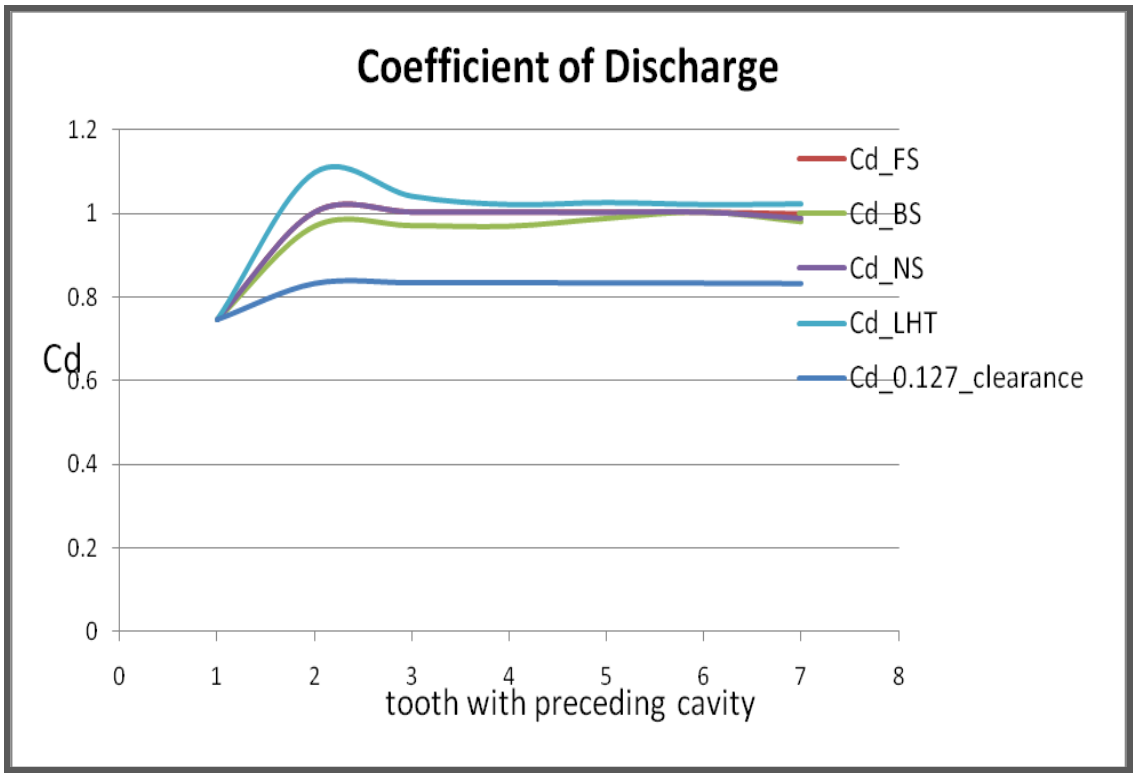

Fig. 35 Coefficient of discharge vs. tooth with preceding cavity

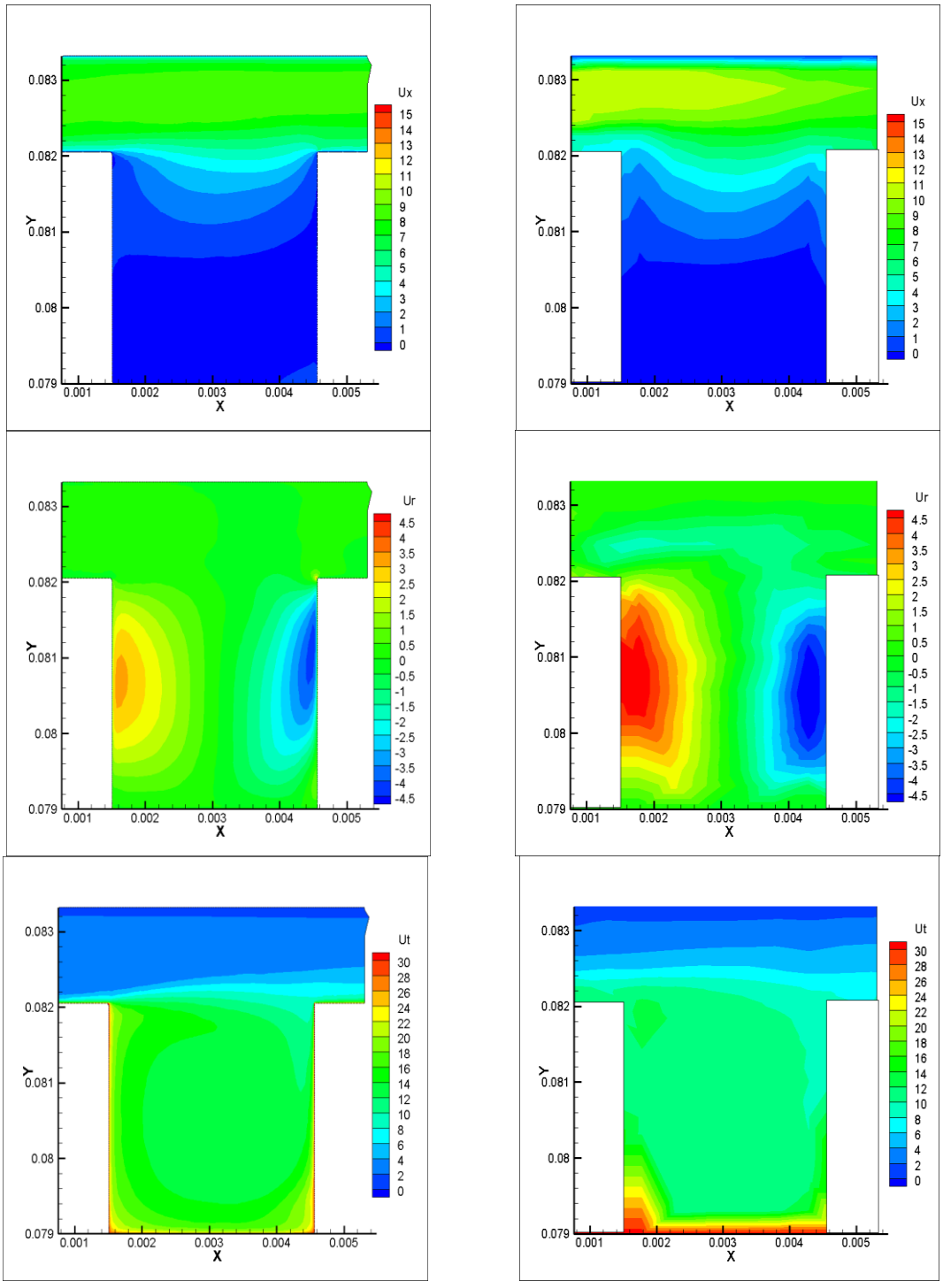

Numerical simulation Experimental LDA data, from ref. 4

Fig. 36 Labyrinth Seal No Swirl- First Cavity

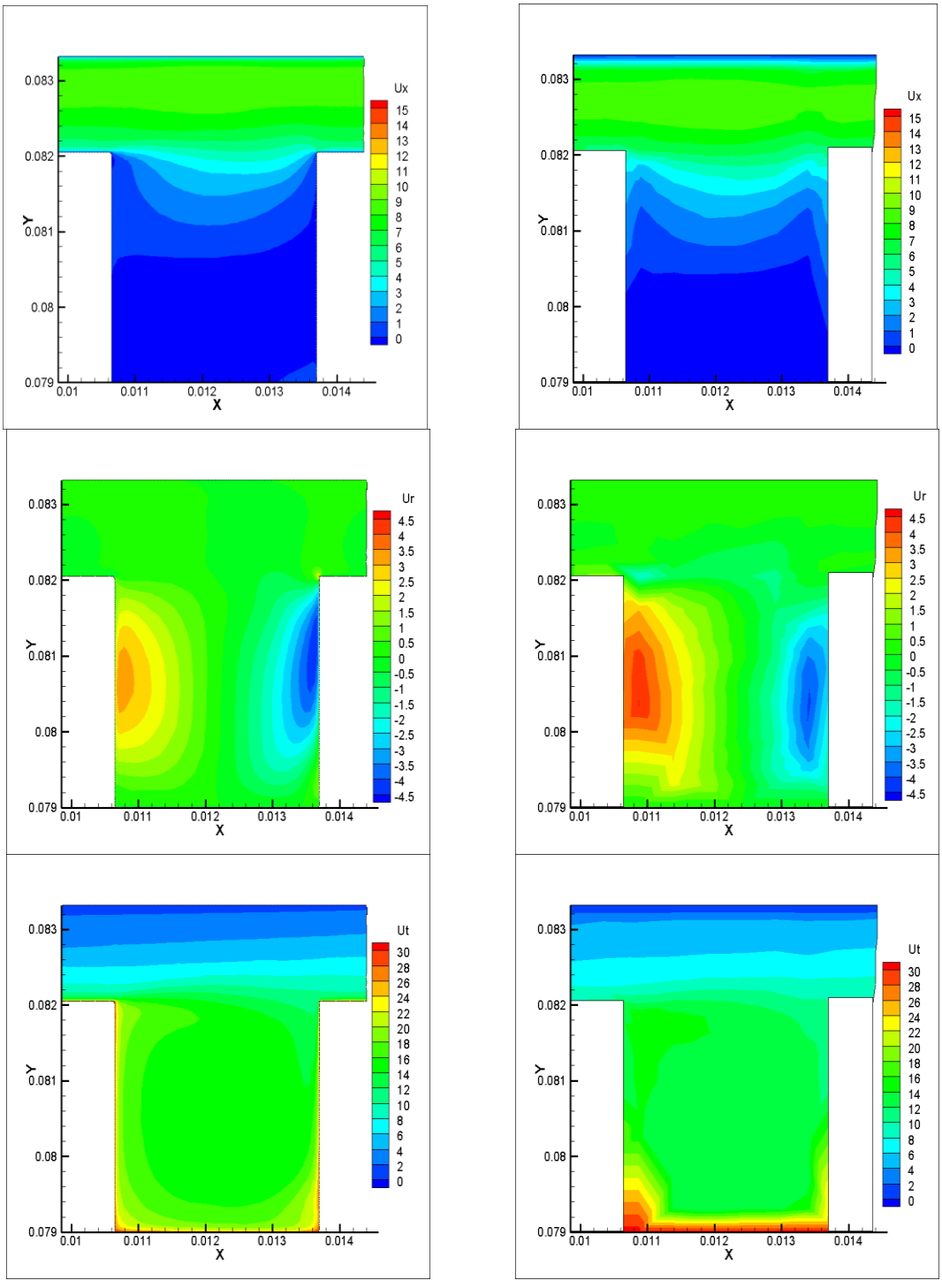

Numerical simulation Experimental LDA data, from ref. 4

Fig. 37 Labyrinth Seal No Swirl- Third Cavity

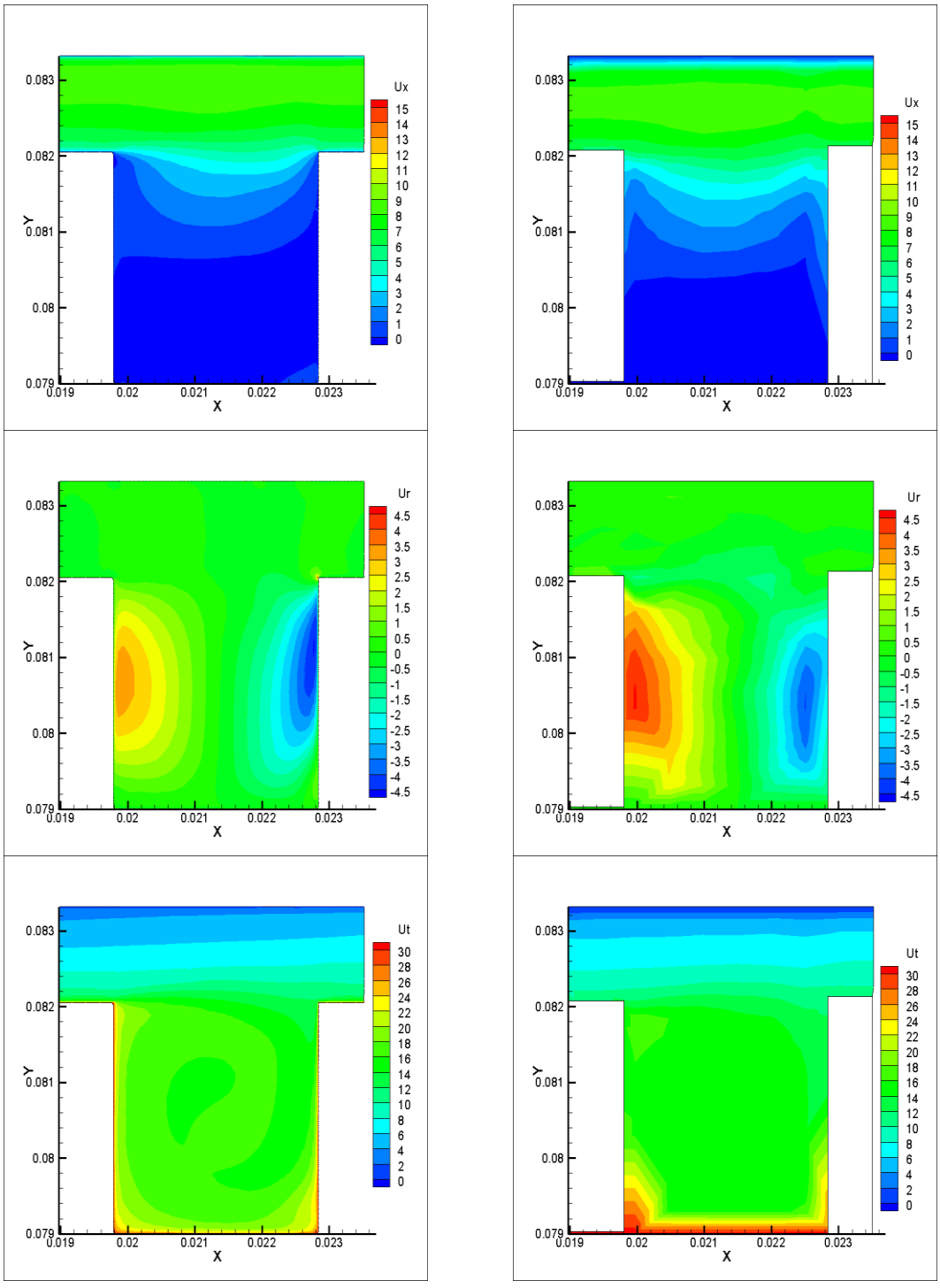

Numerical simulation Experimental LDA data, from ref. 4

Fig. 38 Labyrinth Seal No Swirl- Fifth Cavity

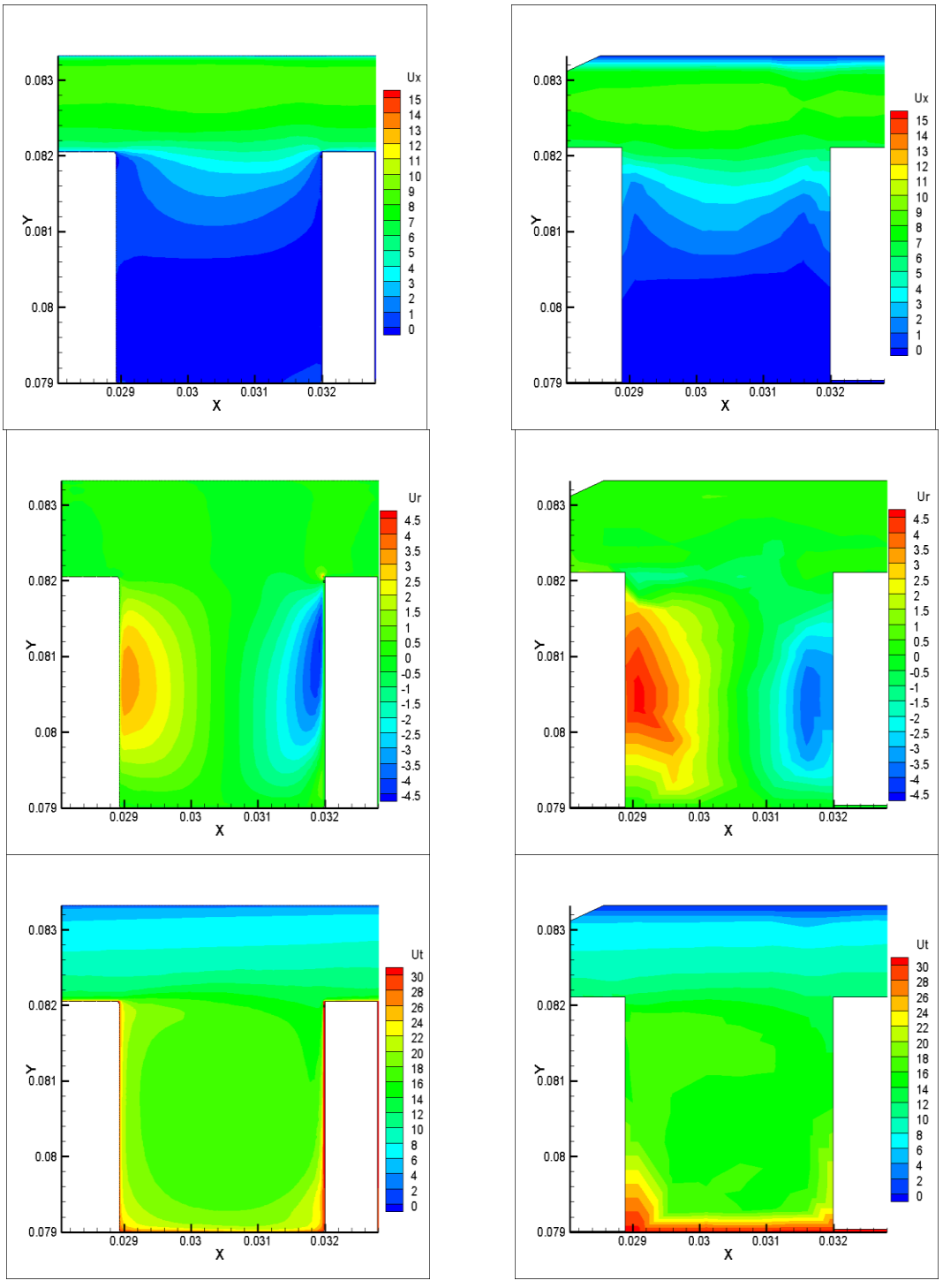

Numerical simulation Experimental LDA data, from ref.4

Fig. 39 Labyrinth Seal No Swirl- Seventh Cavity

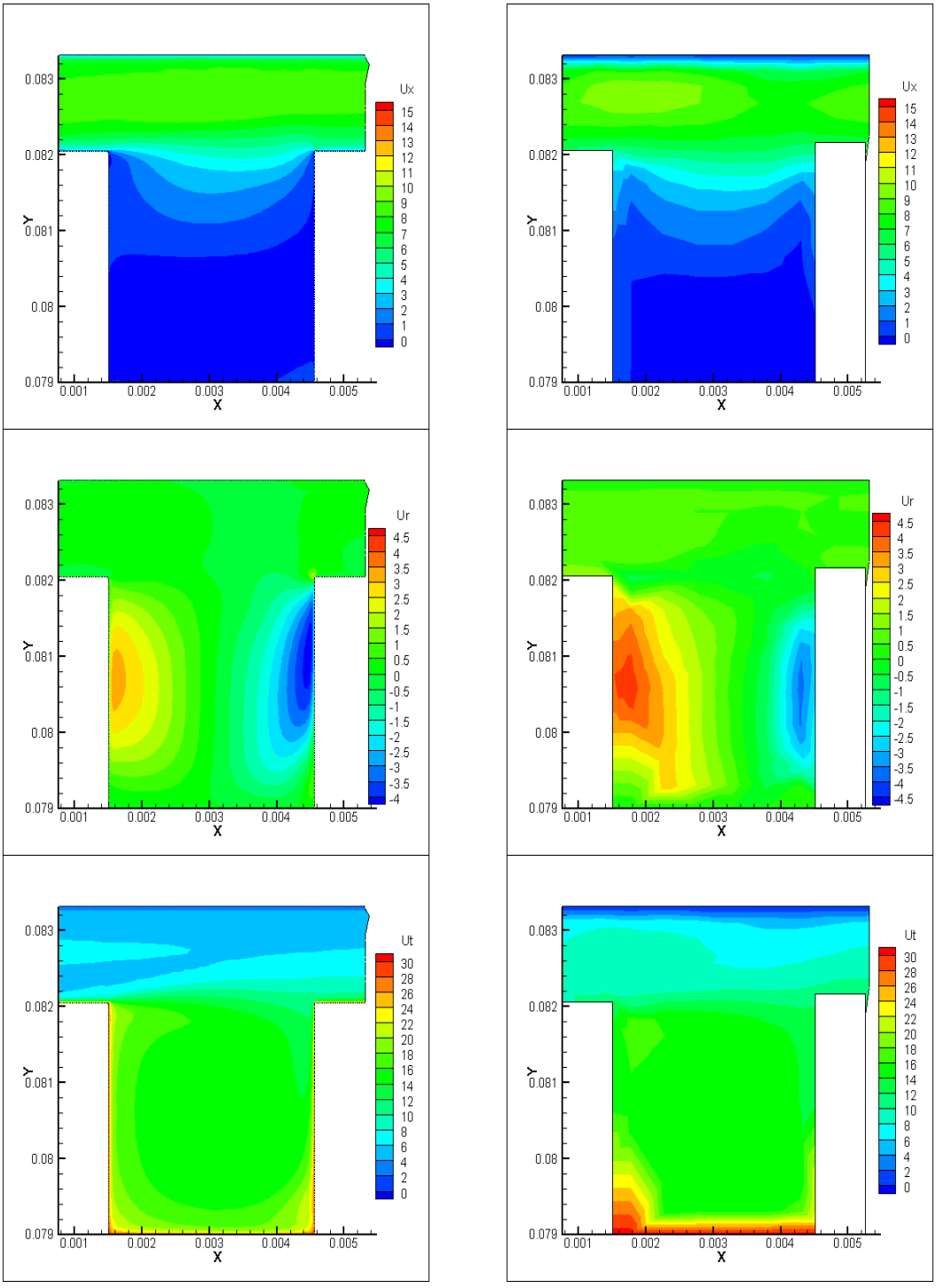

Numerical simulation Experimental LDA data, from ref.4

Fig. 40 Labyrinth Seals Forward Swirl- First Cavity

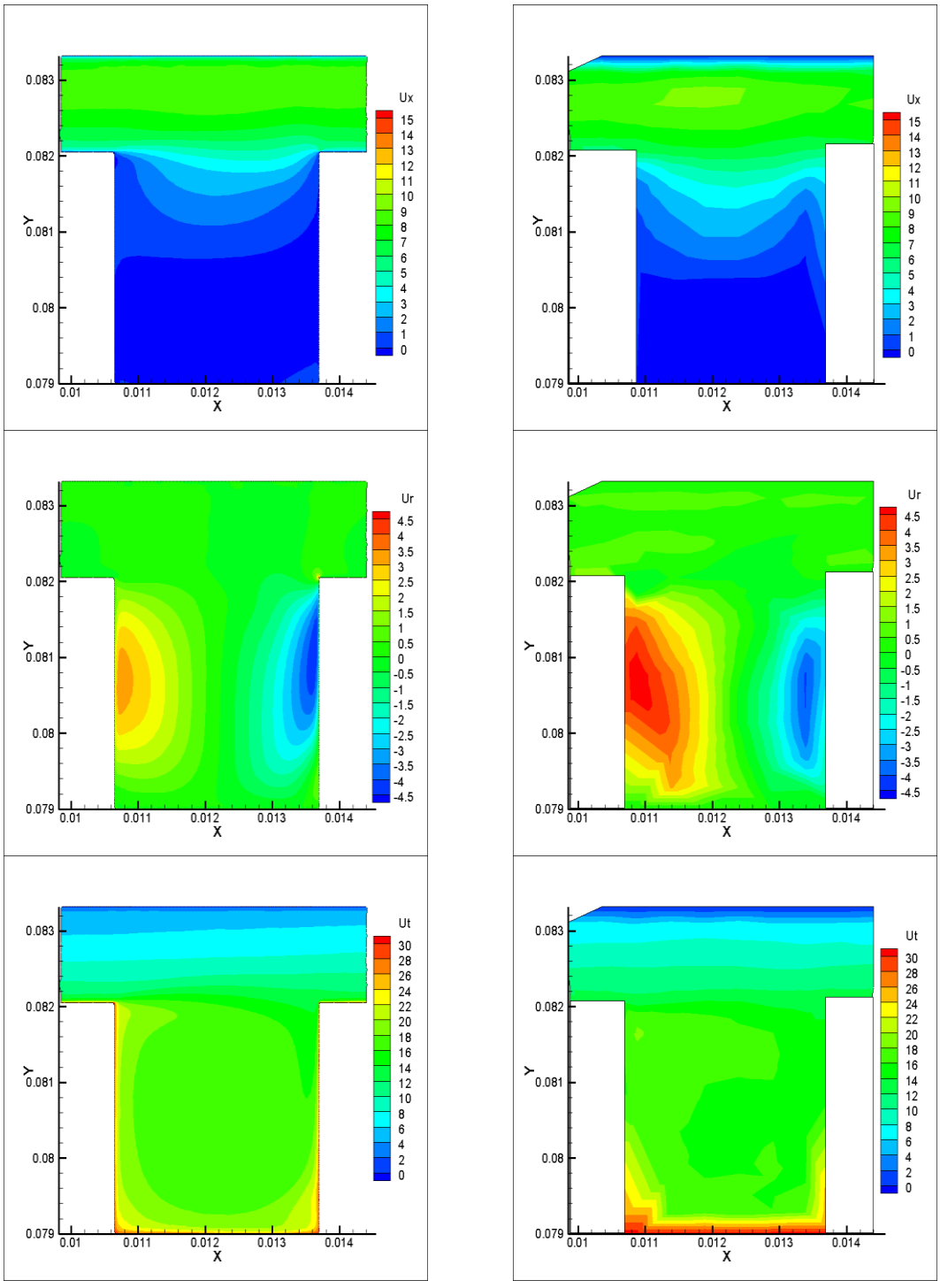

Numerical simulation Experimental LDA data, from ref. 4

Fig. 41 Labyrinth Seals Forward Swirl- Third Cavity

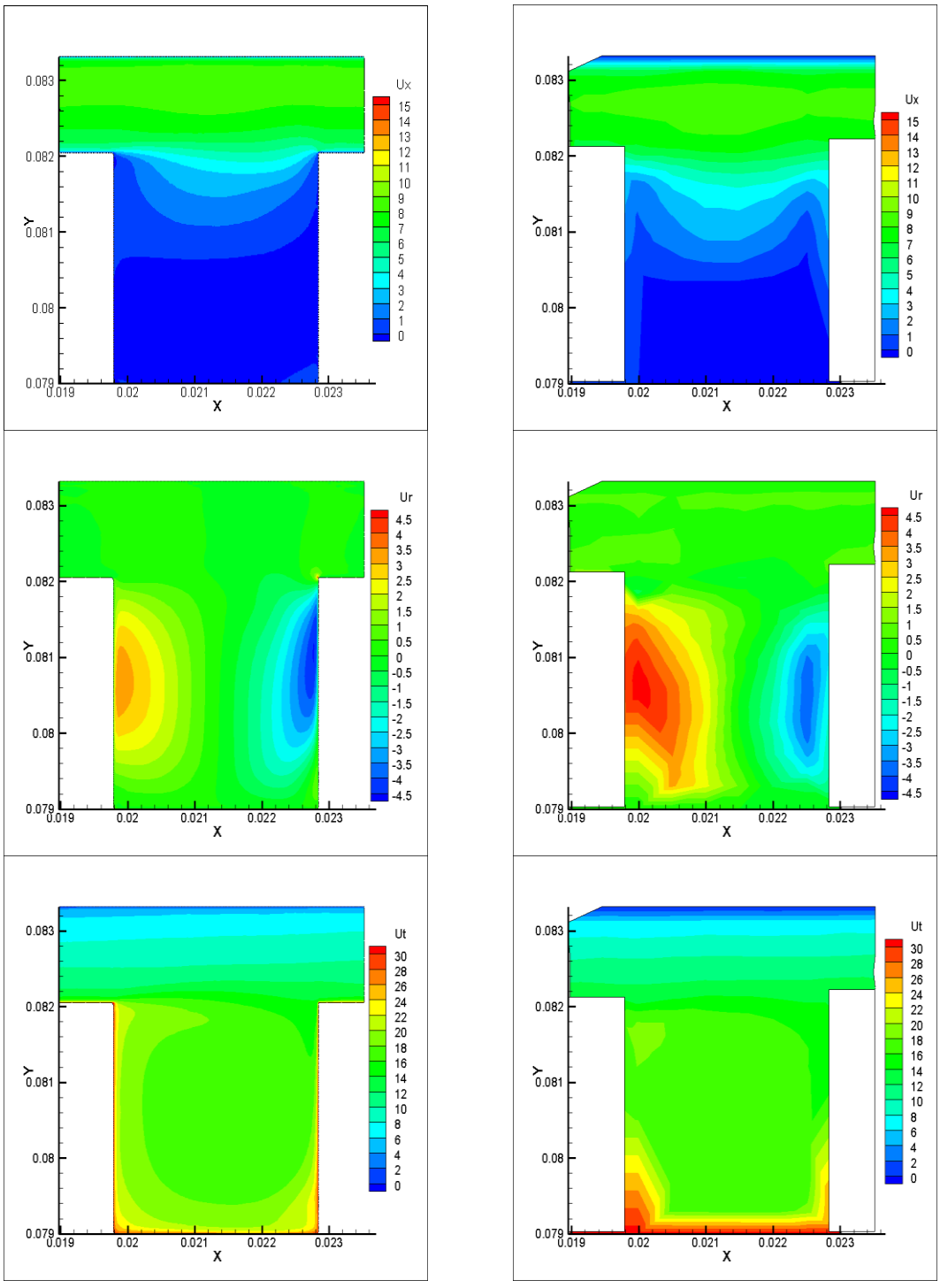

Numerical simulation Experimental LDA data, from ref. 4

Fig. 42 Labyrinth Seals Forward Swirl-Fifth Cavity

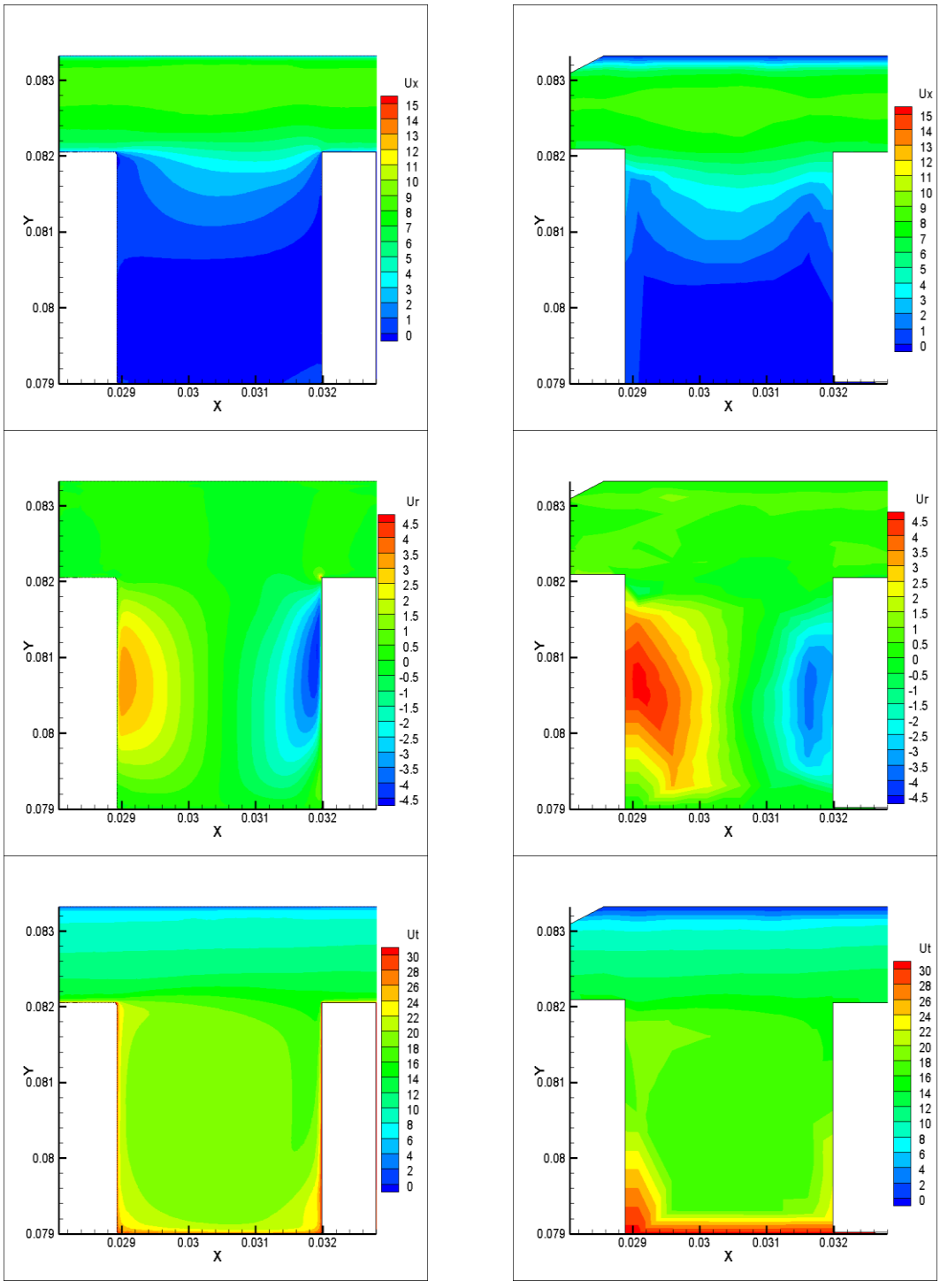

Numerical simulation Experimental LDA data, from ref. 4

Fig. 43 Labyrinth Seals Forward Swirl- Seventh Cavity

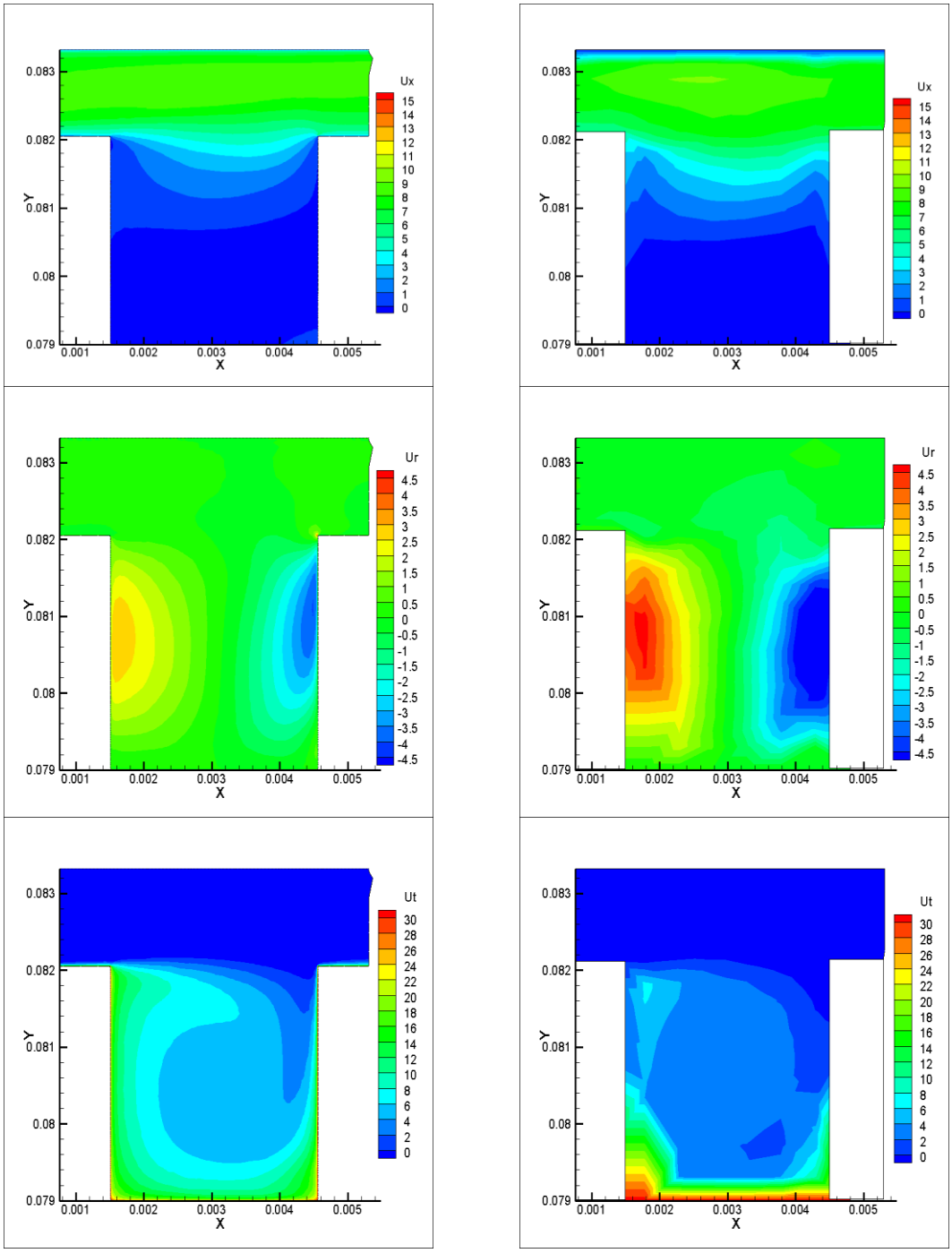

Numerical simulation Experimental LDA data, from ref. 4

Fig. 44 Labyrinth Seals Backward Swirl- First Cavity

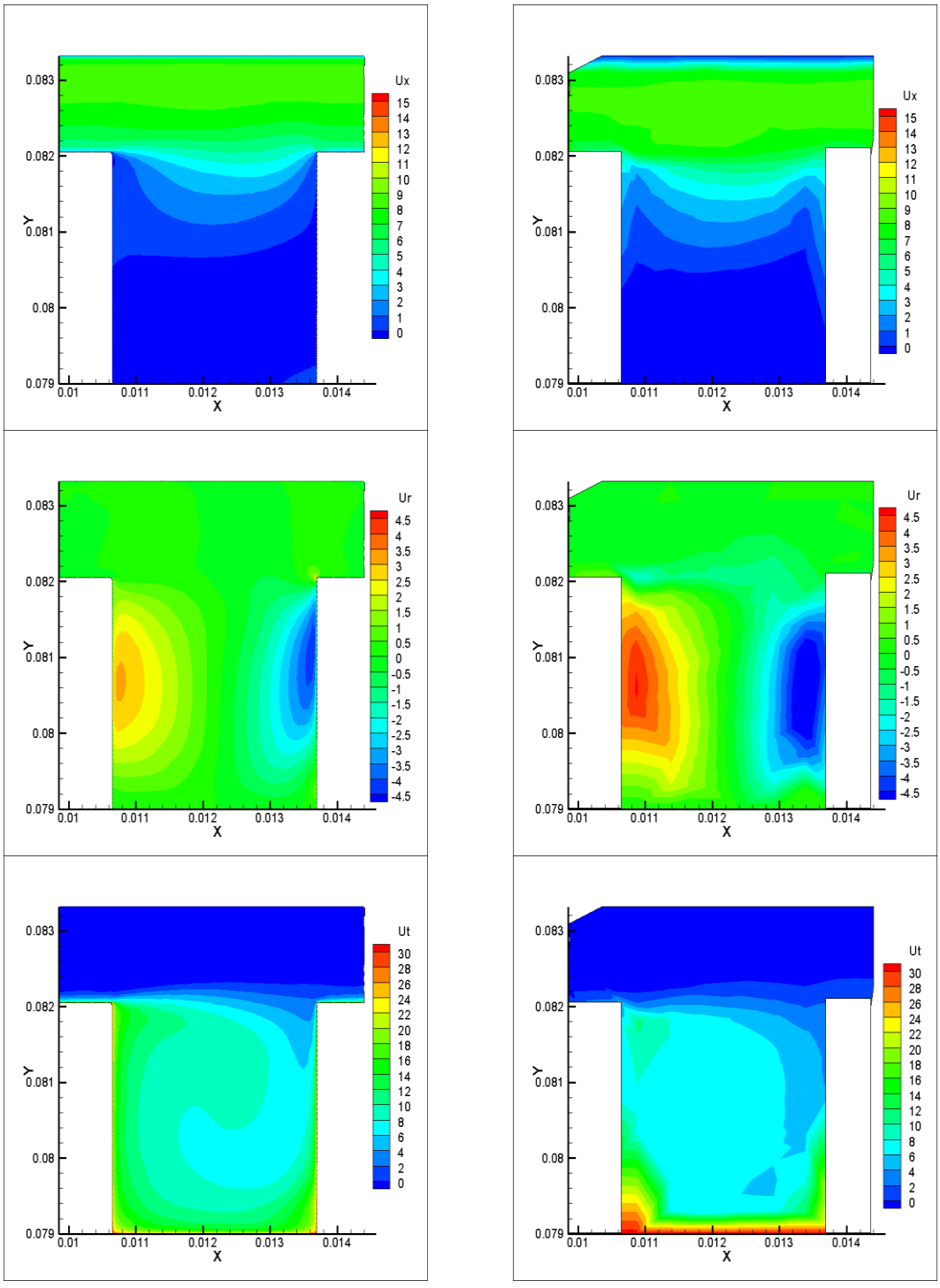

Numerical simulation Experimental LDA data, from ref. 4

Fig. 45 Labyrinth Seals Backward Swirl- Third Cavity

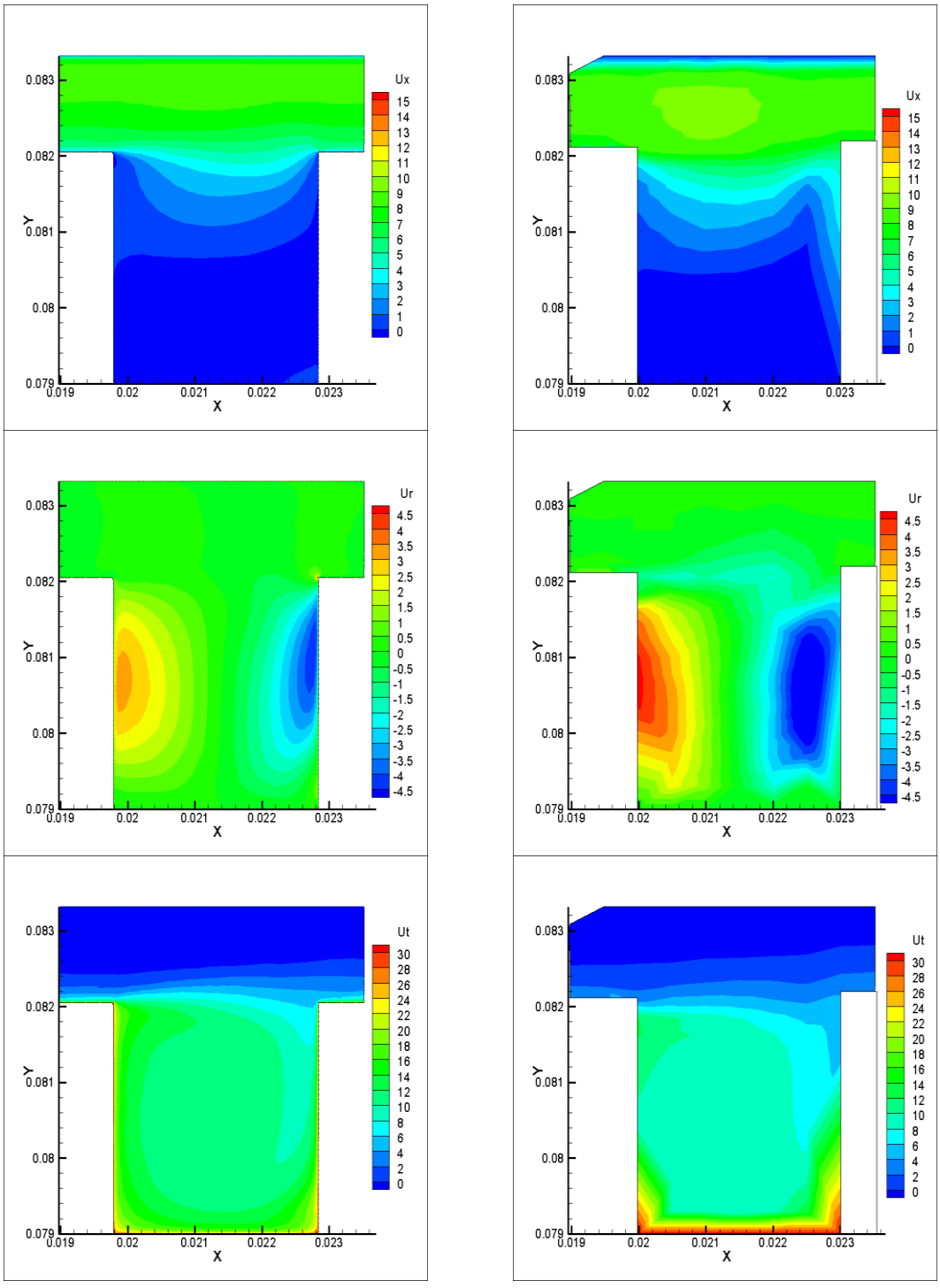

Numerical simulation Experimental LDA data, from ref. 4

Fig. 46 Labyrinth Seals Backward Swirl- Fifth Swirl

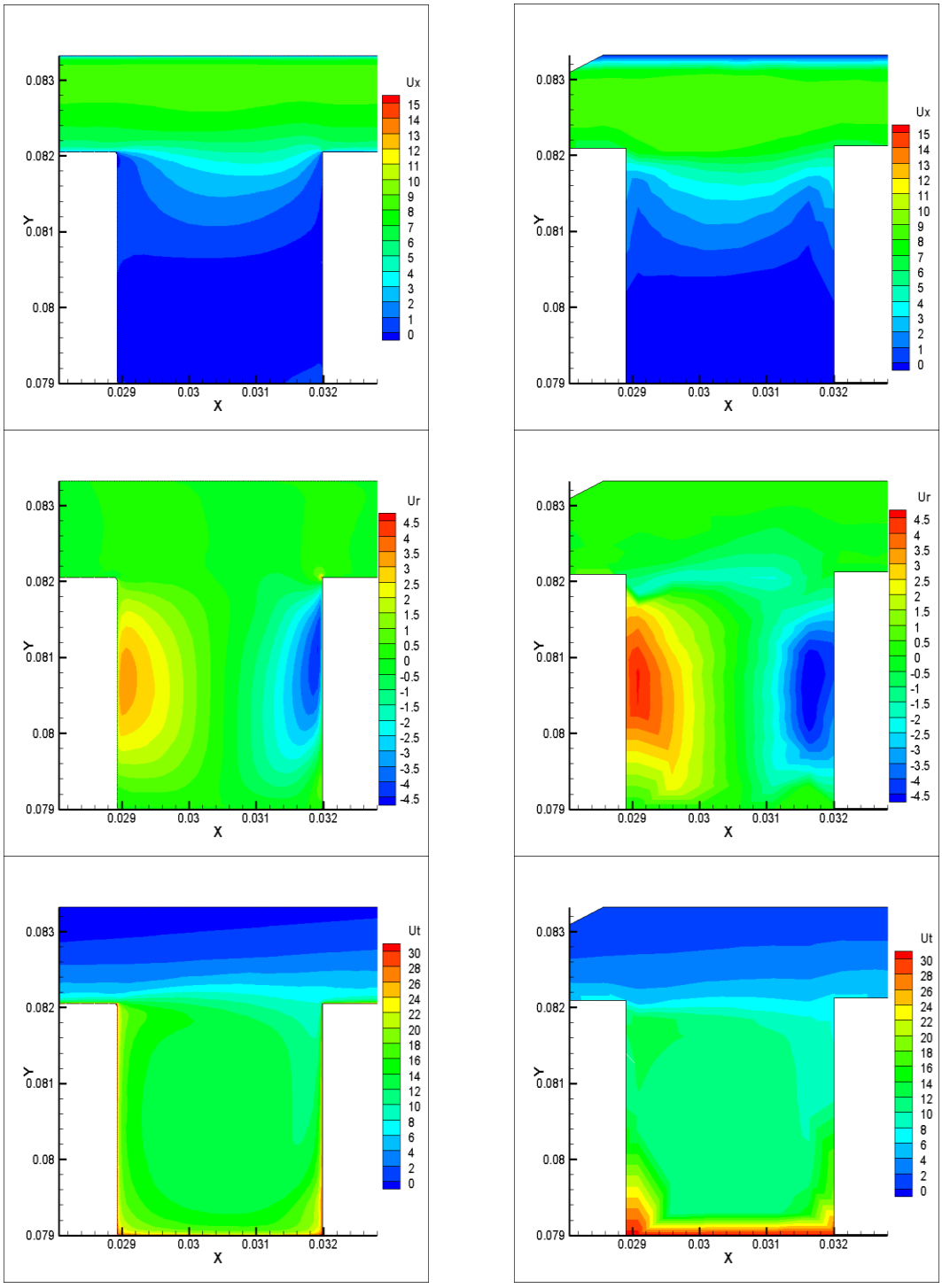

Numerical simulation Experimental LDA data, ref. 4

Fig. 47 Labyrinth Seals Backward Swirl- Seventh Cavity

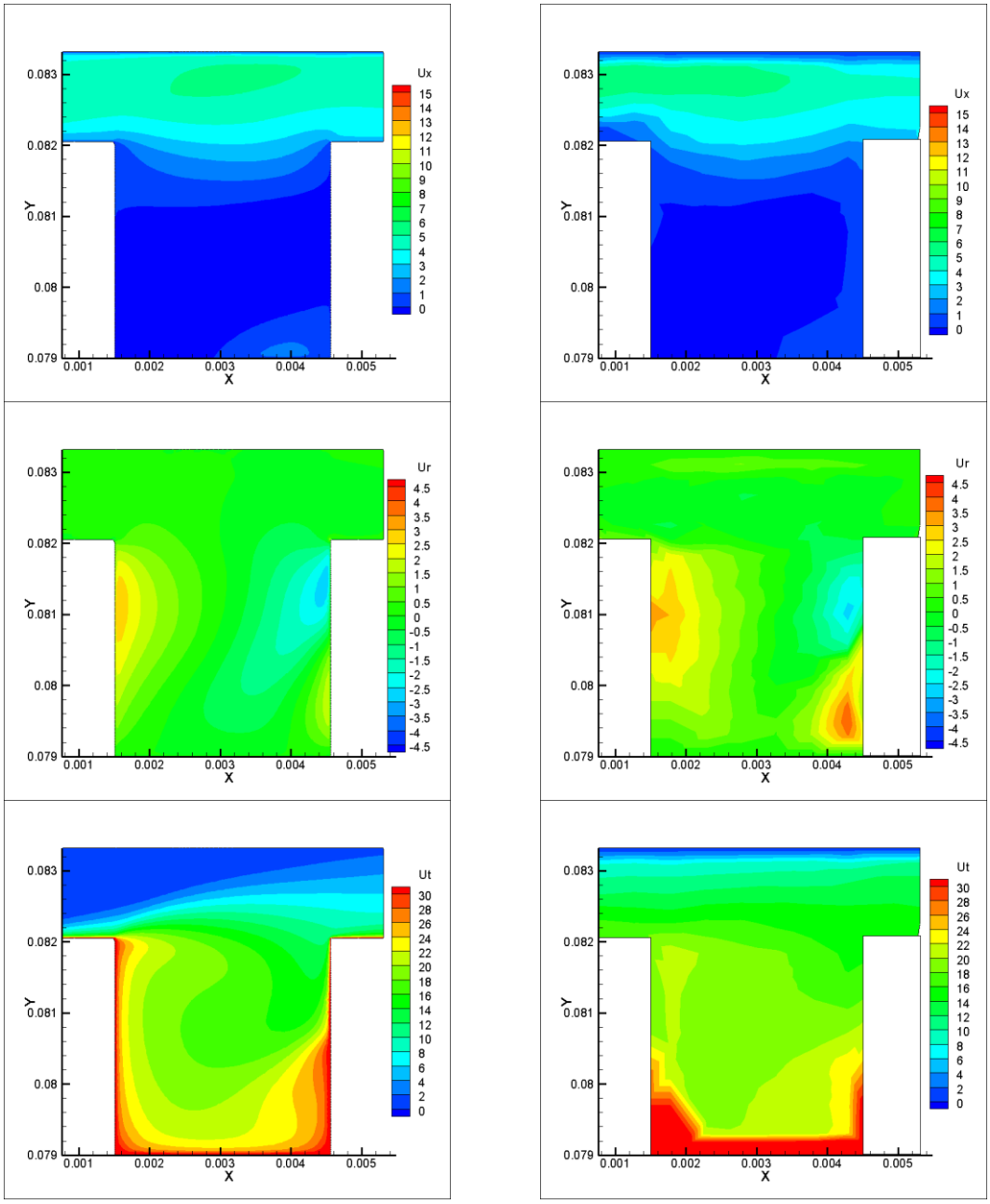

Numerical simulation Experimental LDA data, from ref. 4

Fig. 48 Labyrinth Seal (LHT)- First Cavity

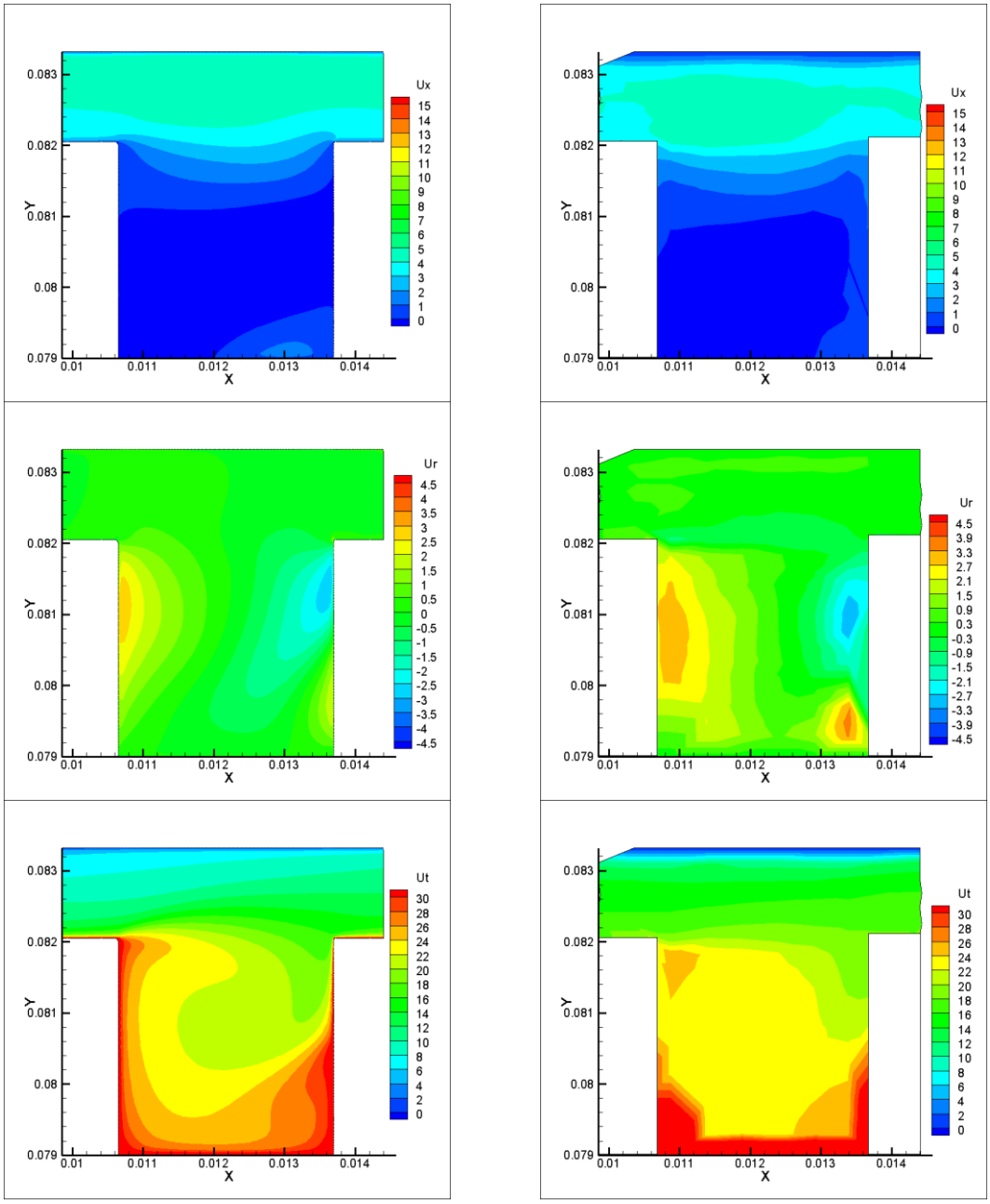

Numerical simulation Experimental LDA data, ref. 4

Fig. 49 Labyrinth Seal (LHT)- Third Cavity

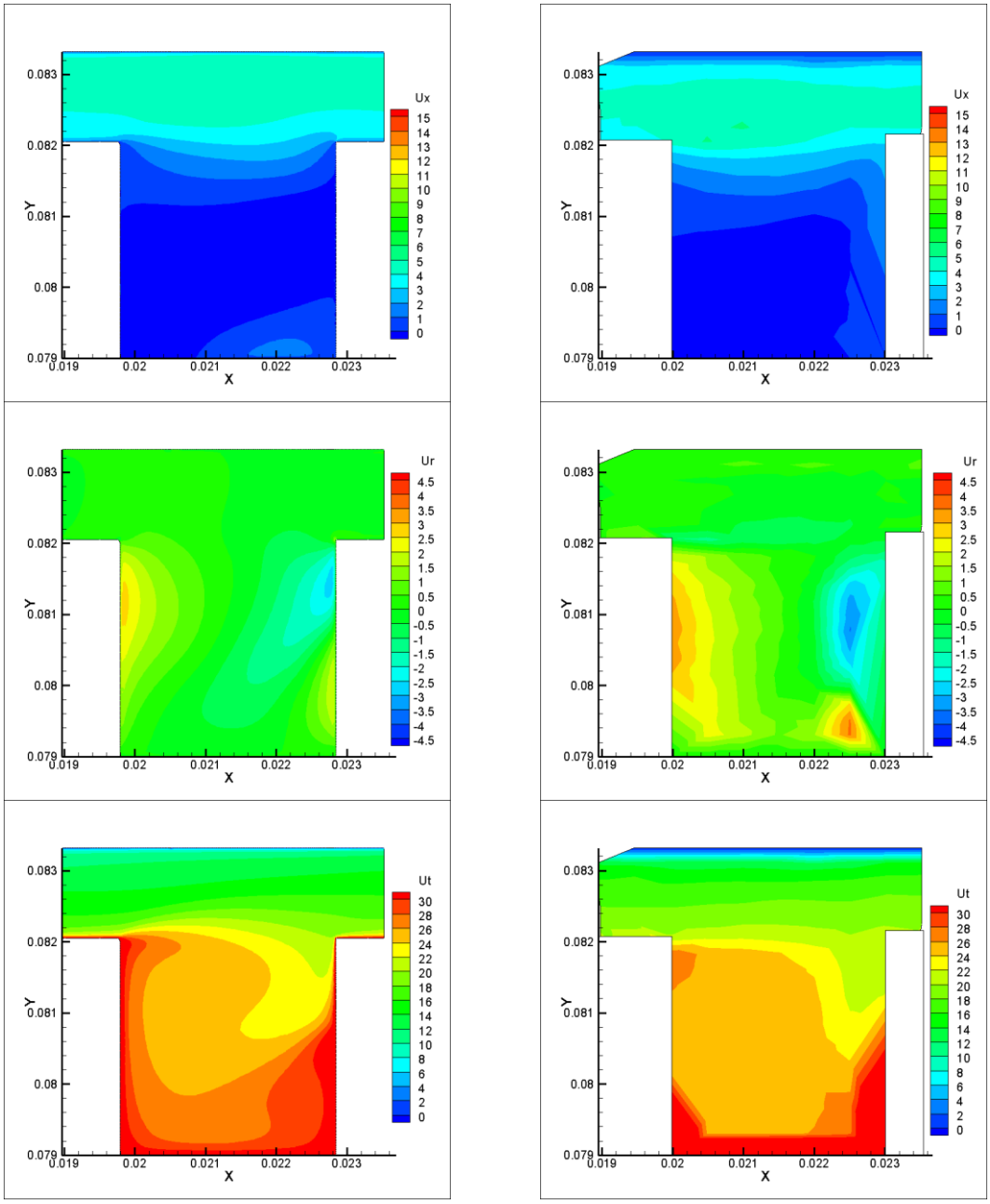

Numerical simulation Experimental LDA data, ref. 4

Fig. 50 Labyrinth Seal (LHT)- Fifth Cavity

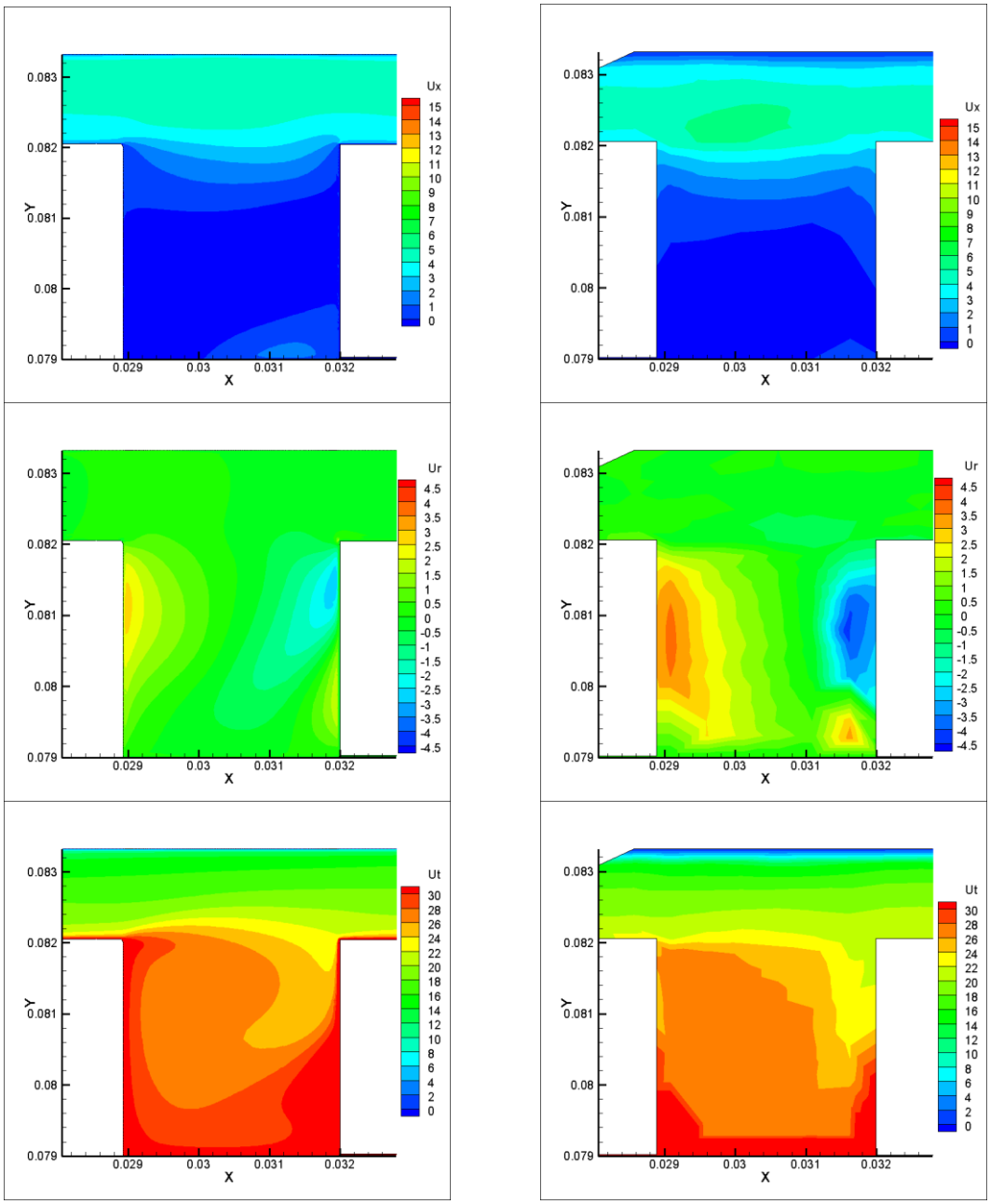

Numerical simulation Experimental LDA data, from ref. 4

Fig. 51 Labyrinth Seal (LHT) - Seventh Cavity

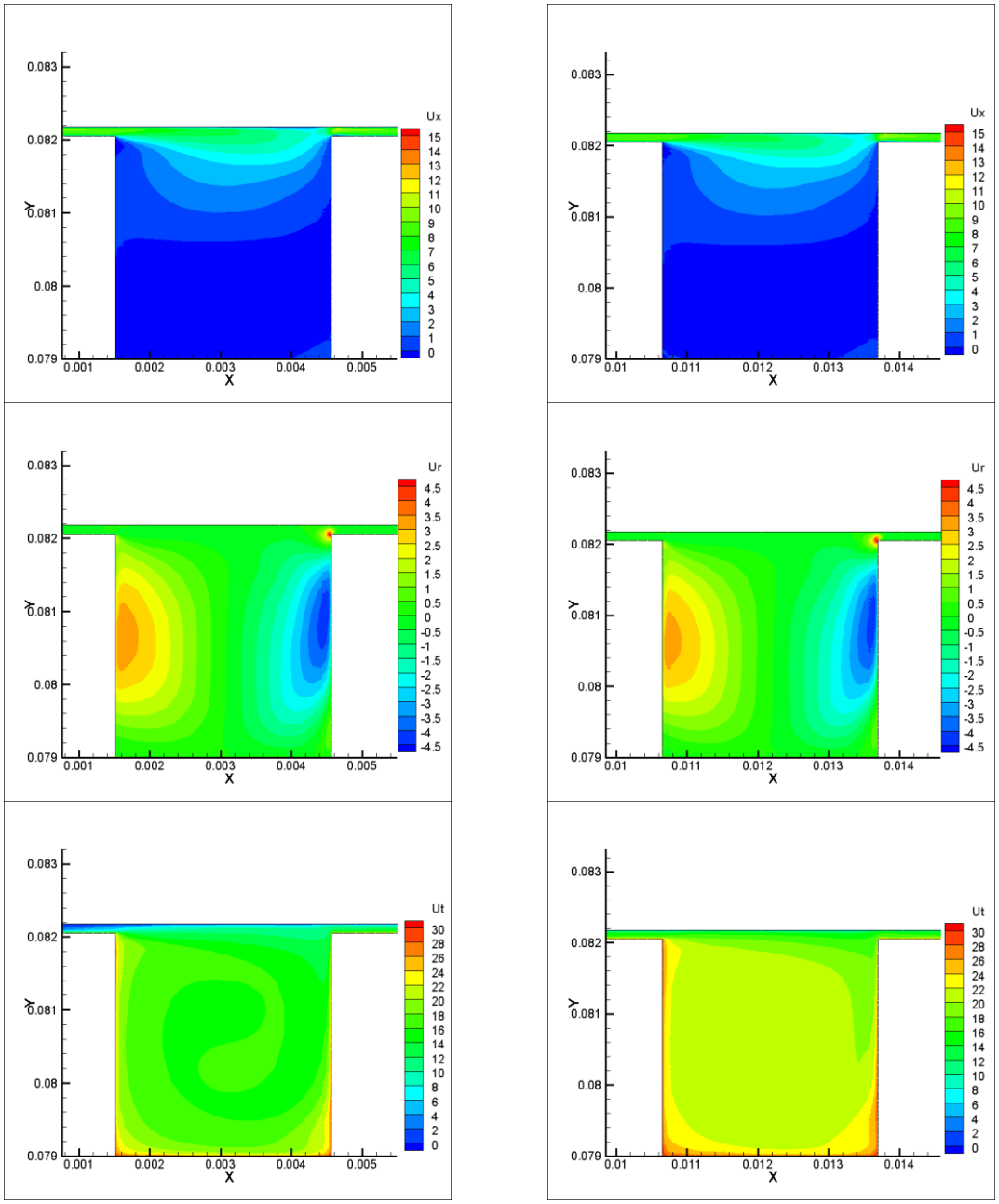

Numerical simulation Experimental LDA data, ref. 4

Fig. 52 Labyrinth Seal Clearance 0.127 mm- First, Third Cavity

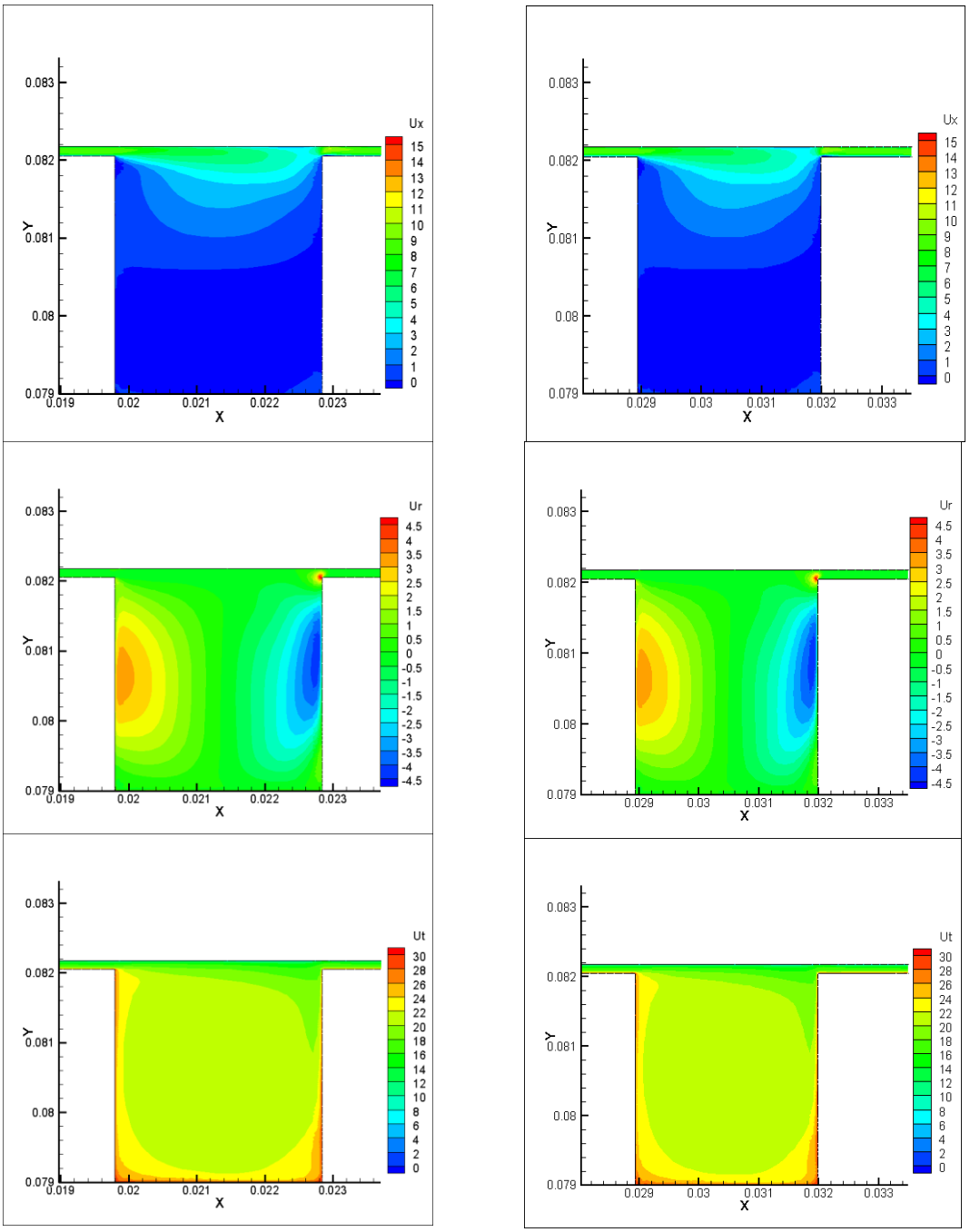

Numerical simulation Experimental LDA data, ref. 4

Fig. 53 Labyrinth Seal Clearance 0.127 mm- Fifth, Seventh Cavity

APPENDIX B

UDF code in ‘c’ language for assigning surface velocity to rotor

```
#include "udf.h"
#include "stdio.h"

DEFINE_PROFILE(Vx_of_Rotor,t,i)
{
real F_Area[ND_ND],x[ND_ND];

real CG[ND_ND];
real one[ND_ND];
real R, w, Theta, del, k;
face_t f;
real time, dtime, Omega;
real a;
time=N_TIME;
dtime=CURRENT_TIMESTEP;
R=0.08205;
del=0.000635;
Omega=150.796416;
w=376.99104;
a=0;

CG[0]=0.0;
CG[1]=0.0;

begin_f_loop(f,t)

{
F_CENTROID(x,f,t);
CG[0] = CG[0] + x[0];
CG[1] = CG[1] + x[1];
a = a + 1;
}
end_f_loop(f,t)

CG[0]=CG[0]/a;
CG[1]=CG[1]/a;

begin_f_loop(f,t)
{
F_CENTROID(x,f,t);
```

```
one[0] = x[0] - CG[0];
one[1] = x[1] - CG[1];
R=sqrt(one[0]*one[0]+one[1]*one[1]);
Theta = atan2(one[1], one[0]);
F_PROFILE(f,t,i) = -R*w*cos(Theta-3.141592/2);
}
end_f_loop(f,t)
}

DEFINE_PROFILE(Vy_of_Rotor,t,i)
{
real F_Area[ND_ND],x[ND_ND];
real CG[ND_ND];
real one[ND_ND];
real R, w, Theta, del;
real a;
face_t f;
real time, dtime, Omega;
time=N_TIME;
dtime=CURRENT_TIMESTEP;
a=0;
del=0.000635;
Omega=150.796416;
w=376.99104;

CG[0] = 0.0;
CG[1] = 0.0;

begin_f_loop(f,t)
{
F_CENTROID(x,f,t);
CG[0]=CG[0]+x[0];
CG[1]=CG[1]+x[1];
a=a+1;
}
end_f_loop(f,t)

CG[0]=CG[0]/a;
CG[1]=CG[1]/a;

begin_f_loop(f,t)
{
F_CENTROID(x,f,t);
one[0] = x[0] - CG[0];
```

```
one[1] = x[1] - CG[1];
R=sqrt(one[0]*one[0]+one[1]*one[1]);
Theta = atan2(one[1], one[0]);
F_PROFILE(f,t,i) = -R*w*sin(Theta-3.141592/2);
}
end_f_loop(f,t)
}
```

UDF code in ‘c’ language for mesh motion

```
#include "udf.h"
#include "stdio.h"
#include<math.h>

DEFINE_CG_MOTION(ROtor_Motion,dt,vel,omega,time,dtime)
{
 Thread *tf = DT_THREAD (dt);
 face_t f;
 Node *v;
 real NV_VEC (axis), NV_VEC (dx);
 real NV_VEC (origin), NV_VEC (rvec), NV_VEC (center), NV_VEC (trans);
 real rotation_radii, RPM;
 real x1,x2,y1,y2;
 real time1, time2, theta1, theta2;
 int n;
 real CGravity[ND_ND];
 real xnew[ND_ND];
 real count;

 SET_DEFORMING_THREAD_FLAG (THREAD_T0 (tf));

 x1 = 0.000635;
 x2 = 0.000635;
 y1 = 0;
 y2 = 0;

 RPM = 150.796416;
 NV_D (axis, =, 0.0, 0.0, 1.0);
 NV_D (origin, =, 0.0, 0.0, 0.0);
 NV_D (center, =, x1, 0.0, 0.0);
 NV_D (trans, =, 0.0,  0.0, 0.0);

 time1 = time;
 time2 = time+dtime;
```

```
	theta1= time1 * RPM;
	theta2= time2 * RPM;
	Message ("\n whirl angle=%f	time=%f\n",theta1*180/3.141592,time);

		if (fabs(theta1) > 6.28318531 && fabs(theta1) < 12.56637062)
		theta1 -= 6.28318531;
		if (fabs(theta2) > 6.28318531 && fabs(theta2) < 12.56637062)
		theta2 -= 6.28318531;

		if (fabs(theta1) > 12.56637062 && fabs(theta1) < 18.84955593)
		theta1 -= 12.56637062;
		if (fabs(theta2) > 12.56637062 && fabs(theta2) < 18.84955593)
		theta2 -= 12.56637062;

	x1		=(25.197841-30.409216*pow(theta1,1)+12.382895*pow(theta1,2)-
2.1840395*pow(theta1,3)+0.146419016*pow(theta1,4))/(1-
0.98597326*pow(theta1,1)+0.42802009*pow(theta1,2)-
0.083464959*pow(theta1,3)+0.0060158968*pow(theta1,4));

	x2		=(25.197841-30.409216*pow(theta2,1)+12.382895*pow(theta2,2)-
2.1840395*pow(theta2,3)+0.146419016*pow(theta2,4))/(1-
0.98597326*pow(theta2,1)+0.42802009*pow(theta2,2)-
0.083464959*pow(theta2,3)+0.0060158968*pow(theta2,4));

	y1=		0.16948823+20.626258*pow(theta1,1)+65.459141*pow(theta1,2)-
165.9372*pow(theta1,3)+187.78591*pow(theta1,4)-
116.481*pow(theta1,5)+42.194318*pow(theta1,6)-
9.207848*pow(theta1,7)+1.1960505*pow(theta1,8)-
0.085357117*pow(theta1,9)+0.0025804057*pow(theta1,10);

	y2=		0.16948823+20.626258*pow(theta2,1)+65.459141*pow(theta2,2)-
165.9372*pow(theta2,3)+187.78591*pow(theta2,4)-
116.481*pow(theta2,5)+42.194318*pow(theta2,6)-
9.207848*pow(theta2,7)+1.1960505*pow(theta2,8)-
0.085357117*pow(theta2,9)+0.0025804057*pow(theta2,10);

	x1= x1*0.001*0.0254;
	x2= x2*0.001*0.0254;
	y1= y1*0.001*0.0254;
	y2= y2*0.001*0.0254;

	Message("\n x1%f\n",x1);
	Message("\n y1%f\n",y1);
	Message("\n x2%f\n",x2);
```

```
      Message("\n y2%f\n",y2);

      trans[0] = x2 - x1;
      trans[1] = y2 - y1;

      Message  ("%f   %f    %f  \n", theta1*180/3.141592, trans[0], trans[1]);

      CGravity[0] =0;
      CGravity[1] =0;
      count =0;

      begin_f_loop (f, tf)
        {
          F_CENTROID(xnew,f,tf);
          CGravity[0] = CGravity[0]+xnew[0];
          CGravity[1] = CGravity[1]+xnew[1];
          count = count + 1;
          f_node_loop (f, tf, n)
            {
              v = F_NODE (f, tf, n);
                   if (NODE_POS_NEED_UPDATE (v))
                                        {
                                        NODE_POS_UPDATED(v);
                                NV_V (NODE_COORD (v), +=, trans);
                                        }
            }
        }
      end_f_loop (f, tf);
      CGravity[0] = CGravity[0]/count;
      CGravity[1] = CGravity[1]/count;
      Message  ("%f   %f \n", CGravity[0], CGravity[1]);
}
```

VITA

Name:	ANAND VIJAYKUMAR
Address:	Texas A&M University, Dept. of Mechanical Engineering 3123 TAMU College Station, TX, 77843-3123
Email Address:	anandvksin2003@gmail.com
Education:	B.S., Mechanical Engineering, Vellore Institute of Technology, 2007 M.S., Mechanical Engineering, Texas A&M University, 2010